Journal of Electrical and Computer Engineering

Power-Line Communications: Smart Grid, Transmission, and Propagation

Guest Editors: Justinian Anatory, Moises V. Ribeiro, Andrea M. Tonello, and Ahmed Zeddam

Power-Line Communications: Smart Grid, Transmission, and Propagation

Journal of Electrical and Computer Engineering

Power-Line Communications: Smart Grid, Transmission, and Propagation

Guest Editors: Justinian Anatory, Moises V. Ribeiro, Andrea M. Tonello, and Ahmed Zeddam

Editorial Board

The editorial board of the journal is organized into sections that correspond to the subject areas covered by the journal.

Circuits and Systems

Communications

Signal Processing

Contents

Hindawi Publishing Corporation
Journal of Electrical and Computer Engineering
Volume 2013, Article ID 948598, 2 pages
http://dx.doi.org/10.1155/2013/948598

Editorial

Power-Line Communications: Smart Grid, Transmission, and Propagation

Justinian Anatory,[1] Moises V. Ribeiro,[2] Andrea M. Tonello,[3] and Ahmed Zeddam[4]

[1] *School of Informatics, College of Informatics and Virtual Education, University of Dodoma, P.O. Box 490, Dodoma, Tanzania*
[2] *Electrical Engineering Department, Faculdade de Engenharia, Federal University of Juiz de Fora, Campus Universitário, 36 033 330 Juiz de Fora, MG, Brazil*
[3] *Wireless and Power Line Communications Lab, Università di Udine, 33100 Udine, Italy*
[4] *France Telecom, Orange Labs, 2, Avenue Pierre Marzin, 22 307 Lannion Cedex, France*

Correspondence should be addressed to Justinian Anatory; janatory@udom.ac.tz

Received 28 January 2013; Accepted 28 January 2013

Power-line communication networks are gaining popularity in various service provisions such as in houses/offices, access networks, in ships, aircrafts, trains, vehicles, in industry systems control, and advanced metering infrastructure. This popularity is also striding towards smart grid implementations. However, the network structure affects the channel response which exhibits frequency selectivity and time variant behavior. These effects are due to different terminal loads connected to such systems, number of branches, and different branched line lengths. In addition, different types of cables and signal injection methods used (i.e., with respect to adjacent lines/grounds and the grounding systems implemented in different countries) for such systems render the propagation difficult. Furthermore, Electromagnetic Compatibility (EMC) issues and more especially Electromagnetic Interference (EMI) occurring at different frequencies of operations still need more investigation. Power-line communications have demonstrated the acceptance to support various applications such as HD Television (HDTV), Internet Protocol Television (IPTV), interactive gaming, whole-home audio, security monitoring, and Smart Grid management. These services have to be supported by the new home networks/access and be deployed and standardized worldwide.

This special issue was launched to gather state-of-the-art research contributions in the field of Power-line communications. It has attracted the submissions of many high-quality papers. After going through a conscientious peer-review process, six papers have been selected. These papers make an inspiring ensemble with a topic spectrum ranging from improved maximum likelihood detection of spread frequency shift keying (S-FSK) in PLC automatic meter reading (AMR), radiation mitigation for PLC, optimal receiver impedance design for SNR maximization in broadband PLC, PLC for Smart Grid applications, improvements of G3-PLC technology for Smart-Home/Building applications, and finally an overview of the HomePlug AV2 technology.

Specifically, in the paper entitled "*Improved maximum likelihood S-FSK receiver for PLC modem in AMR*," Bali and Rebai present an optimized software implementation of a narrow band Power-line modem. The modem is a node in an automatic meter reading (AMR) system which is compliant to the IEC 61334-5-1 profile and operates in the CENELEC-A band. Because of the hostile communication channel, a new design approach is carried out for an S-FSK demodulator capable of providing lower bit error rate (BER) than standard specifications. The best compromise between efficiency and architecture complexity is investigated. Some implementation results are presented to show that a communication throughput of 9.6 kbps is reachable with the designed S-FSK modem.

In the paper entitled "*Radiation mitigation for Power-line communications using time reversal*," Mescco et al. explain the use of the Time Reversal (TR) technique to mitigate radiated emissions from PLC systems. The method was probed

experimentally in real electrical networks with excellent results: in 40% of the observations, the electromagnetic interference generated by PLC transmission can be reduced by more than 3 dB, and this EMI mitigation factor may increase to more than 10 dB in particular configurations. The paper proposes also future research directions in the field of wired TR techniques at higher frequencies and on other media, such as Digital Subscriber Line twisted pairs. In addition, optimal protocols are suggested for development of practical implementation of TR in future standards.

In the paper entitled "*A study on the optimal receiver impedance for SNR maximization in broadband PLC*," Antoniali et al. present the design of the front-end receiver for broadband Power-line communications. The paper focuses on the design of the input impedance that maximizes the signal-to-noise ratio (SNR) at the receiver. The authors show that the amplitude, rather than the power, of the received signal is important for communication purposes. Furthermore, they analyse the receiver impedance impact on the amplitude of the noise term for which a novel model description is provided. Performance results are reported for real in-home grids that have been assessed with experimental measurements. The best attainable performance is studied when the optimal receiver impedance is used and it is shown that conventional power matching is suboptimal with respect to the proposed impedance design approach in terms of achievable information rate.

Two other papers deal with the topic of Smart Grid in various environments. In the paper entitled "*Power-line communications for Smart Grid applications*," Berger et al., surveys PLC technologies that are relevant in the context of Smart Grid. The specifications of G3-PLC, PRIME, HomePlug Green Phy, HomePlug AV2, as well as the standards IEEE 1901/1901.2, and ITU-T G.hn/G.hnem are discussed. Another paper entitled "*Enhancements of G3-PLC technology for Smart-Home/Building applications*," by Di Bert et al., consider the in-home/building scenario, for which a convergent network architecture is proposed to enhance the performance of the narrow band G3-PLC technology through its integration with an Ethernet-based network. The paper defines the protocols implemented by the network modules. Since Ethernet represents a convergent standard for many communication devices, by adding this functionality to G3-PLC, interconnectivity with other heterogeneous nodes can be offered. Furthermore, since the G3-PLC medium access control layer is based on a Carrier Sense Multiple Access (CSMA) scheme, its performance decreases when the number of network nodes contending for the channel increases. Therefore, the paper evaluates the network performance when an optimized time division multiple access scheme is adopted showing that performance improvements are reached.

In the paper entitled "*An overview of the HomePlug AV2 technology*," Yonge et al. provide an overview of the HomePlug AV2 system architecture and the key features at both the PHY and MAC layers. The paper presents the new techniques used at the PHY layer as multiple-input multiple-output transmission, beamforming and precoding, adaptation of the parameters, and power management for improved EMC. Enhancements at the MAC layer are also discussed and they include the implementation of power saving modes, the usage of a short delimiter in the MAC frame, delayed acknowledgment, and the coexistence mechanisms with other PLC systems. The HomePlug AV2 performance is also assessed, through simulations reproducing real home scenarios.

We believe that the papers appearing in this special issue provide a good contribution and representation of significant research topics in the field of PLC.

Acknowledgments

We would like to thank the authors for their contributions and the reviewers for their competent and timely work.

Justinian Anatory
Moises V. Ribeiro
Andrea M. Tonello
Ahmed Zeddam

Hindawi Publishing Corporation
Journal of Electrical and Computer Engineering
Volume 2013, Article ID 712376, 16 pages
http://dx.doi.org/10.1155/2013/712376

Review Article

Power Line Communications for Smart Grid Applications

Lars Torsten Berger,[1] Andreas Schwager,[2] and J. Joaquín Escudero-Garzás[3]

[1] *Kenus Informática, Paterna, Valencia, Spain*
[2] *European Technology Center (EuTEC), Sony Deutschland GmbH, Stuttgart, Germany*
[3] *Department of Telecommunications and Systems Engineering, Universitat Autónoma of Barcelona (UAB), Barcelona, Spain*

Correspondence should be addressed to Lars Torsten Berger; lars.berger@kenus.es

Received 3 August 2012; Accepted 29 December 2012

Academic Editor: Ahmed Zeddam

Power line communication, that is, using the electricity infrastructure for data transmission, is experiencing a renaissance in the context of *Smart Grid*. Smart Grid objectives include the integration of intermittent renewable energy sources into the electricity supply chain, securing reliable electricity delivery, and using the existing electrical infrastructure more efficiently. This paper surveys *power line communications* (PLCs) in the context of Smart Grid. The specifications *G3-PLC*, *PRIME*, *HomePlug Green PHY*, and *HomePlug AV2*, and the standards *IEEE 1901/1901.2* and *ITU-T G.hn/G.hnem* are discussed.

1. Introduction

Smart Grids, for many, the next big technological revolution since the invention of the Internet, will play an important role in tomorrow's societies. Governments around the world are pumping large sums of money into *Smart Grid* (SG) research, development, and deployments, their aims being manifold. Smart Grids have the potential to reduce carbon dioxide emissions through the integration of distributed renewable energy resources, energy storage, and plug-in hybrid electric vehicles. Moreover, they can increase the reliability of the electricity supply (reduced blackout rate) by real-time measurements, monitoring and control of the generation, and transmission and distribution networks. Further, they can render the utilization of base load power plants and electricity transport infrastructure more efficient, deploying dynamic pricing and demand response strategies [1, 2].

Besides achievements in power electronics, sensing, monitoring, and control technology, key Smart Grid enablers are the advances that in the last decade have been made in the area of telecommunications. There is a long list of complementary and sometimes competing wireless and wireline specifications and standards that can be used in Smart Grid deployments [3]. Industry adoption and large-scale customer roll-outs are still in their infancies, and it is hard to make an accurate prediction of the "winners" and "losers." What seems clear is that *power line communications* (PLCs), that is, communications over the existing electrical infrastructure, will have their part to play since they provide the natural upgrade from simple electricity conductors to hybrid and bidirectional electricity and data communication solutions.

The idea of using power lines also for communication purposes has already been around at the beginning of the last century [4]. The obvious advantage is the wide spread availability of electrical infrastructure, so that theoretically deployment costs are confined to connecting modems to the existing electrical grid.

Power line technologies can be grouped into *narrowband PLC* (NB-PLC), operating usually below 500 kHz, and *broadband PLC* (BB-PLC), operating usually at frequencies above 1.8 MHz [5]. These are discussed in Sections 5 and 6, respectively. Nevertheless, the following starts out with an introduction to PLC scenarios, followed by channel, noise, and *electromagnetic compatibility* (EMC) aspects. Freely available complementary reading on PLC state-of-the-art can also be found in [6]. Another valuable source of the PLC-related

Table 1: Domains and actors in the smart grid conceptual model, based on [13, Table 3-1].

Domain	Actors in the domain
Customers	The end users of electricity. May also generate, store, and manage the use of energy. Traditionally, three customer types are discussed, each with its own domain: residential, commercial, and industrial.
Markets	The operators and participants in electricity markets.
Service providers	The organizations providing services to electrical customers and utilities.
Operations	The managers of the movement of electricity.
Bulk generation	The generators of electricity in bulk quantities. May also store energy for later distribution.
Transmission	The carriers of bulk electricity over long distances. May also store and generate electricity.
Distribution	The distributors of electricity to and from customers. May also store and generate electricity.

literature is the recently established IEEE Communication Society's web portal on *Best Readings in Power Line Communications* [7].

2. Communication Scenarios

Many national and international organizations are currently drawing up roadmaps for SG standards [8–12]. For brevity, the following orients itself on the work by the US *National Institute of Standards and Technology* (NIST). To structure the various areas of the Smart Grid, NIST devised a domain-based conceptual model [13]. Each *domain* contains *actors* that with the help of communications might act over domain borders. The definitions of domains and actors are reproduced in Table 1. The interconnections between domains are displayed in Figure 1. It has been common practice to distinguish power line communication scenarios according to operation voltages of the power lines [14]. Figure 1 links this voltage-based differentiation to the NIST conceptual model.

High-voltage (HV) lines, with voltages in the range from 110 kV to 380 kV, are used for nationwide or even international power transfer and consist of long overhead lines with little or no branches. This makes them acceptable wave guides with less attenuation per line length as for their medium- and low-voltage counterparts. However, their potential for broadband SG communication services has up to the present day been limited. Time-varying high-voltage arcing and corona noise with noise power fluctuations in the order of several tens of dBs and the practicalities and costs of coupling communication signals in and out of theses lines have been an issue. Further, there is a fierce competition of fiber optical links. In some cases, these links might even be spliced together with the ground conductor of the HV system [15, 16]. Nevertheless, several successful trials using HV lines have been reported in [17–20].

Medium-Voltage (MV) lines, with voltages in the range from 10 kV to 30 kV, are connected to the HV lines via primary transformer substations. The MV lines are used for power distribution between cities, towns, and larger industrial customers. They can be realized as overhead or underground lines. Further, they exhibit a low level of branches and directly connect to *intelligent electronic devices* (IEDs) such as reclosers, sectionalizers, capacitor banks, and phasor measurement units. IED monitoring and control requires only relatively low data rates, and NB-PLC can provide economically competitive communication solutions for these tasks. MV-related studies and trials can be found in [21–23].

Low-voltage (LV) lines, with voltages in the range from 110 V to 400 V, are connected to the MV lines via secondary transformer substations. A communication signal on an MV line can pass through the secondary transformer onto the LV line, however, with a heavy attenuation in the order of 55 dB to 75 dB [24]. Hence, a special coupling device (inductive, capacitive) or a PLC repeater is frequently required if one wants to establish a high data rate communications path. As indicated in Figure 1, the LV lines lead directly or over street cabinets to the end customers' premises. Note that a considerable regional topology difference exits. For example in the USA a smaller secondary transformer on a utility pole might service a single house or a small number of houses. In Europe, however, it is more common that up to 100 households get served from a single secondary transformer substation. Further, as pointed out in [25], significant differences exist between building types. They may be categorized as *multiflat buildings with riser*, *multiflat buildings with common meter room*, *single family houses*, and *high-rise buildings*. Their different electrical wiring topologies influence signal attenuation as well as interference between neighboring PLC networks [26].

In most cases the electrical grid enters the customers' premises over a *house access point* (HAP) followed by an *electricity meter* (M) and a distribution board (fuse box). One frequently refers to PLC systems operating up to this point as *Access* systems. Delivering broadband Internet Access over the electrical grid, also known as *broadband over power line* (BPL), amounted at the end of 2008 to less then 1% of the worlds Access customers (65% used DSL, 21% used cable) [27]. BPL is, however, on the rise, especially in rural areas and in developing countries with a poorly developed fixed telephone line and coaxial cable infrastructure [16]. Apart from general Internet Access, *automated meter reading* (AMR) systems frequently used *ultranarrowband power line communication* (UNB-PLC) technologies like Turtle [28] and TWACS [29, 30] to gain access and control over the energy meters within private homes. UNB-PLC systems are usually designed to communicate over long distances with their signals passing through the LV/MV transformers. This helps to keep the amount of required modems and repeaters to a minimum. Drawbacks are low data rates in the order of 0.001 bit/s and 60 bit/s for Turtle and TWACS, respectively, and sometimes limitations to unidirectional communications. These UNB-PLC technologies are mentioned here as they are among the pioneers in the AMR

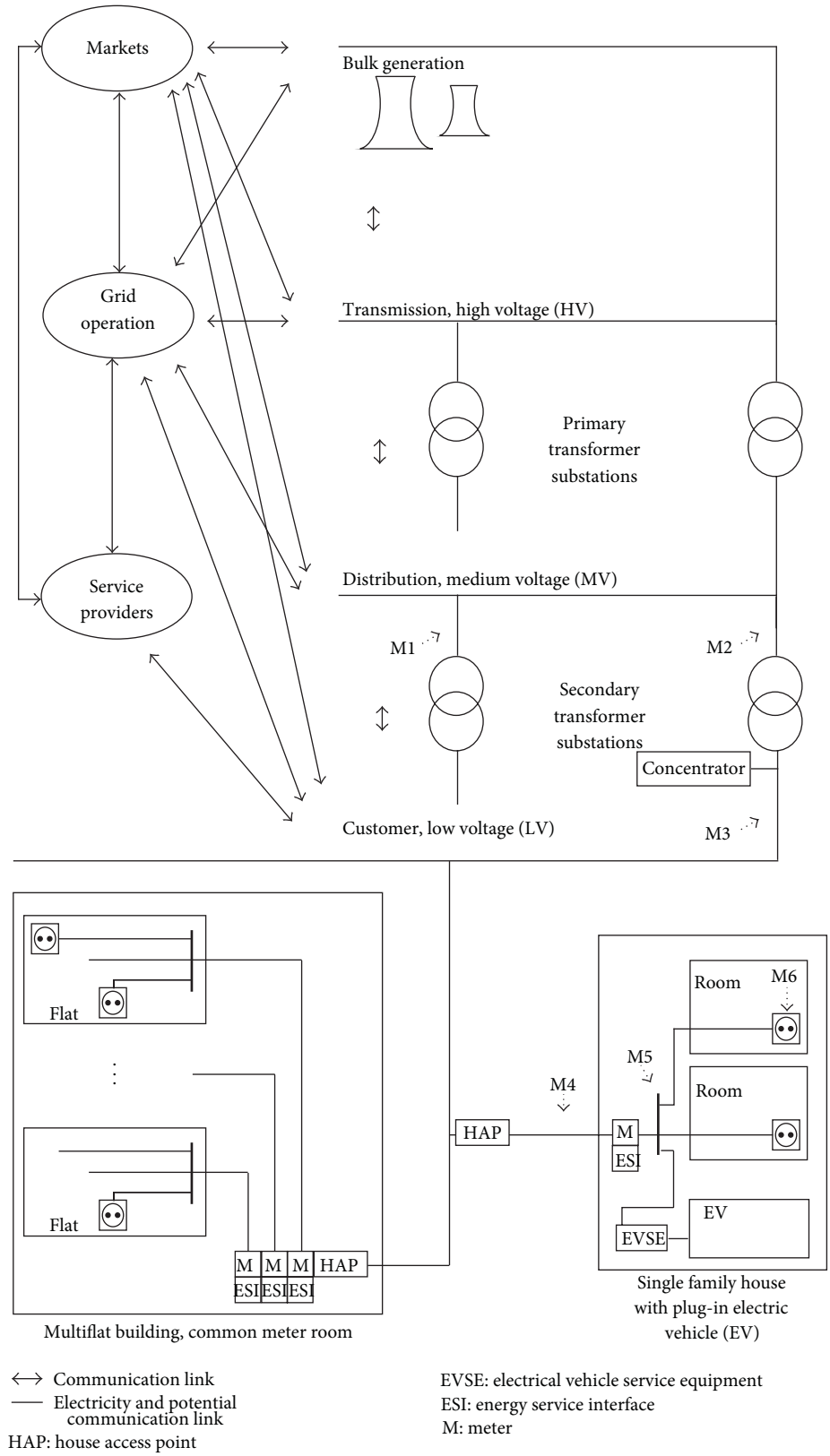

Figure 1: Smart Grid domains and their electrical and communication interconnections, based on Figure 7.1 in [75].

and *distribution automation* field. However, in the light of many upcoming Smart Grid deployments, there are much higher requirements on the communication infrastructure, for example, to support *demand response*, *distributed generation*, and *demand side management* applications. It is believed that these applications can, among others, be supported by PLC-based *Advanced Metering Infrastructure* (AMI). A whole wealth of material on AMI requirements and architectures is available, for example, from the European *OPEN meter* project [31]. To cope with increased AMI requirements, this paper leaves UNB-PLC solutions at a sideline in favour of more recent *narrowband PLC* (NB-PLC) technologies, such as *Power line-Related Intelligent Metering Evolution* (PRIME) [32], and G3-PLC [33, 34]. NB-PLC bidirectional data rates lie in the order of hundred kbit/s, while partly preserving the advantage to communicate over long ranges and through transformers.

From the distribution board the LV lines run up to the different power sockets in every room. Lines may also run to an *electric vehicle service equipment* (EVSE) as indicated in Figure 1. For reliable *home area network* (HAN) high data rate applications, *broadband power line communication* (BB-PLC) technologies are becoming more and more attractive. Field-proven BB-PLC technologies provide data rates of more than 200 Mbit/s [35], making it easy to fulfill the users' home entertainment needs including *high definition television* (HDTV). Upcoming SG services in the home include granular control of smart appliances, the ability to remotely manage electrical devices, and the display of consumption data. Consumer awareness usually leads to a change in consumption habits and in the sequel to energy savings between 10% and 20% [36].

NB-PLC solutions have for a long time been used for home automation applications [14], and it is believed that the well-established automation systems, like BACnet [37], KNX (ISO/IEC 14543-3-5, EN 50090) [38], and LON (ISO/IEC 14908-3, ANSI 709.2) [39, 40], are being integrated into upcoming Smart Home concepts [10]. Nevertheless the following also leaves these technologies at a sideline in favor of more recent standards like IEEE 1901 and ITU-T G.hn for BB-PLC applications and IEEE 1901.2 and ITU-T G.hnem for NB-PLC applications.

3. Channel and Noise Aspects

The power line channel and noise situations heavily depend on the scenario and, hence, span a very large range. Generally, it can be said that the PLC channel exhibits frequency selective multipath fading and a low-pass behaviour. Further, *alternating-current*- (AC) related cyclic short-term variations and abrupt long-term variations can be observed.

3.1. Frequency Selectivity. To understand the effects that lead to frequency selective fading consider, for example, the stub line schematic in Figure 2. An impedance-matched transmitter is placed at A. B marks the point of a branch, also called an electrical T-junction. An impedance-matched receiver is placed at C. A parallel load is connected at D.

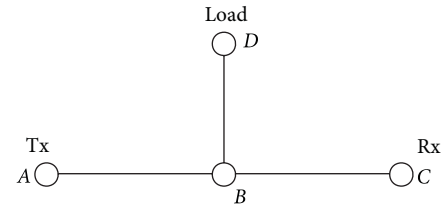

Figure 2: Stub line example.

Transmissions and reflections lead to a situation where a PLC signal travels in form of a direct wave from A over B to C. Another signal travels from A over B to D, bounces back to B, and reaches C. All further signals travel from A to B and undergo multiple bounces between B and D before they finally reach C. The result is a classical multipath situation, where frequency selective fading is caused by in-phase and antiphase combinations of the arriving signal components. The corresponding transfer function can readily be derived in close form as an infinite impulse response filter [41]. One important parameter capturing the frequency selectivity characteristics is the *root mean square* (rms) *delay spread* (DS). For example, designing *orthogonal frequency-division multiplexing* (OFDM) systems, the guard interval might be chosen as 2 to 3 times the rms DS to deliver good system performance [42]. To provide an orientation, the mean of the observed rms DS for a band from 1 MHz up to 30 MHz in the MV, LV-Access and LV-In-Home situations in [24, 42] was reported to be 1.9 μs, 1.2 μs, and 0.73 μs, respectively.

3.2. Time Variation. Besides multipath fading, the PLC channel exhibits time variation due to loads and/or line segments being connected or disconnected [43]. Further, through synchronizing channel measurements with the electrical grid AC mains cycle Cañete et al. were able to show that the In-Home channel changes in a cyclostationary manner [44–46].

3.3. Low-Pass Behavior. Untill now the low-pass behavior of PLC channels has not been considered. It results from dielectric losses in the insulation between the conductors and is more pronounced in long cable segments such as outdoor underground cabling. Transfer function measurements on different cable types and for different lengths can be found in [47, 48]. Using a large set of field trials, low-pass mean gain models are derived in [24]. Over the range from 1 to 30 MHz the mean gain in dB is approximated by linear models. Consider again the PLC scenarios from Figure 1. The mean gain from the secondary transformer to the HAP, labeled M3 and M4, writes [24]

$$\overline{g}_{\text{LV-Access}} = -\left(a_1 \cdot f \cdot d + a_2 \cdot f + a_3 \cdot d + a_4\right), \quad (1)$$

where f is frequency in MHz, d is distance in meters, and the coefficients a_1 to a_4 are 0.0034 dB/(MHz m), 1.0893 dB/MHz, 0.1295 dB/m, and 17.3481 dB, respectively.

The mean gain model in dB for MV lines, as well as for LV-In-Home situations is given by [24]

$$\overline{g}_{\text{MV or LV-In-Home}} = -\left(b_1 \cdot f + b_2\right). \quad (2)$$

For the LV-In-Home situation the mean gain is given from the mains distribution board to a socket in a room, labelled M5 and M6 in Figure 1. The coefficients are $b_1 = 0.596$ dB/MHz and $b_2 = 45.325$ dB. The MV gain describes the channel between two primary transformers on the MV side, indicated by M1 and M2 in Figure 1. Its coefficients are $b_1 = 1.77$ dB/MHz and $b_2 = 37.9$ dB. In both situations the model is not distant dependent. For the MV situation this is due to the fact that not enough measurement results were available to construct a distant-dependent model. Hence, in this case the model is limited to situations where the distance between M1 and M2 is around 510 m. Nevertheless, correction factors are proposed in [24] to determine the mean gain at other distances. For the LV-In-Home situation the model is not distance dependent either as "distance" in an In-Home situation is a hard-to-define term. Power line networks in such situation exhibit usually a large amount of branches, and a detailed floor plan to determine cable length cannot always be obtained. This leads to a situation where the low-pass behavior is less pronounced in the In-Home case. Further, in the MV- and the LV-Access situation the attenuation drastically increases with frequency. This goes well in line with the findings in [49] and is one of the reasons why BB-PLC Access networks are frequently operated in the lower frequency range, for example, between 1 and 10 MHz, while BB-PLC In-Home networks might operate at frequencies above 10 MHz.

3.4. MIMO Channel. For a long time, the power line channel has been regarded as *single-input single-output* (SISO) channel, based on two conductors. Nevertheless, in many In-Home installations three wires, namely, *live* (L) (also called *phase* (P)), *neutral* (N), and *protective earth* (PE), are common [50]. Further, medium- and high-voltage installations often make use of four or more conductors. In this respect, a theoretical framework of multiconductor transmission line theory is extensively treated in [51]. Further, channel characterization and modeling work directly related to multiconductor PLC are available in [52–63].

3.5. MIMO Couplers. In general, the observed channel characteristics are not independent from the coupling devices used to inject and receive the power line signal. Figure 3 presents feeding and receiving possibilities for MIMO power line communication, that is, (a) a *Delta-style* coupler, (b) a *T-style* coupler [55], and (c) a *Star-style* coupler [64]. Coupler designs are tightly related to radiated emission treated in more detail in Section 4 [62]. According to the *Biot-Savart law* the main source of radiated emission is the *common mode* (CM) current [65]. To avoid radiated emission, traditionally PLC modem manufacturers aim at injecting the signal as symmetrically as possible. In this way, two 180° out of phase electric fields are generated that neutralize each other resulting in little radiated emission. This desired symmetrical way of propagation is also known as *differential mode* (DM). Specifically, to avoid the injection of CM, feeding MIMO PLC signals can be done using the delta or T-style couplers from Figures 3(a) or 3(b). The delta, also called transversal probe,

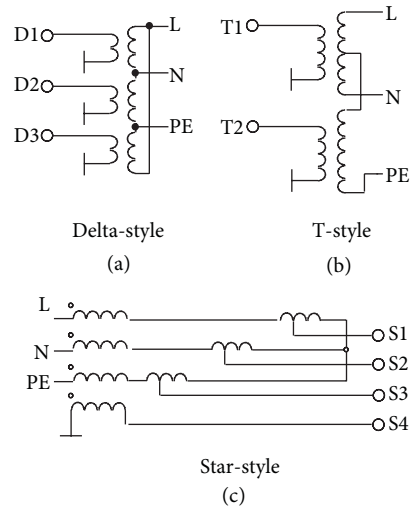

Figure 3: MIMO PLC couplers.

consists of three baluns arranged in a triangle between L, N, and PE. The T-style coupler feeds a differential mode signal between L and N plus a second signal between the middle point of L-N to PE. Receiving the PLC signals is also possible using the star-style or longitudinal coupler. There three wires are connected in a star topology to the center point. The benefit of this coupler is the possibility to receive CM signals which enables a forth reception path. On average CM signals are less attenuated than DM signals [64]. This is why it may be interesting to receive them, especially for highly attenuated channels.

3.6. Noise Characterization and Modeling. Turning from the channel to the noise situation, power line noises can be grouped based on temporal and spectral characteristics. Following, for example, [48, 66] one can distinguish *colored background noise*, *narrowband noise*, *periodic impulsive noise asynchronous to the AC frequency*, *periodic impulsive noise synchronous to the AC frequency*, and *aperiodic impulsive noise*. In [48] all these noises are modeled directly at the receiver using a superposition of spectrally filtered *additive white Gaussian noise* (AWGN), modulated sinusoidal signals, and Markov processes. Instead of modeling the noise directly at the receiver, Cañete et al. proposed to model the noise at its origin and to filter it by the channel transfer function [44, 67]. Besides, specific results on MIMO system noise are presented in [68, 69].

A statistical approach to average colored background noise modeling is presented in [24] based on a large amount of noise measurements in MV, LV-Access and LV-In-Home situations. Although a lot of the details get lost by averaging, the results can still deliver some interesting rule of thumb when one wants to determine a likely average noise level. One general finding is that the mean noise power falls off exponentially with frequency. Derived from [24] the mean noise *power spectral density* (PSD) in dBm/Hz is given by

$$\overline{P}_N = c_1 \cdot e^{(-c_2 \cdot f)} + c_3 - 10 \cdot \log_{10}(30000), \quad (3)$$

Table 2: Mean noise model coefficients [70] © 2010 John Wiley & Sons.

Location	c_1, [dB]	c_2, [1/MHz]	c_3, [dBm/Hz]
M1 and 2, Secondary Transformer, MV	37	0,17	−105
M3, Secondary Transformer, LV	24,613	0,105	−116,72
M4, House access point, LV	29,282	0,12	−114,94
M5, Main distribution board, LV	39,794	0,07	−118,08
M6, Socket in private home, LV	17,327	0,074	−115,172

where the last term normalizes out the 30 kHz bandwidth used in the noise measurement process. The coefficients c_1 to c_3 are given in Table 2. The resulting noise models correspond to the measurement points M1 to M6 in Figure 1.

3.7. Mean SNR Considerations. Details on Tx limits will be discussed in Section 4. For simplicity, assume for now that a power line signal with $\overline{P}_S = -50$ dBm/Hz may be injected. Using the gain and noise models from (1) to (3) the mean *signal-to-noise ratio* (SNR) can then be calculated as

$$\overline{\mathrm{SNR}} = \overline{g} + \overline{P}_S - \overline{P}_N. \quad (4)$$

The mean SNRs for the various connections between the measurement points M1 to M6 in Figure 1 are plotted in Figure 4. One should note that, although the channel gain between two measurement points is symmetric, the noise at the measurement points differs. Hence, five different curves are produced.

It can be seen that especially the lower part of the spectrum, up to 10 MHz, is very well suited for Access and Backhaul applications. Further, for In-Home applications the entire spectrum from 1 to 30 MHz promises high mean SNRs in the order of 40 dB, which goes also well in line with the findings in [71]. Further interesting results for the frequency range up to 100 MHz are available in [61–63, 69, 72].

In general, the results show that there is a high potential for PLC if the estimated mean SNRs can be exploited in PLC modems. However, the presented mean results have to be handled with care. One should bear in mind that the mean SNR models from [24] exhibit a significant standard deviation. Further, effects due to frequency selectivity, narrowband interference, impulsive noise, and time variation are not reflected in Figure 4. Whether the estimated mean SNRs translate into high PLC data rates depends not at last on the PLC modem's signal processing algorithms, its component quality, and permissible implementation complexity.

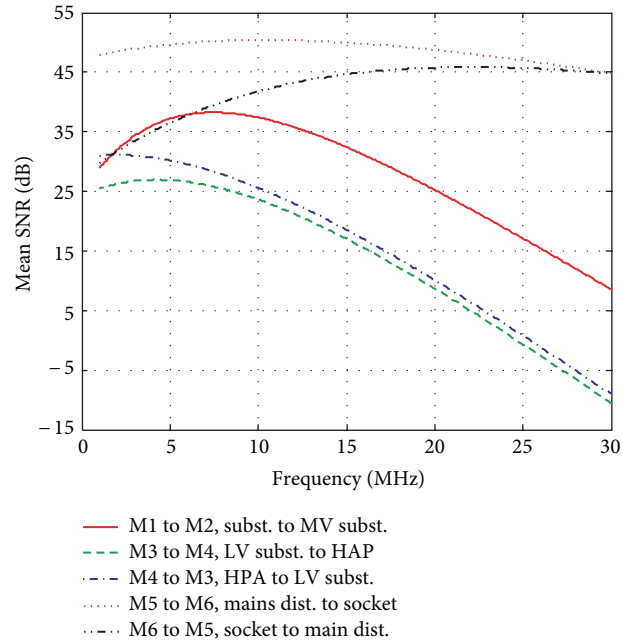

Figure 4: Mean SNR based on −50 dBm/Hz injected PSD, as well as mean channel gain and mean noise power spectral density models.

4. Electromagnetic Compatibility Regulations

Power line cables were not designed to carry communication signals and, hence, give rise to conducted emission, as well as radiated emission that may interfere, for example, with Amateur Radio or radio broadcast receivers. When looking at power line *electromagnetic compatibility* (EMC) regulations, one may distinguish between regulations for NB-PLC and BB-PLC.

The NB-PLC regulations deal with the spectrum from 3 kHz up to around 500 kHz. Important NB-PLC regulations are listed in Table 3. Being a subset of all other bands, the *European Committee for Electrotechnical Standardization* (CENELEC) bands are the only ones available on a global basis. Four CENELEC bands are defined as *A* (3–95 kHz), *B* (95–125 kHz), *C* (125–140 kHz), and *D* (140–148.5 kHz) [73]. Besides specifying transmission limits and their measurement procedures, the CENELEC standard also mandates that the A band may only be used by Energy Suppliers and their licensees, while the other bands may be used by consumers. Further, devices operating in C band have to comply with a *carrier sense medium access/collision avoidance* (CSMA/CA) protocol that allows a maximum channel holding period of 1 s, a minimum durations between channel uses by the same device of 125 ms, and a minimum time of 85 ms before declaring the channel idle. For the USA, there are currently ongoing efforts [74] to specify the band from 9 kHz to 534 kHz for NB-PLC operations with a mandatory CSMA/CA protocol compliant with CENELEC EN 50065-1 [73]. The advantages are that equipment manufacturers would be easily able to adapt their NB-PLC products to the EU and USA market and to many other markets that follow these standards.

Turning the view to BB-PLC one may again distinguish two frequency ranges, that is, 1 MHz to 30 MHz, where conducted emission is at the focus of regulation, and 30 MHz to 100 MHz, where the focus shifts to radiated emission.

The *Comité International Spécial des Perturbations Radioélectriques* (CISPR), founded in 1934 and now part of the *International Electrotechnical Commission* (IEC), was

Table 3: Important regulations related to NB-PLC [75] © 2012 John Wiley & Sons.

States	Frequ. [kHz]	Institution	References
EU	3–148.5	*Comité Européen de Normalisation Électrotechnique (CENELEC)*	[73]
US	10–490	*Federal Communications Commission (FCC)*	[76]
Japan	10–450	*Association of Radio Industries and Businesses (ARIB)*	[77]

making efforts to regulate BB-PLC generated interference. At the beginning CISPR 22 [78] defined two sets of limits and measurement methods for conducted emissions of telecommunication equipment. One set was defined for the telecommunication port, and the other was defined for the mains port. For PLC modems, it is not defined whether the PLC signal port, which at the same time is used for power supply, is considered as a mains or as telecommunication port. The method for telecommunication ports respects the symmetry properties of the attached cable. Asymmetries like an open light switch or asymmetrical parasitic capacitances convert the symmetrically fed signals into common mode signals [65]. However, the method used for devices connected to the mains, specified in CISPR 16 [79], is based on measuring the asymmetric voltage level of either the phase or neutral wire to the ground. From the perspective of a PLC modem, this is the worst case, because this voltage consists of asymmetric and symmetric voltage; that is, not only the emission, and therewith the interference relevant part, but also the desired signal is measured and compared against emission limits. IEC CISPR/I/89/CD [80] tried to clarify the situation by interpreting PLC as an application following the telecommunication limits of CIPSR 22. Therefore, the *longitudinal conversion loss* (LCL) parameter was used in an identical way as, for example, in the testing of *digital subscriber line* (DSL) equipment. The benefit of using the LCL parameter is the simplicity of measuring it. It is a reflection parameter whose measurement requires an equipment to be connected to only one location of the grid. Other possibilities to verify the potential of interference would have been to place antennas and measure the field generated by the fed PLC signal. However, this would make a measurement setup significantly more cumbersome and error prone. Nevertheless, with respect to highly attenuated wires like the power lines the much simpler measurement of a reflection parameter as in [80] only describes the local situation instead of giving detailed insight of what is happening if a PLC signal travels deeply into the electrical network. In 2008, CISPR/I/257/CD [81] was published with an LCL parameter reduced by 6 dB. Simultaneously, CISPR/I/258/CD [82] indicated that mitigation techniques like cognitive notching for PLC modems [64, 83] and dynamic transmit power management are the compromise to solve the never-ending EMC discussions. CIS/I/301/CD [84] answered the question of whether PLC is connected to the telecommunication port or to the mains port by introducing a Power Line Telecommunication (PLT) port. In this document the *electro magnetic interference* (EMI) mitigation techniques are specified as normative. However, CISPR never proposed a *committee draft for voting* (CDV). This is why CENELEC became active after the lifetime of the CISPR committee to find at least in Europe an acceptable solution. The result, prEN 50561-1:2012 [85] additionally excludes the aeronautical frequencies from power line communication and specifies the following.

(i) An emission measurement procedure at the PLT port while no communication takes place.

(ii) A second emission measurement procedure at the PLT port when normal PLC takes place.

(iii) A general cap on the injected PSD of −55 dBm/Hz.

(iv) Permanent notching of certain parts of the radio spectrum, that is related to amateur radio and aeronautical bands.

(v) A procedure for adaptive notching, meaning that the PLC equipment senses the presence of radio services and notches the affected frequencies for its own operation.

(vi) A procedure of adaptive transmit power management, meaning that the transmitting equipment limits its transmit power as a function of channel attenuation and noise to a level below the allowed maximum, that is just sufficient to achieve the required data rate.

EN50561-1:2012 was approved in November 2012, which finally gives certainty to PLC stakeholders on interference limits.

In the USA the *Federal Communications Commission* (FCC) is in charge of regulating electromagnetic emissions. In general, all digital equipments have to comply with the FCC part 15 standard (47 CFR §15) [76]. Specifically, Access PLC systems over medium- and low-voltage power lines and for a frequency range from 1.705 to 80 MHz are treated in the standard's Section G. Conducted emission limits are explicitly not applicable, but radiated emission limits are imposed through a transmit power spectral density mask. Additionally, PLC systems have to be able to notch certain frequencies that might be used by other services. Further, the FCC defines excluded bands where no PLC signal shall be injected, as well as geographical exclusion zones close to which no Access PLC systems may be deployed. Further, procedures in which service providers inform about prospective PLC Access deployments and complaint handling procedures are a requirement.

More details on PLC EMC regulations as well as conducted and radiated interference measurement results can be found in [6, 61, 86]. Besides, the "*IEEE Standard for Power Line Communication Equipment—Electromagnetic Compatibility (EMC) Requirements—Testing and Measurement Methods*" [87] was recently released, intending to provide an internationally recognized EMC measurement and testing methodology. It endorses among others CISPER22 and FCC part 15 as normative references, but does not establish

any emission limits itself. Looking at the developments in CISPR/CENELEC and at FCC part 15, it becomes clear that next generation PLC equipment has to be highly configurable to apply power spectral density-shaping masks, as well as adaptive notching.

5. Narrowband PLC

Narrowband power line communication systems usually operate in the frequency range from 3 kHz to 500 kHz, that is, the CENELEC/ARIB/FCC bands. Following, for example, the nomenclature in [5], they can be subdivided into *low data rate* (LDR) and *high data rate* (HDR) systems. LDR systems have throughputs of a few kbit/s and usually are based on single carrier technology. Example standards, listed in the NIST *Smart Grid Interoperability Panel* (SGIP) *Catalog of Standards* [3, 13], are ISO/IEC 14908-3 (LON, ANSI/EIA 709.2) [39, 40] and ISO/IEC 14543-3-5 (KNX, EN 50090) [38]. These standards span all layers of the *open systems interconnection* (OSI) model and can, besides over power line, also be used over other media such as twisted pair and in some cases even wirelessly. Their main area of application has been industrial and building automation. In this respect a further popular protocol is BACnet (ISO 16484-5 [37]). The following, however, will focus on the *physical layer* (PHY) of high data rate (up to 1 Mbit/s) NB-PLC. As in many other communication systems OFDM has emerged as the modulation scheme of choice for HDR NB-PLC. Example HDR NB-PLC systems are G3-PLC [33] and PRIME [88] that have made it into ITU G.hnem standardization as ITU G.9903 [89] and ITU G.9904 [90], respectively. Both are also supported via interoperability modes in IEEE 1901.2. With respect to coexistence, the NIST *priority action plan 15* (PAP15) working group recently approved that newly developed NB-PLC standards shall all implement a single coexistence protocol as to "have minimal performance impact on the existing deployed devices," that is, devices using ISO/IEC 14543-3-5, IEC 61334-3-1, IEC 61334-5-1, IEC 61334-5-2, and IEC 61334-4-32 [91].

5.1. PRIME. PRIME, for *Power line-Related Intelligent-Metering Evolution*, was developed within the PRIME Alliance, with its steering committee chaired by the Spanish utility heavyweight Iberdrola [32]. The PRIME system uses a total of 96 ODFM subcarriers over the frequencies from 42 kHz to 89 kHz, that is, within the CENELEC A-band. Further, it deploys differential *binary*, *quaternary*, and *eight-phase shift keying* (BPSK, QPSK, and 8PSK) and an optional 1/2-rate convolutional code. Therewith it is able to achieve a PHY peak data rate of 128.6 kbit/s [92]. The OFDM symbol interval is of 2240 μs including a 192 μs cyclic prefix which suffices to deal with most common power line delay spreads. Further, to deal with unpredictable impulsive noise PRIME offers the option to implement *automatic retransmission request* (ARQ), based on the *selective repeat* mechanism. Turning to the system architecture, PRIME is forming subnetworks, where each subnetwork has one *Base Node* and several *Service Nodes*. The base node is the "master" that manages the subnetwork's resources and connections using a periodically sent *beacon* signal. The base node is further responsible for PLC channel access arbitration. A contention free and a contention-based access mechanism exists, whose usage time and duration are decided by the base node. Within the contention-free *time division multiplex* (TDM) channel access period, the base node assigns the channel to only one node at a time. The contention-based access uses CSMA/CA [88, 92]. To assure *privacy*, *authentication*, and *data integrity* a *Security Profile 1* is defined, that uses 128-bit AES encryption [93]. The specification also defines a *Security Profile 0* equivalent to no encryption and leaves room for the definition of two further security profiles in future releases. To interface MAC and *application layer*, PRIME defines a *convergence layer* (CL) between the two. The CL can be split into a *Common Part Convergence Sublayer* (CPCS) and a *Service Specific Convergence Sublayer* (SSCS). The CPCS performs tasks of data segmentation and reassembling and is adjusted to the specific application. Three SSCSs are currently defined: the "*NULL Convergence Sublayer* provides the MAC layer with a transparent way to the application, being as simple as possible and minimizing the overhead. It is intended for applications that do not need any special convergence capability." "The *IPv4 Convergence Layer* provides an efficient method for transferring IPv4 packets over the PRIME network." Finally, the *IEC 61334-4-32 Convergence Layer* "supports the same primitives as the IEC 61334-4-32 standard" [94], making it easy, for example, to support advanced metering applications that make use of the standardised data models of IEC 62056-62 [95]. PRIME could therefore also be used to replace the aging PHY and MAC layer of the single carrier power line standard IEC 61334-5-1 [96], also known as S-FSK, for *spread frequency shift keying*.

5.2. G3-PLC. The other OFDM-based HDR NB-PLC specification, G3-PLC [97–99] was published in August 2009. It can be configured to operate in the internationally accepted bands from 10 kHz to 490 kHz (FCC, CENELEC, and ARIB). Using differential BPSK, QPSK, and 8PSK for constellation mapping and concatenated convolutional Reed-Solomon forward error correction coding, it reaches PHY peak data rates close to 300 kbit/s. Peak and typical data rates for various frequency bands have been reported in [100] and are, for convenience, also listed in Table 4. The MAC layer is based on IEEE 802.15.4-2006 [101]. 6LoWPAN [102] is used to adapt the IEEE 802.15.4-2006 MAC to IPv6 [103]. This allows the application layer to comply with ANSI C12.19/C12.22 [104] or IEC 62056-61/62 (DLMS/COSEM) [105, 106] to run standard Internet services.

A comparison between PRIME and G3-PLC, mainly focusing on physical layer aspects is presented in [107]. There it is found that G3-PLC is slightly more robust when disturbed by AWGN and narrowband interference, while PRIME is the less complex system, which could allow cheaper implementations.

5.3. IEEE 1901.2 and ITU-T G.hnem. The specifications PRIME and G3-PLC form the baseline in the ongoing NB-PLC standardization processes within IEEE 1901.2 [108]. Compliant devices are supposed to support interoperability modes with PRIME and G3-PLC in the CENELEC A band

Table 4: G3-PLC data rates, based on [100].

Frequency band	Peak rate, [kbit/s]	Typical rate, [kbit/s]
CENELEC (36 kHz to 91 kHz)	46	44
FCC (150 kHz to 487.5 kHz)	234	187
FCC (10 kHz to 487.5 kHz)	298	225

and have as minimum a requirement to implement one of the PHY/MACs referred to as *Main 1901.2*, *G3 CENELEC A*, and *PRIME CENELEC A* [109]. G3-PLC and PRIME have also been approved as ITU recommendations G.9903 [89] and G.9904 [90], respectively in October 2012. Together with ITU G.9901 [110] and ITU G.9902 [111] they now supersede what was formally ITU G.9955/G9956. ITU G.hnem development is oriented on Smart Grid use cases, like support of *pricing awareness*, *load control*, and *demand response*, and it has been agreed to meet the requirements set forth by NIST PAP15.

There are still some open issues, for example, with respect to ITU G.hnem IEEE 1901.2 coexistence. Implementers that cannot wait might consider that due to relatively low signal processing complexity, NB-PLC modems can be implemented on a *digital signal processor* (DSP). This allows for upgradeability via software updates and can especially be an advantage for early stage customer premises deployments where a hardware update would be prohibitively expensive. An upgradeable DSP solution that supports PRIME as well as G3-PLC is, for example, offered by Texas Instruments [112].

6. Broadband PLC

In the last decade, BB-PLC chips by semiconductor vendors, such as Intellon (in 2009 acquired by Atheros, Atheros in 2011 acquired by Qualcomm) [113], DS2 (in 2010 acquired by Marvell) [114], Gigle (in 2010 acquired by Broadcom) [115], and Panasonic [116], came to market that operate in the band from around 1 MHz to 300 MHz. The chips are mainly based on three consortia backed specifications developed within the frameworks of the *HomePlug Powerline Alliance* (HomePlug) [117], the *Universal Powerline Association* (UPA) [118], and the *High Definition Power Line Communication* (HD-PLC) Alliance [119]. Related products allow data rates around 200 Mbit/s and are not interoperable. However, to make PLC systems a broad success, an internationally adopted BP-PLC standard became essential. The *International Telecommunications Union* (ITU) as well as the *Institute of Electrical and Electronics Engineers* (IEEE) commenced work on such next generation standards, namely, *ITU-T G.hn* and *IEEE 1901*. ITU-T G.hn is not only applicable to power lines, but also to phone lines and coaxial cables, therewith for the first time defining a single standard for all major wireline communications media. At the end of 2008, the PHY layer and the overall architecture were consented in ITU-T Recommendation G.9960 [120]. The *Data Link Layer* (DLL) Recommendation G.9961 [121] was approved in June 2010, and a MIMO transceiver extension G.9963 was consented in September 2011 [122]. Alongside, the *HomeGrid Forum* was founded to promote the ITU-T G.hn standard and to address certification and interoperability issues [123]. Simultaneously, IEEE P1901 [124] was working on the "*Draft Standard for Broadband over Power Line Networks: Medium Access Control and Physical Layer Specifications*" [125]. It covers the aspects Access, In-Home, and coexistence of Access-In-Home and In-Home-In-Home networks, and the official IEEE Std 1901–2010 was published on December, 30, 2010, with the HomePlug Powerline Alliance [117] being a certifying body for IEEE 1901 compliant products. In analogy to the introduction of MIMO to ITU G.hn, the HomePlug Alliance introduced the HomePlug AV2 specification in January 2012. The HomePlug AV2 specification includes features like MIMO with beamforming, an extended frequency range of up to 86 MHz, efficient notching, several transmit power optimization techniques, 4096-QAM, power save modes, short delimiter, and delayed acknowledgement, boosting the maximum PHY rate to around 2 Gbit/s. Further, to cover multiple home networking media under one umbrella, IEEE P1905.1 is working on a standard for a convergent digital home network for heterogeneous technologies [126]. It defines an abstraction layer for multiple home networking technologies like IEEE 1901, IEEE 802.11 (Wi-Fi), IEEE 802.3 (Ethernet), and MoCA 1.1 and is extendable to work with other home networking technologies.

6.1. IEEE 1901 and ITU-T G.hn. IEEE 1901 uses the band from 2 MHz up to 50 MHz with services above 30 MHz being optional. ITU-T G.hn (G.9960/G.9961) operates from 2 MHz up to 100 MHz using bandwidth scalability, with three distinct and interoperable bands defined as 2–25, 2–50, and 2–100 MHz. The architectures defined by IEEE 1901 and ITU-T G.hn (G.9960/G.9961) are similar in several aspects. In G.hn one refers to a subnetwork as *Domain*. Operation, as well as communication is organized by the *Domain Master* who communicates with various *Nodes*. Similarly, the subnetwork in 1901 is referred to as *Basic Service Set* (BSS). The equivalent to the domain master is the *BSS Manager*, which connects to so-called *Stations*. These basic network components with their system specific terminology are summarized in Table 5.

While the general concepts are similar, one should note that G.hn defines a PHY/DLL used for operation over any wireline medium. Primarily, the OFDM parameters are adjusted to account for different medium-dependent channel and noise characteristics. On the contrary, IEEE 1901 defines two disparate PHY/MAC technologies based on HomePlug AV and HD-PLC. One of the key differences is their frequency division-multiplexing scheme. The HomePlug AV-based version uses the *Fast Fourier Transform* (FFT), while the HD-PLC based version uses Wavelets. Hence, they are sometimes also referred to as FFT-PHY and Wavelet-PHY, respectively. A special coexistence mechanism has to be used when operating IEEE 1901 devices from both PHYs on the same power line which is standardized within IEEE 1901 as *Inter-System Protocol* (ISP) (see also [127] or [128]). A nearly identical mechanism was standardized by ITU-T in G.9972 [129], also known as G.cx. Technical contributions to ITU, and IEEE from members of the NIST PAP15 assured the alignment of both standards. As a result, it is likely that the

Table 5: Synopsis of terms used in the BB-PLC standards ITU-T G.hn and IEEE 1901 [75] © 2012 John Wiley & Sons.

Network item	ITU-T G.hn	IEEE P1901
Sub-network	Domain	*Basic Service Set (BSS)*
Transceiver	Node	*Station (STA)*
Sub-network controller	Domain Master	BSS Manager
Access control schedule	*Media Access Plan (MAP)*	Beacon
Timeframe	MAC cycle	Beacon Interval
Access methods	CSMA/CA, TDMA, STXOP (*shared transmission opportunities*)	CSMA/CA, TDMA
Relaying	Relay (L2)	Repeater (L2)
Network controller	Relay (assigned	Proxy BSS
proxy	as a proxy)	Manager
Transceiver	Hidden	Hidden
(not directly reached)	Node	Station

NIST SGIP will mandate that all BB-PLC technologies implement Recommendation ITU-T G.9972 or ISP [130]. ISP/G.cx provides coexistence by splitting time equally among systems present on the line. IEEE 1901 additionally specifies the optional *Coexistence Protocol* (CXP), that provides coexistence among multiple technologies based on a first-come-first-serve basis.

The coexistence mechanism is thought for the case where disparate networks would otherwise be interfering with each other. Another likely scenario is that same technology networks exist in close proximity, with the risk of so-called *neighboring network* interference. To deal with neighboring network interference G.hn uses different preamble-symbol seeds in each network. Therewith, G.hn networks are able to coexist and communicate simultaneously, that is, not using time division. Instead, link adaptation procedures adjust the throughput to cope with degraded *signal to interference plus noise ratios* (SINR). In many cases the throughput will be throttled only slightly allowing G.hn networks to coexist nearly unimpeded. On the other hand, IEEE 1901 relies on a CSMA/CA medium access strategy, which may lead to an increased number of collisions. As countermeasure, IEEE 1901 introduces a *coordinated mode* that allows neighboring networks to allocate times over the shared medium for specific communications. This coordinated *time division multiple access* (TDMA) mode enables traffic to get through unimpeded albeit at the price of time division (orthogonal throughput sharing).

6.2. ITU-T G.hn Low Complexity Profile. It is envisioned that G.hn nodes are in the future embedded into *Smart Grid home* (SGH) *area network* devices. SGH nodes will typically make use of the G.hn *low complexity profile* (LCP), operating in the frequency range 2–25 MHz. This allows for reduced component cost and power consumption. Example SGH nodes could be heating and air conditioning appliances, Plug-in Electric Vehicles (PEV), and Electric Vehicle Service Equipments (EVSEs) as indicated in Figures 1 and 5. Together they form a multi-domain HAN.

The SGHs interact with the *utility's access network* (UAN) and its *advanced metering infrastructure* (AMI) through an *energy service interface* (ESI). The AMI domain comprises *AMI Meters* (AM), *AMI Submeters* (ASM), and an AMI *Head End* (HE). The HE is a local hub (concentrator), that controls all meters downstream from it and interfaces to the utility's wide area/backhaul network upstream from it. Each AMI HE supports up to 250 AM and/or ASM nodes forming an AMI domain (in dense urban areas 150 to 200 meters are a frequently encountered maximum). Further, a network supports up to 16 AMI domains, delivering support for up to $16 \cdot 250 = 4000$ AMI devices. The ability to support 16 domains with 250 nodes each is a general property of G.hn not limited to Smart Grid/AMI applications. Domains may be formed over any kind of wiring. The nodes within a domain are grouped into SGH and non-SG nodes. For security reasons, non-SG nodes are logically separated from SGH nodes using a secure upper-layer protocol.

In every domain there is a domain master that coordinates operation of all nodes. G.hn nodes of different domains communicate with each other via *Interdomain Bridges* (IDBs). IDBs are simple data communications bridges on OSI Layer 3 and above, enabling a node in one domain to pass data to a node in another domain. In a multi-domain situation, a *Global Master* (GM) provides coordination of resources, priorities, and operational characteristics between G.hn domains. Besides, G.hn domains can be bridged to alien (non-G.hn) domains, for example, to IEEE 1901/1901.2, wireless technologies, and so forth. For example, besides the UAN/AMI connection through the ESI, the HAN might be connected to the outside world via a DSL or cable modem gateway communicating with the G.hn HAN via an alien domain bridge.

6.3. HomePlug Green PHY. In analogy to the ITU G.hn *low complexity profile* (LCP), the HomePlug Powerline Alliance has released the HomePlug Green PHY specification. HomePlug GreenPhy is a subset of HomePlug AV that is intended for use within Smart Grid applications. It is compatible to HomePlug AV, AV2, and IEEE 1901 and is optimized for low power applications and costs. GreenPhy uses the most robust communication mode (called ROBO) of HomePlug AV technology. OFDM carrier spacing, signal preamble, frame control, and FEC are identical to HomePlug AV to ensure interoperability. This also results in identical coverage and reliability to Smart Grid functions. CSMA/CA is used as channel access scheme. Data rates are up to 10 Mbit/s. GreenPhy nodes may use long power save periods if a higher latency is acceptable. In the sleep state modems have only a 3% power consumption compared to the awake time resulting in an average power reduction of more than 90% with respect to standard HomePlug AV products.

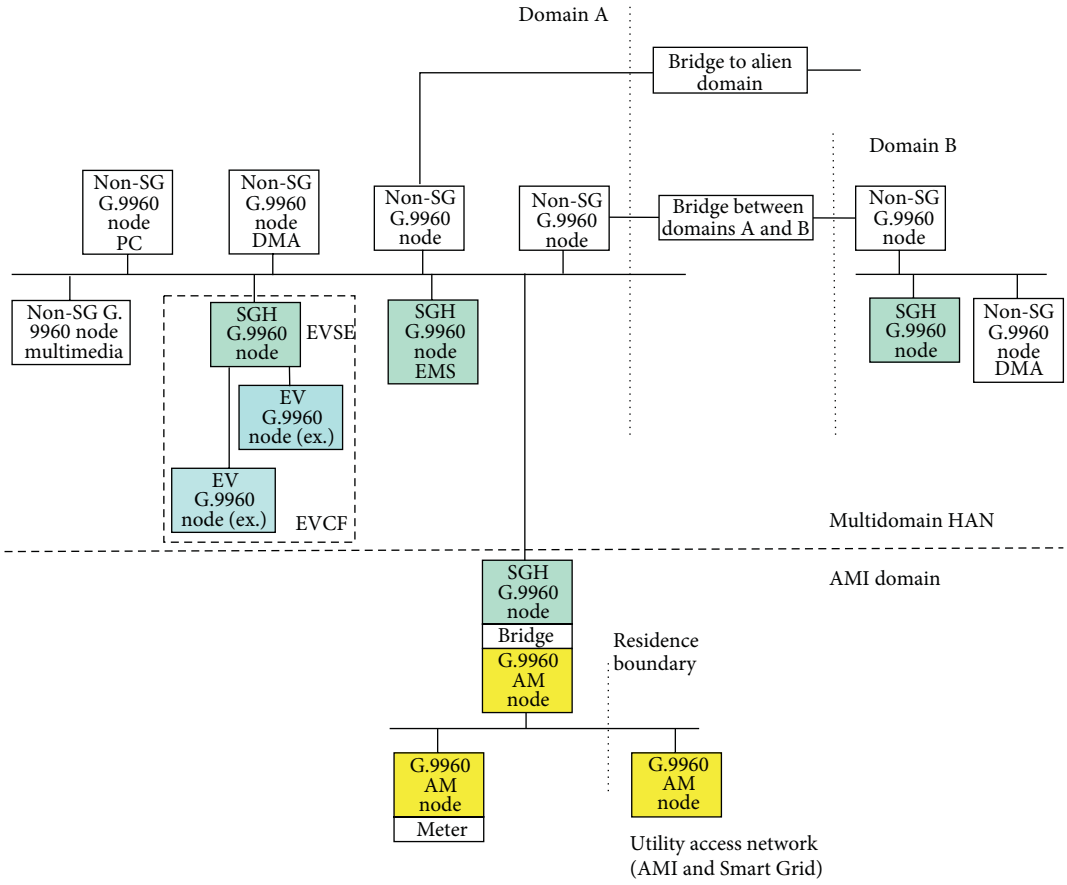

Figure 5: Smart Grid HAN implementation based on G.9960, based on Figure 22 in [138].

7. Application Layer Interoperability

Although there is still an ongoing struggle between stakeholders promoting the various NB-PLC and BB-PLC technologies, it seems clear that IP support will become paramount to assure Smart Grid interoperability. Along these lines, the *HomePlug Alliance* (promoting IEEE P1901) and the *HomeGrid Forum* (promoting ITU G.hn/G.hnem) have joint forces with wireless stakeholders, namely, the *Wi-Fi Alliance* and the *ZigBee Alliance*. Together they formed the *Consortium for Smart Energy Profile 2 (SEP2) Interoperability* with the intention "to develop common testing documents and processes for certifying SEP 2 interoperability" [131].

Smart Energy Profile 2 (SEP2) originates from smart energy-related upper-layer developments (OSI layer 5 to 7) within the ZigBee Alliance [132]. It is compatible to the International Electrotechnical Commission's *Common Information Model* (CIM) [133, 134] and is kept link layer agnostic. Further, it is described using *extensible markup language* (XML) [135] and follows a *Representational State Transfer* (REST) [136] architecture. Moreover, data transport takes place using *Hypertext Transfer Protocol* (HTTP) [137].

By opting for these widely adopted building blocks, SEP 2 can benefit from a large knowledge and developer base and is regarded by NIST as an import specification to allow interoperability between various home area network devices [13].

8. Conclusions

Although there are strong wireless and wireline communication competitors, it is believed that *power line communications* (PLCs) will fulfill various communication tasks in upcoming Smart Grid deployments as PLC provides the natural upgrade from simple electricity conductors to hybrid and bidirectional electricity and data communication solutions.

Seen from a utility point of view, one of the main advantages of PLC is the full control over the physical medium, without the need to depend on third party providers like telecommunication companies or cellular operators. Especially, PLC standardization and harmonization as, for example, fostered by NIST PAP15, are important for the PLC industry as a whole when defending territory against competing wireless and wireline options.

In terms of *broadband PLC* (BB-PLC), the coexisting standards ITU-T G.hn and IEEE P1901 with the expanded HomePlug AV2 specification are currently the most promising, while *narrowband PLC* (NB-PLC) standardization, that is, IEEE P1901.2 and ITU-T G.hnem, is still ongoing.

Cases where NB-PLC and BB-PLC systems operate on the same physical medium will become more frequent with increasing PLC system penetration. Nevertheless, coexistence of the two should be straight forward as they are using different frequency ranges. In general, interconnections between different coexisting NB-PLC and BB-PLC standards

can then be established by OSI Layer 3 bridges as suggested, for example, in [108, 138].

When looking at higher layer interoperability, the recent foundation of the Consortium for Smart Energy Profile 2 Interoperability, is a promising step forward to allow users and operators to deploy various wireless and wireline technologies with seamless interoperability at the application layer which is regarded as essential for widespread Smart Grid acceptance.

Acknowledgments

Although this article is distributed under the Creative Commons Attribution License, it should be noted that it is in parts based on [70, 75]. The material from [70] and [75] is reproduced with explicit permission of John Wiley & Sons, Ltd. and John Wiley & Sons, Inc., respectively. However, related copyrights and the right to grant reprint permissions of the affected parts remain with John Wiley & Sons. This work is cofinanced by the Spanish Ministry of Science and Innovation (MICINN) Program INNCORPORA-Torres Quevedo 2011, and Grant SICCNALS, TEC2011-28219. Further it is cofunded by the European Social Fund and the European Regional Development Fund within the ERDF Operational Programme of the Valencian Community 2007–2013, grant no. IMIDTA/2011/905. Special thanks also to the BreezeSolve Team for editorial support.

References

[1] B. A. Hamilton, J. Miller, and B. Renz, "Understanding the benefits of smart grid," Tech. Rep. DOE/NETL-2010/1413, U.S. Department of Energy, 2010.

[2] L. T. Berger and K. Iniewski, *Smart Grid—Applicacions, Communications and Security*, John Wiley & Sons, 2012.

[3] M. Burns, "NIST SGIP catalog of standards," October 2010, http://collaborate.nist.gov/twiki-sggrid/bin/view/SmartGridSGIPCatalogOfStandards.

[4] P. A. Brown, "Power line communications—past present and future," in *Proceedings of the International Symposium on Power Line Communicatons and Its Applications (ISPLC '99)*, pp. 1–8, September 1999.

[5] S. Galli, A. Scaglione, and Z. Wang, "For the grid and through the grid: the role of power line communications in the smart grid," *Proceedings of the IEEE*, vol. 99, no. 6, pp. 998–1027, 2011.

[6] The OPEN meter Consortium, "Description of current state-of-the-art of technology and protocols description of state-of-the-art of PLC-based access technology," European Union Project Deliverable FP7-ICT-2226369, d 2.1 Part 2, Version 2.3, March 2009, http://www.openmeter.com/files/deliverables/OPEN-Meter%20WP2%20D2.1%20part2%20v2.3.pdf.

[7] IEEE Communication Society, "Best readings in power line communications," http://www.comsoc.org/best-readings.

[8] SMB Smart Grid Strategic Group (SG3), "IEC smart grid standardization roadmap," June 2010, http://www.iec.ch/smartgrid/downloads/sg3_roadmap.pdf.

[9] ITU Telecommunication Standardization Bureau Policy & Technology Watch Division, "Activities in smart grid standardization repository," version 1.0., April 2010, http://www.itu.int/dmspub/itu-t/oth/48/01/T48010000020002PDFE.pdf.

[10] DKE German Commission for Electrical, Electronic & Information Technologies of DIN and VDE, "The German roadmap e-energy/smart grid," April 2010, http://www.e-energy.de/documents/DKE%20Roadmap%20SmartGrid%20230410%20Englllish.pdf.

[11] State Grid Corporation of China, "SGCC framework and roadmap for strong and smart grid standards," August 2010, http://collaborate.nist.gov/twiki-sggrid/pub/SmartGrid/SGIPDocumentsAndReferencesSGAC/China_State_Grid_Framework_and_Roadmap_for_SG_Standards.pdf.

[12] International Energy Agency, "Technology roadmap smart grids," April 2011, http://www.iea.org/publications/freepublications/publication/smartgrids_roadmap.pdf.

[13] National Institute of Standards and Technology (NIST) and U.S. Department of Commerce, "NIST framework and roadmap for smart grid interoperability standards," NIST Draft Publication, Release 1. 0, January 2010.

[14] K. Dostert, *Powerline Communications*, Prentice-Hall, 2001.

[15] G. Held, *Understanding Broadband Over Power Line*, CRC Press, 2006.

[16] P. Sobotka, R. Taylor, and K. Iniewski, "Broadband over power line communications: Home networking, broadband access, and smart power grids," in *Internet Networks: Wired, Wireless, and Optical Technologies*, K. Iniewski, Ed., Devices, Circuits, and Systems, chapter 8, CRC Press, New York, NY, USA, 2009.

[17] R. Pighi and R. Raheli, "On multicarrier signal transmission for high-voltage power lines," in *Proceedings of the 9th International Symposium on Power Line Communications and Its Applications (ISPLC '05)*, pp. 32–36, Vancouver, Canada, April 2005.

[18] H. Duckhwa and L. Younghun, "A study on the compound communication network over the high voltage power line for distribution automation system," in *Proceedings of the 2nd International Conference on Information Security and Assurance (ISA '08)*, pp. 410–414, Busan, Korea, April 2008.

[19] R. Aquilu, I. G. J. Pijoan, and G. Sanchez, "Highvoltage multicarrier spread-spectrum system field test," *IEEE Transactions on Power Delelivery*, vol. 24, no. 3, pp. 1112–1121, 2009.

[20] N. Strandberg and N. Sadan, "HV-BPL phase 2 field test report," Tech. Rep. DOE/NETL-2009/1388, U.S. Department of Energy, 2009.

[21] P. A. A. F. Wouters, P. C. J. M. van der Wielen, J. Veen, P. Wagenaars, and E. F. Wagenaars, "Effect of cable load impedance on coupling schemes for MV power line communication," *IEEE Transactions on Power Delivery*, vol. 20, no. 2, pp. 638–645, 2005.

[22] R. Benato and R. Caldon, "Application of PLC for the control and the protection of future distribution networks," in *Proceedings of the IEEE International Symposium on Power Line Communications and Its Applications (ISPLC '07)*, pp. 499–504, Pisa, Italy, March 2007.

[23] A. Cataliotti, A. Daidone, and G. Tinè, "Power line communication in medium voltage systems: characterization of MV cables," *IEEE Transactions on Power Delivery*, vol. 23, no. 4, pp. 1896–1902, 2008.

[24] P. Meier, M. Bittner, H. Widmer et al., "Pathloss as a function of frequency, distance and network topology for various LV and MV European powerline networks," The OPERA Consortium, Project Deliverable, EC/IST FP6 Project no. 507667 D5v0.9, April 2005.

[25] A. Rubinstein, F. Rachidi, M. Rubinstein et al., "EMC guidelines," The OPERA Consortium, IST Integrated Project Deliverable D9v1. 1, IST Integrated Project No 026920, October 2008.

[26] A. Vukicevic, *Electromagnetic compatibility of power line communication systems [Ph.D. thesis]*, École Polytechnique Fédérale de Lausanne, Lausanne, Switzerland, 2008.

[27] Broadband Forum, "Next generation broadband access," White Paper MR-185, Issue: 1, August 2009, http://www.broadband-forum.org/marketing/download.

[28] D. E. Nordell, "Communication systems for distribution automation," in *Proceedings of the IEEE Transmission and Distribution Conference and Exposition*, Bogota, Colombia, April 2008.

[29] S. Mak and D. Reed, "TWACS, a new viable twoway automatic communication system for distribution networks. Part I: outbound communication," *IEEE Transactions on Power Apparatus and Systems*, vol. 101, no. 8, pp. 2941–2949, 1982.

[30] S. Mak and T. Moore, "TWACS, a new viable twoway automatic communication system for distribution networks. Part II: inbound communication," *IEEE Transactions on Power Apparatus and Systems*, vol. 103, no. 8, pp. 2141–2147, 1984.

[31] The OPEN meter Consortium, "Open Public Extended Network Metering, Home page," http://www.openmeter.com/.

[32] PRIME Alliance, "Powerline related intelligent metering evolution (PRIME)," http://www.prime-alliance.org,.

[33] Électricité Réseau Distribution France, "G3-plc: Open standard for smart grid implementation," http://www.maximintegrated.com/products/powerline/g3-plc/.

[34] K. Razazian, M. Umari, A. Kamalizad, V. Loginov, and M. Navid, "G3-PLC specification for powerline communication: Overview, system simulation and field trial results," in *Proceedings of the 14th Annual International Symposium on Power Line Communications and its Applications (ISPLC '10)*, pp. 313–318, Rio de Janeiro, Brazil, March 2010.

[35] P. Siohan, A. Zeddam, G. Avril et al., "State of the art, application scenario and specific requirements for PLC," OMEGA, European Union Project Deliverable D3.1 v1.0, IST Integrated Project No ICT-213311, 2008, http://www.ict-omega.eu/publications/deliverables.html.

[36] G. Wood and M. Newborough, "Dynamic energy-consumption indicators for domestic appliances: environment, behaviour and design," *Energy and Buildings*, vol. 35, no. 8, pp. 821–841, 2003.

[37] International Organization for Standartization, "Building automation and control systems—part 5: data communication protocol," international standard ISO 16484-5, 2010.

[38] International Organization for Standartization, "Information technology—Home electronic system (HES) architecture—part 3–5: Media and media dependent layers Powerline for network based control of HES class 1," international standard ISO/IEC 14543-3-5, First edition, May 2007.

[39] International Organization for Standartization, "Interconnection of information technology equipment—Control network protocol—Part 3: Power line channel specification," international standard ISO/IEC 14908-3, Rvision 11, January 2011.

[40] American National Standards Institute/Electronic Industries Association (ANSI/EIA), "Control network power line (PL) channel specification," ANSI/CEA-709.2-A, September 2006.

[41] L. T. Berger and G. Moreno-Rodríguez, "Power line communication channel modelling through concatenated IIR-filter elements," *Academy Publisher Journal of Communications*, vol. 4, no. 1, pp. 41–51, 2009.

[42] S. Galli, "A simplified model for the indoor power line channel," in *Proceedings of the IEEE International Symposium on Power Line Communications and its Applications (ISPLC '09)*, pp. 13–19, Dresden, Germany, April 2009.

[43] F. J. Cañete Corripio, L. Díez del Río, and J. T. Entrambasaguas Muñoz, "A time variant model for indoor power-line channels," in *Proceedings of the International Symposium on Power Line Communications (ISPLC '01)*, pp. 85–90, Malmö, Sweden, March 2001.

[44] F. J. Cañete, L. Díez, J. A. Cortñs, and J. T. Entrambasaguas, "Broadband modelling of indoor powerline channels," *IEEE Transactions on Consumer Electronics*, vol. 48, no. 1, pp. 175–183, 2002.

[45] J. A. Cortñs, F. J. Cañete, L. Díez, and J. T. Entrambasaguas, "Characterization of the cyclic short-time variation of indoor power-line channels response," in *Proceedings of the International Symposium on Power Line Communications and Its Applications (ISPLC '05)*, pp. 326–330, Vancouver, Canada, April 2005.

[46] F. J. Cañete Corripio, J. A. Cortñs Arrabal, L. Díez del Río, and J. T. Entrambasaguas Muñoz, "Analysis of the cyclic short-term variation of indoor power line channels," *IEEE Journal on Selected Areas in Communications*, vol. 24, no. 7, pp. 1327–1338, 2006.

[47] M. Zimmermann and K. Dostert, "A multipath model for the powerline channel," *IEEE Transactions on Communications*, vol. 50, no. 4, pp. 553–559, 2002.

[48] M. Babic, M. Hagenau, K. Dostert, and J. Bausch, "Theoretical postulation of PLC channel model," The OPERA Consortium, IST Integrated Project Deliverable D4v2.0, March 2005.

[49] H. Liu, J. Song, B. Zhao, and X. Li, "Channel study for medium-voltage power networks," in *Proceedings of the IEEE International Symposium on Power Line Communications (ISPLC '06)*, pp. 245–250, Orlando, Fla, USA, March 2006.

[50] European Telecommunication Standards Institute (ETSI), "Powerline Telecommunications (PLT); MIMO PLT; Part 1: Measurement Methods of MIMO PLT," February 2012.

[51] C. R. Paul, *Analysis Of Multiconductor Transmission Lines*, John Wiley & Sons, 1994.

[52] T. Magesacher, P. Ödling, P. O. Börjesson et al., "On the capacity of the copper cable channel using the common mode," in *Proceedings of the IEEE Global Telecommunications Conference*, pp. 1269–1273, November 2002.

[53] T. Sartenaer, *Multiuser communications over frequency selective wired channels and applications to the powerline access network [Ph.D. thesis]*, Faculty of Applied Sciences of the Université Catholique de Louvain, Louvain-la-Neuve, Belgium, 2004.

[54] D. Sabolic, A. Bazant, and R. Malaric, "Signal propagation modeling in power-line communication networks," *IEEE Transactions on Power Delivery*, vol. 20, no. 4, pp. 2429–2436, 2005.

[55] T. Banwell and S. Galli, "A novel approach to the modeling of the indoor power line channel part I: circuit analysis and companion model," *IEEE Transactions on Power Delivery*, vol. 20, no. 2, pp. 655–663, 2005.

[56] S. Galli and T. Banwell, "A novel approach to the modeling of the indoor power line channel—part II: transfer function and its properties," *IEEE Transactions on Power Delivery*, vol. 20, no. 3, pp. 1869–1878, 2005.

[57] T. Magesacher, P. Ödling, P. O. Börjesson, and S. Shamai, "Information rate bounds in common-mode aided wireline communications," *European Transactions on Telecommunications*, vol. 17, pp. 533–545, 2006.

[58] R. Hashmat, P. Pagani, A. Zeddam, and T. Chonave, "MIMO communications for inhome PLC Networks: Measurements and results up to 100 MHz," in *Proceedings of the 14th Annual International Symposium on Power Line Communications and its Applications (ISPLC '10)*, pp. 120–124, Rio de Janeiro, Brasil, March 2010.

[59] R. Hashmat, P. Pagani, A. Zeddam, and T. Chonave, "A channel model for multiple input multiple output in-home power line networks," in *Proceedings of the IEEE International Symposium on Power Line Communications and Its Applications (ISPLC '11)*, pp. 35–41, April 2011.

[60] F. Versolatto and A. M. Tonello, "A MIMO PLC random channel generator and capacity analysis," in *Proceedings of the IEEE International Symposium on Power Line Communications and Its Applications (ISPLC '11)*, pp. 66–71, Udine, Italy, April 2011.

[61] L. T. Berger, A. Schwager, P. Pagani, and D. Schneider, *MIMO Power Line Communications: Narrow and Broadband Standards, EMC, and Advanced Processing*, CRC Press, 2013.

[62] A. Schwager, W. Bäschlin, J. Moreno et al., "European MIMO PLC field measurements: overview of the ETSI STF410 campaign & EMI analysis," in *Proceedings of the International Symposium on Power Line Communications and Its Applications (ISPLC '12)*, Beijing, China, 2012.

[63] D. Schneider, A. Schwager, W. Baschlin, and P. Pagani, "European MIMO PLC field measurements: channel analysis," in *Proceedings of the 16th IEEE International Symposium on Power Line Communications and Its Applications (ISPLC '12)*, pp. 304–309, March 2012.

[64] A. Schwager, *Powerline communications: significant technologies to become ready for integration [Ph.D. thesis]*, Universität Duisburg-Essen, Fakultät für Ingenieurwissenschaften, Duisburg-Essen, Germany, 2010.

[65] A. Schwager, D. Schneider, W. Baschlin, A. Dilly, and J. Speidel, "MIMO PLC: theory, measurements and system setup," in *IEEE International Symposium on Power Line Communications and Its Applications (ISPLC '11)*, pp. 48–53, April 2011.

[66] M. Zimmermann and K. Dostert, "An analysis of the broadband noise scenario in power-line networks," in *Proceedings of the International Symposium on Power Line Communications and Its Applications (ISPLC '00)*, pp. 131–138, Limerick, Ireland, April 2000.

[67] F. J. Cañete, J. A. Cortñs, L. Díez, and J. T. Entrambasaguas, "Modeling and evaluation of the indoor power line transmission medium," *IEEE Communications Magazine*, vol. 41, no. 4, pp. 41–47, 2003.

[68] R. Hashmat, P. Pagani, A. Zeddam, and T. Chonavel, "Measurement and analysis of inhome MIMO PLC channel noise," in *Proceedings of the 4th Workshop on Power Line Communications*, Boppard, Germany, September 2010.

[69] P. Pagani, R. Hashmat, A. Schwager, D. Schneider, and W. Baschlin, "European mimo plc field measurements: noise analysis," in *Proceedings of the 16th IEEE International Symposium on Power Line Communications and Its Applications (ISPLC '12)*, pp. 310–315, March 2012.

[70] L. T. Berger, "Broadband powerline communications," in *Convergence of Mobile and Stationary Next Generation Networks*, K. Iniewski, Ed., chapter 10, pp. 289–316, John Wiley & Sons, Hoboken, NJ, USA, 2010.

[71] A. Schwager, L. Stadelmeier, and M. Zumkeller, "Potential of broadband power line home networking," in *Proceedings of the 2nd IEEE Consumer Communications and Networking Conference (CCNC '05)*, pp. 359–363, January 2005.

[72] M. Tlich, P. Pagani, G. Avril et al., "PLC channel characterization and modelling," OMEGA, European Union Project Deliverable D3.3 v1.0, IST Integrated Project No ICT-213311, December 2008, http://www.ict-omega.eu/publications/deliverables.html.

[73] European Committee for Electrotechnical Standardization (CENELEC), "Signalling on low-voltage electrical installations in the frequency range 3 kHz to 148,5 kHz - Part 1: General requirements, frequency bands and electromagnetic disturbances," Standard EN 50065-1, September 2010.

[74] National Institute of Standards and Technology (NIST), "Priority Action Plan 15 (PAP15): Harmonize Power Line Carrier Standards for Appliance Communications in the Home," Coexistence of narrow band power line communication technologies in the unlicensed FCC band, April 2010, http://www.fcc.gov/encyclopedia/rules-regulations-title-47.

[75] L. T. Berger, "Wireline communications in smart grids," in *Smart Grid—Applicacions, Communications and Security*, L. T. Berger and K. Iniewski, Eds., chapter 7, John Wiley & Sons, Hoboken, NJ, USA, 2012.

[76] FCC, "Title 47 of the code of federal regulations (CFR)," Tech. Rep. 47 CFR §15, Federal Communications Commission, 2008, http://www.fcc.gov/encyclopedia/rules-regulations-title-47,.

[77] Association of Radio Industries and Businesses (ARIB), "Power line communication equipment (10kHz-450kHz)," sTD-T84, Ver. 1.0, (in Japanese), November 2002, http://www.arib.or.jp/english/html/overview/doc/1-STD-T84v1_0.pdf.

[78] Comité International Spécial des Perturbations Radioélectriques, "Information technology equipment; Radio disturbance characteristics; Limits and methods of measurement," ICS CISPR, International Standard Norme CISPR 22:1997, 1997.

[79] Comité International Spécial des Perturbations Radioélectriques, "Specification for radio disturbance and immunity measuring apparatus and methods part 1-1: Radio disturbance and immunity measuring apparatus—Measuring apparatus," 2003.

[80] Comité International Spécial des Perturbations Radioélectriques, "Amendment to CISPR 22: Clarification of its application to telecommunicationsystem on the method of disturbance measurement at ports used for PLC," 2003.

[81] Comité International Spécial des Perturbations Radioélectriques, "CISPR 22 am3 f1 ed. 5.0, Limits and method of measurement of broadband telecommunication equipment over power lines," February 2008.

[82] Comité International Spécial des Perturbations Radioélectriques, "Report on mitigation factors and methods for power line telecommunications," February 2008.

[83] European Telecommunication Standards Institute (ETSI), "PowerLine Telecommunications (PLT); Coexistence between PLT Modems and Short Wave Radio broadcasting services," August 2008.

[84] Comité International Spécial des Perturbations Radioélectriques, "Amendment 1 to CISPR 22 ed. 6.0: Addition of limits and methods of measurement for conformance testing of power line telecommunication ports intended for the connection to the mains," July 2009.

[85] C. European Committee for Electrotechnical Standardization, "Power line communication apparatus used in low-voltage installations—Radio disturbance characteristics—Limits and methods of measurement—Part 1: Apparatus for in-home use," November 2012.

[86] R. Razafferson, P. Pagani, A. Zeddam et al., "Report on electro magnetic compatibility of power line communications," OMEGA, European Union Project Deliverable D3.3 v3.0, IST Integrated Project No ICT-213311, April 2010, http://www.ict-omega.eu/publications/deliverables.html.

[87] Institute of Electrical and Electronics Engineers, "IEEE standard for power line communication equipment–Electromagnetic compatibility (EMC) requirements–Testing and measurement methods," January 2011.

[88] PRIME Alliance, "Draft standard for PoweRline Intelligent Metering Evolution," 2010, www.prime-alliance.org/Docs/Ref/PRIME-Spec_v1.3.6.pdf.

[89] ITU - Telecommunication Standardization Sector STUDY GROUP 15, "Narrowband orthogonal frequency division multiplexing power line communication transceivers for G3-PLC networks," Recommendation ITU-T G.9903, October 2012, approved.

[90] ITU - Telecommunication Standardization Sector STUDY GROUP 15, "Narrowband orthogonal frequency division multiplexing power line communication transceivers for PRIME networks," Recommendation ITU-T G.9904, October 2012, approved.

[91] NIST Priority Action Plan 15, "Narrowband PLC coexistence requirement," October 2011, http://collaborate.nist.gov/twiki-sggrid/pub/SmartGrid/PAP15PLCForLowBitRates/Requirements_on_NB_PLC_coexistence_Final_Oct_11r1.xls.

[92] I. Berganza, A. Sendin, and J. Arriola, "Prime: powerline intelligent metering evolution," in *Proceedings of the CIRED Seminar 2008: SmartGrids for Distribution*, pp. 1–3, Frankfurt, Germany, June 2008.

[93] National Institute of Standards and Technology (NIST), U.S. Department of Commerce, "Specification for the advanced encryption standard (AES)," Federal Information Processing Standards Publication 197, November 2001.

[94] International Electrotechnical Commission (IEC), "Distribution automation using distribution line carrier systems—Part 4: Data communication protocols—Section 32: Data link layer—Logical link control (LLC)," November 1997.

[95] International Electrotechnical Commission (IEC), "Electricity metering—Data exchange for meter reading, tariff and load control—Part 62: Interface classes," Standard IEC 62056-62, 2nd ed., November 2006.

[96] International Electrotechnical Commission (IEC), "Distribution automation using distribution line carrier systems—Part 5-1: Lower layer profiles—The spread frequency shift keying (S-FSK) profile," Standard IEC 61334-5-1, 2nd ed., 2001.

[97] Electricité Réseau Distribution France (ERDF), "G3-PLC physical layer specification," August 2009, http://www.maximintegrated.com/products/powerline/pdfs/G3-PLC-Physical-Layer-Specification.pdf.

[98] Electricité Réseau Distribution France (ERDF), "G3-PLC MAC layer specification," August 2009, http://www.maximintegrated.com/products/powerline/pdfs/G3-PLC-MAC-Layer-Specification.pdf.

[99] Electricité Réseau Distribution France (ERDF), "G3-PLC profile specification," August 2009, http://www.maximintegrated.com/products/powerline/pdfs/G3-PLC-Profile-Specification.pdf.

[100] K. Razazian, "G3-PLC provides an ideal communication platform for the smart gird," in *Proceedings of the IEEE Internatinal Symposium on Power Line Communications and Its Applications (ISPLC '10)*, Rio de Janeiro, Brazil, March 2010.

[101] Institute of Electrical and Electronics Engineers, "Local and metropolitan area networks—Specific requirements part 15.4: Wireless medium access control (MAC) and physical layer (PHY) specifications for low-rate wireless personal area networks (WPANs)," standard for Information Technology—Telecommunications and Information Exchange Between Systems, September 2006.

[102] Z. Shelby and C. Bormann, *6LoWPAN: The Wireless Embedded Internet*, John Wiley & Sons, 2009.

[103] S. Deering and R. Hinden, "Internet protocol, version 6 (IPv6) specification," RFC 2460, December 1998, http://tools.ietf.org/html/rfc2460.

[104] American National Standards Institute (ANSI), "Utility industry end device data tables," ANSI Standard C12.19, 2008.

[105] International Electrotechnical Commission (IEC), "Electricity metering—Data exchange for meter reading, tariff and load control—Part 61: Object identification system (OBIS)," international standard IEC 62056-61, second edition, November 2006.

[106] International Electrotechnical Commission (IEC), "Electricity metering—Data exchange for meter reading, tariff and load control—Part 62: Interface classes," international standard IEC 62056-62, second edition, November 2006.

[107] M. Hoch, "Comparison of PLC G3 and PRIME," in *Proceedings of the IEEE International Symposium on Power Line Communications and Its Applications (ISPLC '11)*, pp. 165–169, Udine, Italy, April 2011.

[108] V. Oksman and J. Zhang, "G.HNEM: the new ITU-T standard on narrowband PLC technology," *IEEE Communications Magazine*, vol. 49, no. 12, pp. 36–44, 2011.

[109] J. LeClare, "IEEE 1901.2 PAP15 update," Presentation to NIST PAP-15 SGIP Plenary Meeting, Chicago, Ill, USA, at Grid Interop, December 2010, http://collaborate.nist.gov/twiki-sggrid/pub/SmartGrid/PAP15PLCForLowBitRates/PAP15_IEEE_1901_2_Update.ppt.

[110] ITU - Telecommunication Standardization Sector STUDY GROUP 15, "Narrowband orthogonal frequency division multiplexing power line communication transceivers—Power spectral density specification," Recommendation ITU-T G.9901, November 2012, approved.

[111] ITU - Telecommunication Standardization Sector STUDY GROUP 15, "Narrowband orthogonal frequency division multiplexing power line communication transceivers for G.hnem networks," Recommendation ITU-T G.9902, October 2012, approved.

[112] O. Monnier, "TI delivers flexible power line communications solutions," White Paper, September 2010, http://www.ti.com/lit/wp/slyy026/slyy026.pdf.

[113] Intellon, http://www.intellon.com/.

[114] DS2, Design of Systems on Silicon, "Your world. Connected," http://www.marvell.com/.

[115] Gigle Networks Inc., http://www.giglenetworks.com/.

[116] Panasonic Communications Co., Ltd., "Ideas for life," http://panasonic.net/corporate/segments/psn/.

[117] HomePlug Powerline Alliance, https://www.homeplug.org/home.

[118] Universal Powerline Association (UPA), http://en.wikipedia.org/wiki/Universal_Powerline_Association.

[119] High Definition Power Line Communication Alliance (HD-PLC), http://www.hd-plc.org/.

[120] International Telecommunications Union (ITU), "ITU-T Recommendation G.9960," Unified highspeed wire-line based home networking transceivers—Foundation, August 2009.

[121] International Telecommunications Union (ITU), "ITU-T Recommendation G.9961, Data link layer (DLL) for unified high-speed wire-line based home networking transceivers," June 2010.

[122] International Telecommunications Union (ITU), "ITU-T Recommendation G.9963, Unified high-speed wire-line based home networking transceivers—Multiple Input/Multiple Output (MIMO)," g.9963 (ex G.hn-MIMO), September 2011.

[123] HomeGrid Forum, "For any wire, anywhere in your home," http://www.homegridforum.org/.

[124] Institute of Electrical and Electronic Engineers (IEEE), "Standards Association, Working group P1901," IEEE standard for broadband over power line networks: Medium access control and physical layer specifications, http://grouper.ieee.org/groups/1901/.

[125] Institute of Electrical and Electronics Engineers (IEEE) Standards Association and P1901 Working Group, "IEEE P1901 Draft standard for broadband over power line networks: Medium access control and physical layer specifications," July 2009.

[126] Institute of Electrical and Electronics Engineers Standards Association and Working Group P1905.1, "Draft standard for a convergent digital home network for heterogeneous technologies," 2012, http://standards.ieee.org/develop/project/1905.1.html.

[127] S. Galli, A. Kurobe, and M. Ohura, "The inter-PHY protocol (IPP): A simple coexistence protocol for shared media," in *Proceedings of the IEEE International Symposium on Power Line Communications and its Applications (ISPLC '09)*, pp. 194–200, Dresden, Germany, April 2009.

[128] H. C. Ferreira, L. Lampe, J. Newbury, and T. G. Swart, Eds., *Power Line Communications: Theory and Applications For Narrowband and Broadband Communications Over Power Lines*, John Wiley & Sons, 2010.

[129] International Telecommunications Union (ITU), "ITU-T Recommendation G.9972, Coexistence mechanism for wireline home networking transceivers," June 2010.

[130] D. Su and S. Galli, "PAP 15 recommendations to SGIP on broadband PLC coexistence," December 2010, http://collaborate.nist.gov/twiki-sggrid/pub/SmartGrid/PAP15PLCForLowBitRates/PAP15_-_Recommendation_to_SGIP_BB_CX_-_Final_-_APPROVED_2010-12-02.pdf.

[131] Consortium for Smart Energy Profile 2 Interoperability, "CSEP consortium for SEP2 interoperability," 2011, http://www.csep.org/.

[132] ZigBee Alliance, "Smart Energy Profile 2.0 Application Protocol Specification," v 0.7, April 2010, http://zigbee.org/Standards/ZigBeeSmartEnergy/Version20Documents.aspx.

[133] International Electrotechnical Commission (IEC), "Application integration at electric utilities—System interfaces for distribution management," international standard IEC 61968, under development.

[134] International Electrotechnical Commission (IEC), "Energy management system application program interface (EMS-API)," international standard IEC 61970, under development.

[135] World Wide Web Consortium (W3C), "Extensible markup language (XML) 1.0," W3C Recommendation, 5th ed., November 2008, http://www.w3.org/TR/REC-xml/.

[136] R. T. Fielding, *Architectural styles and the design of network-based software architectures [Ph.D. thesis]*, University of California, Irvine, Calif, USA, 2000, http://www.ics.uci.edu/~fielding/pubs/dissertation/top.htm.

[137] R. T. Fielding, J. Gettys, J. C. Mogul et al., "RFC 2616: Hypertext Transfer Protocol – HTTP/1.1," June 1999, http://tools.ietf.org/html/rfc2616.

[138] V. Oksman and J. Egan, "Applications of ITUT G.9960, ITU-T G.9961 transceivers for Smart Grid applications: Advanced metering infrastructure, energy management in the home and electric vehicles," Telecommunication Standartization Sector of ITU; Series G: Transmission Systems and Media, Digital Systems and Networks, ITU-T Technical Paper, June 2010, http://www.itu.int/dms_pub/itu-t/opb/tut/T-TUT-HOME-2010-PDF-E.pdf.

Hindawi Publishing Corporation
Journal of Electrical and Computer Engineering
Volume 2013, Article ID 402514, 9 pages
http://dx.doi.org/10.1155/2013/402514

Research Article

Radiation Mitigation for Power Line Communications Using Time Reversal

Amilcar Mescco,[1] Pascal Pagani,[2] Michel Ney,[2] and Ahmed Zeddam[1]

[1] *Orange Labs Networks, 2 Avenue Pierre Marzin, 22200 Lannion, France*
[2] *Telecom Bretagne, Microwave Department, Technopôle Brest-Iroise, 29238 Brest, France*

Correspondence should be addressed to Amilcar Mescco; amescco@gmail.com

Received 4 August 2012; Revised 16 January 2013; Accepted 21 January 2013

Academic Editor: Moises V. Ribeiro

Power Line Communication (PLC) is the response for nowadays high demand of multimedia services in domestic environment, not only for its fast and reliable transfer characteristics but also for its flexible low cost implementation, since the PLC technology uses the existing electrical network infrastructure and the omnipresent outlets throughout the home. The transfer of such a high bit rate through the mains network generates acceptable radiated emission regulated by international standards, but the increment in speed for new generation PLC may cause higher levels of emissions. This paper explains the use of the Time Reversal (TR) technique to mitigate radiated emissions from PLC systems. This method was probed experimentally in real electrical networks with excellent results: in 40% of the observations, the Electromagnetic Interference (EMI) generated by PLC transmission could be reduced by more than 3 dB, and this EMI mitigation factor could increase to more than 10 dB in particular configurations.

1. Introduction

With the increasing demand for both high data rate applications and reliable links for command and control systems, Power Line Communication (PLC) has emerged in recent years as an attractive communication technique [1]. The main advantage of this technology is its ability to benefit from the existing electrical network infrastructure for the transmission of electromagnetic signals. Hence, it becomes possible to build large communication networks without the need for installing new wires.

In the home or office environment, indoor PLC uses the Low Voltage (LV) infrastructure. The presence of several electrical outlets in each room of the house allows ubiquitous coverage of the communication network. In addition, the relatively short distance between different outlets allows the system to operate within a limited attenuation. Current Broad Band (BB) in-home systems primarily operate in the frequency range from 2 MHz to 30 MHz. However, recent specifications, such as IEEE 1901 [2] or ITU-T G.9960 [3] allow signal transmission at higher frequencies up to 100 MHz. On the other hand, Narrow Band (NB) PLC systems are deployed at frequencies below 500 kHz, in both indoor and outdoor configurations, using LV or Medium Voltage (MV) infrastructures [4]. These systems allow the transmission of command and control information over longer distances for Smart Grid applications. The ITU-T G.9955 standard is an example of such NB PLC systems [5].

LV or MV electrical wires were not initially designed to propagate communication signals at frequencies above 1 kHz. As a consequence, the communication channel between the transmitter and the receiver is a difficult channel, generating attenuation and multiple propagation paths. The channel capacity is, hence, limited, and signal processing needs to be optimized so as to maximize the offered data rate and Quality of Service (QoS).

This paper focuses on one of the main limitations related to the PLC technology, namely, the generation of unintentional radiated signal. This phenomenon is mainly due to the unbalanced nature of the electrical network [6]. The variation of the impedances of the loads connected to the network as well as the unequal length of the phase and neutral wires (due to single-phase switches) converts the differential PLC signal into common mode current flowing

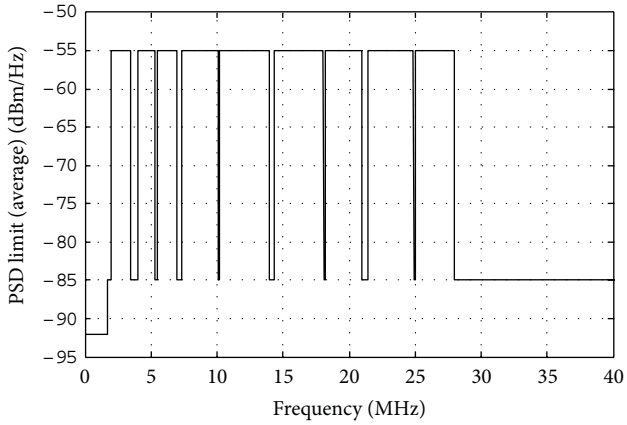

Figure 1: Example of PSD limit (average) for North America.

through the network. Consequently, the copper wires used for transmitting the useful signal act as an antenna, and part of the transmitted power is radiated. This not only results in stronger signal attenuation at the receiver but also leads to Electromagnetic Compatibility (EMC) issues, as the radiated signal may interfere with other existing services, such as amateur radio (HAM) or Short Wave (SW) broadcasting. The impact of PLC transmission on EMC has been studied, for example, within the ICT FP7 project OMEGA [7] and through the ETSI Specialist Task Force 410 [8].

In order to avoid interference between PLC systems and other users of the spectrum, regulation authorities impose strict emission masks for the transmission of electromagnetic signals on the power lines. In the USA, the Federal Communications Commission (FCC) Part 15 [9] specifies a maximum level of radiated field for carrier-current systems (including PLC), leading system specifications to define constrained power transmission masks. Figure 1 represents an example of Power Spectral Density (PSD) limits provided in the IEEE 1901 standard for North America. The observed notches are defined to protect specific systems, such as HAM bands. In Europe, CENELEC is currently developing a draft on regulation standard applying to in-home PLC systems [10].

Regardless of the regulation limits in place, the research presented in this paper focuses on the mitigation of unintentional radiation due to PLC systems. Several attempts to solve this problem have been presented in the literature. Reference [11] presents a method to reduce radiated emissions by applying an auxiliary signal cancelling the electromagnetic field on a given point in space. Simulations demonstrated good performance, with the drawback that the Electro Magnetic Interference (EMI) could only be mitigated at a single location. The authors in [12] used additional hardware connected at the wall outlets, in order to reduce asymmetries on power lines, at the cost of an increased complexity of the PLC network.

In our approach, we tried to simultaneously reach two complementary goals by the means of digital signal processing. First, we intend to focus the transmitted signal at the receiver location. The power gain linked to this energy focalization allows in turn relaxing the required power level at the transmitter, hence generating less Electro Magnetic Interference (EMI). Second, we target to reduce the level of energy dissipated at any location except the intended receiver. In particular, it is desirable to minimize the level of radiated power from the electrical wires. These two benefits already appear as features of a known technique in the field of wireless transmission: Time Reversal (TR) [13]. Experimental investigations conducted using Ultra Wide Band (UWB) radio waves demonstrated both the focusing and interference mitigation properties of this technique [14, 15].

In this paper, we present for the first time an experimental analysis of TR as a mean to mitigate radiation effects for wired signal transmission. Our investigation focuses on High Frequency (HF) BB PLC signals but could be extended to NB PLC and other wired transmission systems, such as Digital Subscriber Line (DSL) access. The paper is organized as follows. Section 2 presents the concepts of the TR technique and its application to wired systems. Section 3 details the experiment conducted to assess the merits of TR for BB PLC, and the results are statistically analyzed in Section 4. Finally, conclusions are drawn in Section 5.

2. Time Reversal for Power Line Communications

2.1. Time Reversal for Wireless Transmission. The TR technique, also known as phase conjugation in the frequency domain, was first used in the fields of acoustics [16, 17]. More recently, this concept has been successfully extended to electromagnetic waves, where the rich multipath channel provides excellent conditions for its application [13]. The basic concept of TR is simple. Let $\delta(\tau)$ be an ideal, Dirac impulse emitted by a transmitter (Tx) antenna (Figure 2(a)). By definition, at any receiver (Rx) location $\mathbf{r}_0$, the received signal is given by the Channel Impulse Response (CIR) $h(\tau, \mathbf{r_0})$. The CIR is composed of multiple echoes reflecting the multiple propagation paths of the propagation channel.

TR uses this Channel State Information (CSI) at the Tx to prefilter the signal to be transmitted. More specifically, the CIR $h(\tau, \mathbf{r_0})$ is time reversed and normalized to serve as an input filter for the signal to be transmitted (Figure 2(b)). Physically, each delayed echo constituting the TR filter travels, among other multiple paths, through its original propagation path. As a result, the multiple echoes sum up coherently at the receiver, hence focusing the received energy in time.

Mathematically, applying TR leads for any Rx situated at an arbitrary location $\mathbf{r}$ to the equivalent perceived CIR $h_{\mathrm{TR}}(\tau, \mathbf{r})$ (note that this formulation holds for a real valued CIR) [18]:

$$h_{\mathrm{TR}}(\tau, \mathbf{r}) = \frac{h(-\tau, \mathbf{r}_0)}{\sqrt{\int |h(\tau, \mathbf{r}_0)|^2 d\tau}} \otimes h(\tau, \mathbf{r}), \tag{1}$$

where the symbol $\otimes$ denotes time domain convolution. Formulating (1) in the frequency domain leads to

$$H_{\mathrm{TR}}(f, \mathbf{r}) = \frac{H^*(f, \mathbf{r}_0)}{\sqrt{\int |H(f, \mathbf{r}_0)|^2 df}} \times H(f, \mathbf{r}), \tag{2}$$

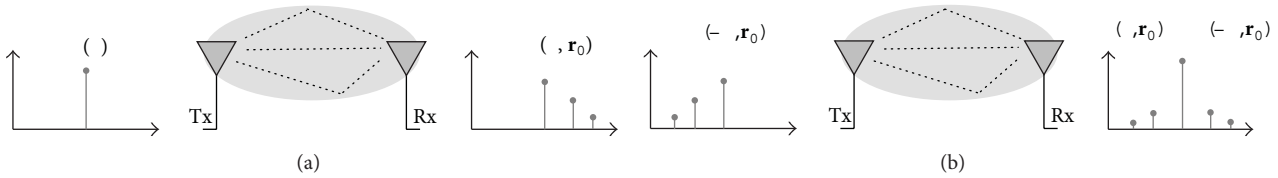

Figure 2: Transmission over an ideal multipath propagation channel (a) of a Dirac impulse, (b) of the time-reversed CIR.

where $H(f, \mathbf{r})$ represents the complex valued Channel Transfer Function (CTF), and the superscript * denotes the complex conjugate operation. For this reason, TR is sometimes called frequency domain phase conjugation.

Two conclusions can be drawn from (1) and (2). First, at the intended Rx location $\mathbf{r}_0$, the perceived CIR simplifies to

$$h_{\mathrm{TR}}(\tau, \mathbf{r}_0) = \frac{1}{\sqrt{\int |h(\tau, \mathbf{r}_0)|^2 d\tau}} \times R_h(\tau, \mathbf{r}_0), \quad (3)$$

where $R_h(\tau, \mathbf{r}_0)$ denotes the time domain autocorrelation of the function $h(\tau, \mathbf{r}_0)$. Similarly, the perceived CTF simplifies to

$$H_{\mathrm{TR}}(f, \mathbf{r}_0) = \frac{1}{\sqrt{\int |H(f, \mathbf{r}_0)|^2 df}} \times |H(f, \mathbf{r}_0)|^2. \quad (4)$$

In the time domain, the effect of the TR filter is to transform the CIR into its autocorrelation. For a rich multipath environment, the autocorrelation of the CIR presents a large peak at $\tau = 0$, with reduced side echoes. Experimental studies demonstrated that the resulting channel is less spread in time [14, 15], hence reducing the possible Intersymbol Interference (ISI). In the frequency domain, the perceived CTF is proportional to the square of the magnitude of the actual CTF. Besides the fact that TR provides a real valued CTF, which could be exploited at the receiver, this also leads to a significant gain in terms of Rx power, due to a better exploitation of the frequency selective nature of the channel. It was demonstrated in [18] that the application of TR in a flat channel (i.e., without frequency domain power decay) under Rayleigh fading leads to a gain of 3 dB in the total received power. This gain was increased to 5 dB when considering the frequency domain power decay observed in practical UWB radio channels.

The second conclusion drawn from (1) and (2) is that, for any other location $\mathbf{r}$ different from $\mathbf{r}_0$, TR creates a mismatch between the Tx filter and the channel. This is particularly observable in the frequency domain representation of TR given in (2). The perceived CTF corresponds to the product of two independent CTF, $H(f, \mathbf{r})$ and $H^*(f, \mathbf{r}_0)$, with possibly very different frequency fading structures. More precisely, minima of the first CTF can happen randomly at maxima of the second CTF. Hence, averaging over all frequencies, the total received power at untargeted locations is reduced. In wireless TR analysis, this effect is called spatial focusing and is generally assessed as the ratio between the maximum of $h_{\mathrm{TR}}(\tau, \mathbf{r})$ and the maximum of $h_{\mathrm{TR}}(\tau, \mathbf{r}_0)$ for a given distance $\|\mathbf{r} - \mathbf{r}_0\|$. Spatial focusing factors of −10 dB have been reported in [18, 19].

2.2. Extension of Time Reversal to Wired Transmission. As observed through the study of TR for wireless transmission, the TR scheme provides two main features, namely, an increase of the Rx power at the intended Rx location and a decrease of the Rx power at any other location. These features are highly desirable in the context of wired transmission, where the level of Tx power is constrained by the unintentional radiation from the wires, causing possible EMI to other systems.

Based on this observation, we conducted experimental studies to analyze the potential of TR to mitigate unwanted emissions for PLC systems. The main principles of the extension of TR to PLC transmission can be explained with the help of Figure 3.

We assume an intended transmission between a Tx PLC modem and an Rx PLC modem, over an LV indoor electrical network. Different experimental investigations reported the PLC channel as a rich multipath propagation channel, due to the multiple branches present in a classical electrical network and to the impedance mismatch occurring at the network terminations (outlets) and nodes [20–23]. This similarity of the PLC channel with wireless channels suggests promising results when applying TR to PLC.

With reference to Figure 3, the Rx modem is situated at the intended location $\mathbf{r}_0$, and the Tx modem is situated at the origin. By applying TR filtering at the Tx, the Rx power will be increased at location $\mathbf{r}_0$; hence, the Rx modem will benefit from an increased Signal-to-Noise Ratio (SNR). This power increased can also in turn be applied as a reduction of the Tx power to achieve similar performance. At other outlets in the network, situated, for example, at locations $\mathbf{r}_1$ or $\mathbf{r}_2$, the Rx power will be reduced. This effect can be further exploited in the design of multiuser transmission schemes.

For our purpose of radiation mitigation, let us now consider a location $\mathbf{r}_3$, situated at any point in space in the vicinity of the electrical network. The level of radiated field at this location can be evaluated, for instance, by the means of an equivalent transfer function $H(f, \mathbf{r}_3)$ between the Tx modem and an ideal antenna situated at location $\mathbf{r}_3$. By the virtue of the TR scheme (2), the perceived transfer function at location $\mathbf{r}_3$ after applying TR will be proportional to the product $H^*(f, \mathbf{r_0}) \times H(f, \mathbf{r}_3)$. As the functions $H^*(f, \mathbf{r}_0)$ and $H(f, \mathbf{r}_3)$ are not correlated, their frequency fading structures are different. In particular, the deep notches due to frequency selective fading do not appear at the same frequencies. As a result, the product $H^*(f, \mathbf{r}_0) \times H(f, \mathbf{r}_3)$ will provide more average attenuation when compared to $H(f, \mathbf{r}_3)$ alone, and therefore, the total power radiated at location $\mathbf{r}_3$ will be reduced. A similar observation is made in previous studies

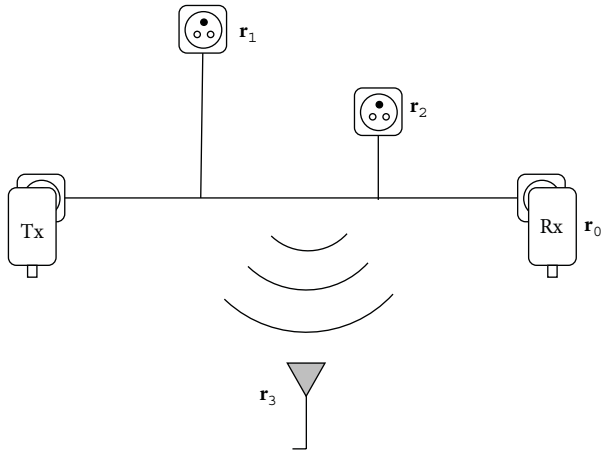

Figure 3: Principle of the extension of TR to wired transmission.

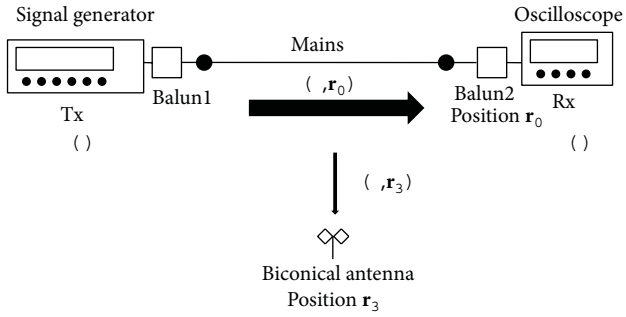

Figure 4: Equipment used in the experimental setup.

dedicated to wireless channels [14, 15, 18]. Hence, TR appears as an efficient method to mitigate EMI for wired communications.

The theoretical basis for the application of TR to wired transmission being set, we will now describe the experimental assessment of this method in the next Sections.

3. Experimental Setup

3.1. Equipment. In order to experimentally assess the use of TR as a method to mitigate EMI for wired communication, we used the experimental setup presented in Figure 4. In this setup, a signal generator Tektronix AWG7082C was used as a generic Tx. A Digital Sampling Oscilloscope (DSO) LeCroy WaveRunner 715Zi-A was used to sample the received signal at Rx. The signal generated at Tx is denoted $s(t)$, and the signal received at the DSO is denoted $y(t)$. Two Universal PLC Couplers were used as baluns to couple the Tx and Rx signals with the power lines. The Tx coupler is situated at the origin, and the Rx coupler is connected to a plug at location $\mathbf{r}_0$. These couplers were developed within the ETSI Specialist Task Force 410 [24]. In order to measure the power density of the radiated emission received at any arbitrary location $\mathbf{r}_3$, a biconical antenna Schwarzbeck EFS921 was connected to a second port of the DSO.

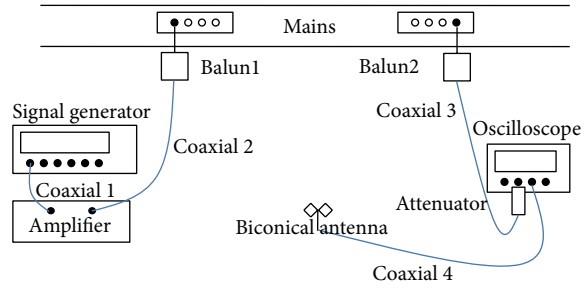

Figure 5: Experimental setup calibration.

3.2. Calibration. With reference to Figure 5, two measurement paths can be distinguished. Path 1 serves for the measurement of the CTF and is composed of the following elements: the transmitter, coaxial cable 1, a 30 dB amplifier IFIM50, coaxial cable 2, balun 1, mains, balun 2, coaxial cable 3, a 20 dB attenuator Radial R412720000, and the receiver. The baluns were considered as part of the channel. The calibration for measurement path 1 was made by directly connecting coaxial cable 2 and coaxial cable 3.

Path 2 is composed by the transmitter, coaxial cable 1, a 30 dB amplifier IFIM50, coaxial cable 2, the wire to free space propagation channel (represented by the CTF $H(f, \mathbf{r}_3)$), the biconical antenna, coaxial cable 4, and the DSO. The calibration for this second path was made by connecting coaxial cable 2 and coaxial cable 4. The gain of the antenna was removed from the measurements by postprocessing.

The signal generator and the DSO were synchronized by a direct connection of their 10 MHz reference clocks. The sampling rates of both devices were set to $f_s = 100$ MHz.

3.3. Signal Processing. After initial system calibration, the measurements are performed in 3 steps.

(1) The CTF $H(f, \mathbf{r}_0)$ is evaluated using a specific Tx frame (see below). The considered frequency band extends from 2.8 MHz to 37.5 MHz.

(2) The TR filter is generated using the phase and magnitude of $H(f, \mathbf{r}_0)$.

(3) The CTFs $H(f, \mathbf{r}_0)$ and $H(f, \mathbf{r}_3)$ as well as the perceived CTFs $H_{\mathrm{TR}}(f, \mathbf{r}_0)$ and $H_{\mathrm{TR}}(f, \mathbf{r}_3)$ are measured using a single Tx frame (see below). Measurements at the location of the Rx outlet ($\mathbf{r}_0$) and at arbitrary locations in space ($\mathbf{r}_3$) are made simultaneously using two ports of the oscilloscope, one connected to the Rx balun and the other connected to the biconical antenna.

The Tx signal is generated according to the HomePlug standard [25]. The used frame is called PHY Protocol Data Unit (PPDU) and it is composed by a preamble (including a Frame Control) and a number of payload symbols as shown in Figure 6. Each payload symbol consists of a 3072-sample OFDM symbol as defined in the HomePlug specification [25]. In order to estimate the CTFs $H(f, \mathbf{r})$ and $H_{\mathrm{TR}}(f, \mathbf{r})$, the OFDM symbols were loaded with predefined constellations.

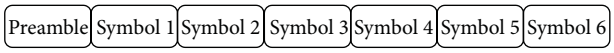

Figure 6: HomePlug frame.

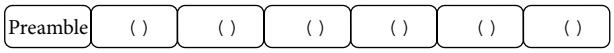

Figure 7: HomePlug frame for calibration and CTF measurement before computation of the TR filter.

The frame used for the calibration and the initial measurement of the CTF before computation of the TR filter is represented in Figure 7.

The frame used for the measurement of the CTF and EMI after computation of the TR filter is represented in Figure 8. Note that in this frame, the TR filter is applied on the 3 last symbols only (represented by the signal $s'(t)$). From this particular frame scheme, the CTF and EMI can be evaluated with and without application of TR quasi-simultaneously. Recomputing the CTF at this stage also allows monitoring any possible temporal evolution of the channel between calibration and measurement.

In essence, the overall channel estimation process is similar to the channel sounding procedure defined in the HomePlug AV specification. In our experiment, the computation of the CTF from the received signal uses a classical Zero Forcing (ZF) channel estimation procedure. This is suitable in our experiment involving high levels of Signal-to-Noise Ratio (SNR) at the Rx. In practical systems operating at lower SNR, more sophisticated methods such as the Minimum Mean Square Error channel estimation would be more efficient against noise enhancement. Note that we chose to actually implement the TR filter in the time domain at the transmitter using a programmable waveform generator, in order to measure results as close as possible to a realistic implementation of the TR scheme in practical PLC modems.

In order to estimate channel attenuation continuously over the measured frequency band, no spectral notches were implemented for this study. In practical systems, a Tx PSD mask is defined, where the Tx power is notched at predefined frequencies, to protect existing services using the same spectrum. The HomePlug specification uses windowing in order to better exploit the power allocated within the PSD mask while protecting out-of-band services. The present study concentrates on reducing the EMI within the band effectively used by PLC systems. Therefore, the results also hold for practical systems including notches.

3.4. Measured Environment. The measurement campaign was conducted using 13 different topologies of 230 V mains networks within the premises of Orange Labs in Lannion. The campaign took place in different rooms of about $5 \times 4\,\mathrm{m}^2$. Figure 9 presents a picture of the experimental setup in an exemplar location.

The Tx and Rx modems were connected to two outlets in the same room, with distances varying between 2 m and 8 m. In general, the rooms are equipped with several other

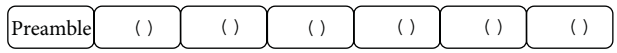

Figure 8: HomePlug frame for CTF and EMI measurement after application of TR.

Figure 9: Picture of experimentation.

electrical outlets (between 4 and 10). About half of the outlets were connected to classical office appliances (lamps, desktops, etc.). For each topology, one CTF was measured, first without applying TR and then after applying TR filtering. In addition, for each topology, between 3 and 5 locations were selected to measure the received electrical field with the help of the biconical antenna. In total, 13 CTF and 43 measurements of the electrical field were collected for statistical analysis.

4. Results and Statistical Analysis

4.1. Preliminary Results. The preliminary results for an exemplar network will be presented in two parts: first, the CTF at $\mathbf{r}_0$ and second the electric field and its associated power density at $\mathbf{r}_3 \neq \mathbf{r}_0$.

For the CTF at $\mathbf{r}_0$, we show its attenuation characteristics in Figure 10.

Let us first consider the measured CTF (black curve). The deep notches at some frequencies are due to reflections at the terminations of the network and reflect the multipath nature of the PLC network. We define the average attenuation before TR $\overline{H(\mathbf{r}_0)}$ in dB as:

$$\overline{H(\mathbf{r}_0)} = 10\log_{10}\left(\frac{1}{f_{\max} - f_{\min}} \int_{f_{\min}}^{f_{\max}} \left|H\left(f, r_0\right)\right|^2 df\right), \tag{5}$$

where $f_{\min}$ and $f_{\max}$ respectively represent the minimum and maximum sounded frequencies. The average attenuation corresponds to the signal attenuation perceived by a receiver capable of exploiting all the power received in the frequency band from $f_{\min}$ to $f_{\max}$. Typically, an OFDM system like the HomePlug AV specification is able to exploit the total received power over a wide frequency band. In our example, the average attenuation is about 11 dB.

Let us now focus on the perceived CTF after applying TR. Owing to the mathematical definition of the TR filter, TR allocates more power to frequencies showing minimal

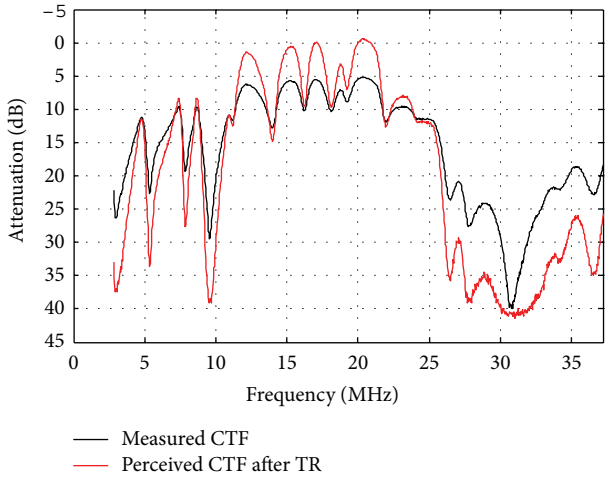

Figure 10: Channel attenuation before and after TR.

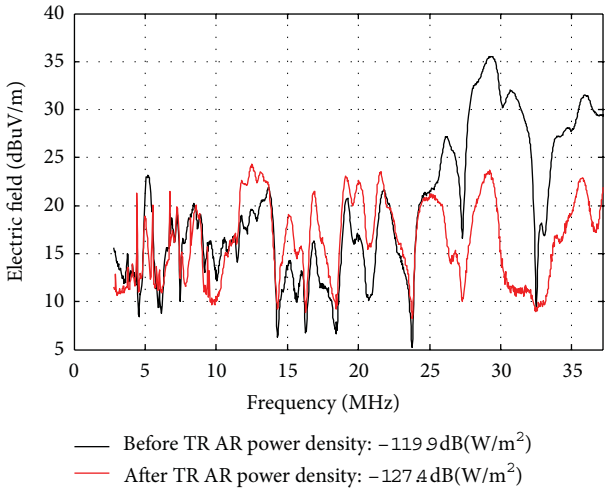

Figure 11: Electric field before and after TR.

attenuation, while strongly attenuated frequencies are more power constrained. In particular, for all frequencies where the attenuation of the channel $H(f, \mathbf{r_0})$ is higher than the average attenuation $\overline{H(\mathbf{r}_0)}$, the perceived channel is more attenuated after applying TR. This can be clearly seen in the frequency range from 26 MHz to 37.5 MHz. For the frequencies where the attenuation of the channel is less than $\overline{H(\mathbf{r}_0)}$, the response of the channel is improved using TR. We can see this clearly in the frequency range from 11 MHz to 22 MHz. If we define the average attenuation after TR $\overline{H_{\mathrm{TR}}(\mathbf{r}_0)}$ in dB as

$$\overline{H_{\mathrm{TR}}(\mathbf{r}_0)} = 10\log_{10}\left(\frac{1}{f_{\max}-f_{\min}}\int_{f_{\min}}^{f_{\max}}\left|H_{\mathrm{TR}}(f, r_0)\right|^2 df\right), \tag{6}$$

we observe that the average attenuation after applying TR is about 7.5 dB. Hence, the application of TR provided a gain in the total received power of 3.5 dB in this particular example.

Note that only the measured CTF (black curve) is physical. Therefore, the measured CTF will always degrade the transmission with some degree of channel attenuation. On the contrary, the CTF perceived at Rx after application of TR (red curve) corresponds to a logical channel, where the effects of the measured CTF are combined with the effects of the TR filter at Tx. Hence, the perceived CTF may exhibit some gain over a limited frequency range.

We now consider the electrical field and its associated power density at $\mathbf{r}_3 \neq \mathbf{r}_0$. The value of the electrical field $E(f, \mathbf{r}_3)$ in dBμV/m was computed from the CTF $H(f, \mathbf{r}_3)$ measured between the Tx balun and the antenna connector assuming an injected PSD $P_{\mathrm{feed}} = -55$ dBm/Hz and using the following formula [24]:

$$E(f, \mathbf{r}_3) = P_{\mathrm{feed}} + 20\log_{10}\left(\left|H(f, \mathbf{r}_3)\right|\right) + 107 + \mathrm{AF}(f), \tag{7}$$

where AF(f) represents the antenna factor and 107 represents the conversion from dBm to dBμV. In addition, we computed the average radiated power density $\overline{S(\mathbf{r}_3)}$ in dB(W/m^2) as

$$\overline{S(\mathbf{r}_3)} = 10\log_{10}\left(\frac{1}{f_{\max}-f_{\min}}\int_{f_{\min}}^{f_{\max}}\frac{1}{120\pi}\left|E(f, \mathbf{r}_3)\right|^2 df\right), \tag{8}$$

where $f_{\min}$ and $f_{\max}$, respectively, represent the minimum and maximum sounded frequencies, and $E(f, \mathbf{r}_3)$ is expressed in V/m. In (8), the term $120 \times \pi$ provides the value of the impedance of free space in Ohm.

Note that both $E(f, \mathbf{r}_3)$ and $\overline{S(\mathbf{r}_3)}$ can also be computed after applying TR filtering, using the following equations:

$$E_{\mathrm{TR}}(f, \mathbf{r}_3) = P_{\mathrm{feed}} + 20\log_{10}\left(\left|H_{\mathrm{TR}}(f, \mathbf{r}_3)\right|\right) + 107 + \mathrm{AF}(f) \tag{9}$$

$$\overline{S_{\mathrm{TR}}(\mathbf{r}_3)} = 10\log_{10}\left(\frac{1}{f_{\max}-f_{\min}}\int_{f_{\min}}^{f_{\max}}\frac{1}{120\pi}\left|E_{\mathrm{TR}}(f, \mathbf{r}_3)\right|^2 df\right). \tag{10}$$

An example of radiated emission measurement is given in Figure 11. For this particular electrical network, the mitigation of radiated emissions is clear in the frequency band from 26 MHz to 37.5 MHz, and the average radiated power density has reduced by about 7.5 dB. Thus, we can observe with this example that the application of TR filtering can reduce significantly the level of undesired radiated power.

4.2. Statistical Analysis. In this section, we present the statistical analysis of the measurement database collected within 13 rooms of the office building at Orange Labs in Lannion. The total measurement set is composed of 13 CTF and 43 measurements of the electrical field.

We first computed the channel gain G_{TR} observed on the perceived CTF $H_{\mathrm{TR}}(f, \mathbf{r}_0)$ after application of TR filtering. As OFDM systems can exploit the total power received over a given frequency band, we computed this gain in dB for the total received power as

$$G_{\mathrm{TR}} = \overline{H(\mathbf{r}_0)} - \overline{H_{\mathrm{TR}}(\mathbf{r}_0)}. \tag{11}$$

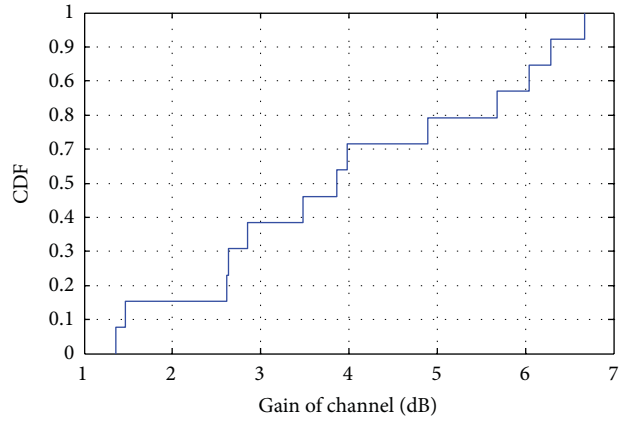

Figure 12: CDF of the channel gain G_{TR}.

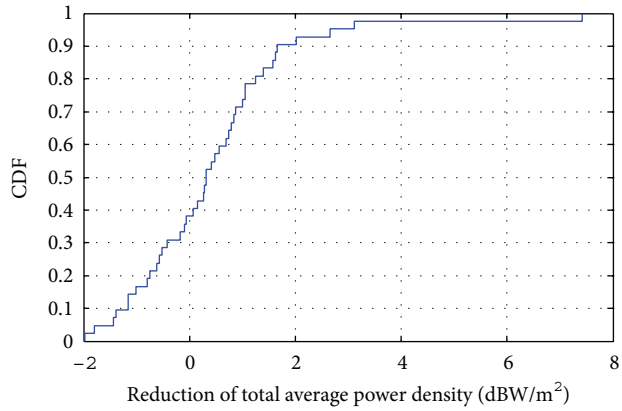

Figure 13: CDF of the EMI reduction coefficient R_{TR}.

The cumulative distribution function (CDF) of G_{TR} is given in Figure 12. This parameter shows always a positive gain, between 1.4 dB and 6.6 dB in our experiment, which is in line with results reported in similar wireless experiments [18]. In about 60% of cases, the channel gain is higher than 3 dB. This means that at Rx we have always a better reception using TR. This channel gain can in turn be used to reduce the injected PSD at Tx, hence reducing by the same factor the unwanted EMI.

We then computed the EMI reduction coefficient R_{TR}, corresponding to the reduction of the undesired radiated power due to the application of a TR filter. This figure of merit of the reduction of radiated signal is computed in dB as follows:

$$R_{TR} = \overline{S(\mathbf{r}_3)} - \overline{S_{TR}(\mathbf{r}_3)} \quad (12)$$

The CDF of the EMI reduction coefficient R_{TR} is given in Figure 13. Results show that the simple application of TR reduces the EMI in more than 60% of cases. In the best case, the EMI reduced by more than 7 dB using TR. In the worst case, the EMI increased by 2 dB. The observations of particular cases indicates that the reduction of EMI is more effective when the CTFs $H(f, \mathbf{r}_0)$ and $H(f, \mathbf{r}_3)$ are highly decorrelated. This is more likely to happen in complex

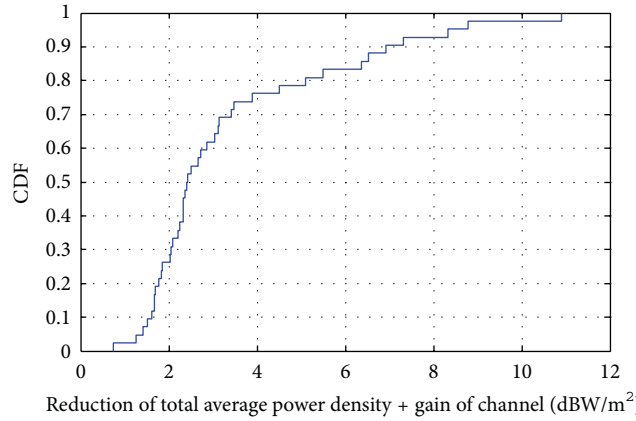

Figure 14: CDF of the effective EMI mitigation, M_{TR}.

electrical network topologies, where the rich multipath environment results in different frequency fading structures for different Rx locations.

Observing the statistics of the channel gain G_{TR} and of the EMI reduction coefficient R_{TR}, an optimal strategy can be proposed in order to minimize EMI for a PLC system. Indeed, Figure 12 shows that the application of TR provides better system performance due to the reduced channel attenuation. This gives us in turn the flexibility to reduce the level of the Tx power to further reduce EMI while keeping the system performance constant. More precisely, when TR is applied, a Tx power back-off of G_{TR} dB can be applied without modifying the total received power. Finally, following this power backoff strategy, the effective EMI mitigation factor M_{TR} can be computed as the sum of the power backoff and the EMI reduction coefficient:

$$M_{TR} = G_{TR} + R_{TR}. \quad (13)$$

The CDF of the effective EMI mitigation factor M_{TR} is depicted in Figure 14. Several conclusions can be drawn from this statistical result.

(i) First, the TR method is able to mitigate EMI generated by PLC transmission in 100% of our experimental observations. To this respect, one can conclude that the gain G_{TR} provided by the application of TR allows a Tx power backoff that largely compensates for the possible EMI increment observed in Figure 13.

(ii) Second, in 40% of the cases, the undesired radiated power is reduced by more than 3 dB.

(iii) Finally, in the most favorable configurations, a reduction of the EMI by more than 10 dB can be observed. Such configurations correspond to cases where the CTF between the Tx and Rx modem and the EMI spectrum are particularly decorrelated.

5. Conclusion

In this paper, we proposed for the first time the application of TR in order to mitigate EMI generated by wired communication systems. TR was originally used in the field of wireless

transmission as a mean to focus the transmitted signal in both time and space around the intended receiver. We proposed to use the same property to focus the signal injected in a wired medium, such as the electrical network in the case of PLC for instance. As a result, the energy lost through undesired radiation is expected to decrease significantly.

We presented an experimental setup in order to demonstrate this method. The experiment was conducted in the time domain using signal frames similar to the industrial specification HomePlug AV. In addition, the TR filter was actually implemented using an arbitrary wave generator, thus providing results encompassing the possible drawbacks of a practical implementation.

Results demonstrated that, on the wired medium, TR could provide a transmission channel gain between 1 dB and 7 dB, which is similar to the gain observed in wireless transmission. In addition, the application of a TR filter alone could effectively reduce EMI for 60% of the observations, with a maximum EMI mitigation of 7 dB. Finally, by combining the channel gain and the EMI reduction features, we experimentally demonstrated that TR was efficient in 100% of the observed cases to reduce EMI. In 40% of the cases, the EMI mitigation was larger than 3 dB, with maxima higher than 10 dB. TR is, thus, seen as a promising technique to help resolving EMC issues related to PLC and other wired media.

In the TR strategy presented in this paper, the CTF gain provided by the TR technique was fully dedicated as a power backoff to minimize the EMI. Another strategy could target an increase of the offered capacity while maintaining a constant EMI. Further analyses will, therefore, be dedicated to analyze the tradeoff between channel throughput increase and EMI reduction. In addition, future research will focus on the study of wired TR at higher frequencies and on other media, such as DSL cables. Finally, optimal protocols will be developed to practically implement TR in future standards. In particular, the application of TR to multicast or broadcast scenarios, involving one Tx modem and several Rx modems, could be further investigated.

References

[1] H. C. Ferreira, L. Lampe, J. Newbury, and T. G. Swart, Eds., *Power Line Communications: Theory and Applications for Narrowband and Broadband Communications Over Power Lines*, Wiley, Chichester, UK, 2010.

[2] IEEE, 1901-2010, "IEEE standard for broadband over power line networks: medium access control and physical layer specifications," 2010.

[3] ITU-T G. 9960, "Unified high-speed wireline-based home networking transceivers—system architecture and physical layer specification," 2010.

[4] S. Galli, A. Scaglione, and Z. Wang, "For the grid and through the grid: the role of power line communications in the smart grid," *Proceedings of the IEEE*, vol. 99, no. 6, pp. 998–1027, 2011.

[5] V. Oksman and J. Zhang, "G.HNEM: the new ITU-T standard on narrowband PLC Technology," *IEEE Communications Magazine*, vol. 49, no. 12, pp. 36–44, 2011.

[6] M. Ishihara, D. Umehara, and Y. Morihiro, "The correlation between radiated emissions and power line network components on indoor power line communications," in *Proceedings of the IEEE International Symposium on Power Line Communications and Its Applications (ISPLC '06)*, pp. 314–318, Orlando, Fla, USA, March 2006.

[7] Seventh Framework Programme: Theme 3 ICT-213311 OMEGA, Deliverable D3.3, "Report on Electro Magnetic Compatibility of Power Line Communications", 2009.

[8] A. Schwager, W. Bäschlin et al., "European MIMO PLC Field Measurements: overview of the ETSI STF410 Campaign & EMI Analysis," in *IEEE International Symposium on Power Line Communications and Its Applications (ISPLC '12)*, pp. 304–309, Beijing, China, March 2012.

[9] Federal Communications Commission, "Title 47 of the code of federal regulations part 15," 2007.

[10] CENELEC, Final Draft European Standard FprEN 50561-1, "Power line communication apparatus used in low voltage installations—Radio disturbance characteristics—Limits and methods of measurement—Part 1: Apparatus for in-home use" 2011.

[11] A. Vukicevic, M. Rubinstein, F. Rachidi, and J. L. Bermudez, "On the impact of mitigating radiated emissions on the capacity of PLC systems," in *Proceedings of the IEEE International Symposium on Power Line Communications and Its Applications (ISPLC '07)*, pp. 487–492, Pisa, Italy, March 2007.

[12] P. Favre, C. Candolfi, and P. Krahenbuehl, "Radiation and disturbance mitigation in PLC networks," in *Proceedings of the 20th International Zurich Symposium on Electromagnetic Compatibility (EMC Zurich '09)*, pp. 5–8, Zürich, Switzerland, January 2009.

[13] G. Lerosey, J. De Rosny, A. Tourin, A. Derode, G. Montaldo, and M. Fink, "Time reversal of electromagnetic waves," *Physical Review Letters*, vol. 92, no. 19, Article ID 193904, 4 pages, 2004.

[14] A. E. Akogun, R. C. Qiu, and N. Guo, "Demonstrating the leverages of time reversal in ultra-wideband communications using time domain measurements," in *Proceedings of the 51st International Instrumentation Symposium*, pp. 737–742, Knoxville, Tenn, USA, May 2005.

[15] A. Khaleghi, G. El Zein, and I. H. Naqvi, "Demonstration of time-reversal in indoor ultra-wideband communication: time domain measurement," in *Proceedings of the 4th IEEE International Symposium on Wireless Communication Systems (ISWCS '07)*, pp. 465–468, October 2007.

[16] A. Derode, P. Roux, and M. Fink, "Acoustic time-reversal through high-order multiple scattering," in *Proceedings of the IEEE International Ultrasonics Symposium*, vol. 2, pp. 1091–1094, Seattle, Wash, USA, November 1995.

[17] D. R. Jackson and D. R. Dowling, "Phase conjugation in underwater acoustics," *Journal of the Acoustical Society of America*, vol. 89, pp. 171–181, 1991.

[18] P. Pajusco and P. Pagani, "On the use of uniform circular arrays for characterizing UWB time reversal," *IEEE Transactions on Antennas and Propagation*, vol. 57, no. 1, pp. 102–109, 2009.

[19] C. Zhou and R. C. Qiu, "Spatial focusing of time-reversed UWB electromagnetic waves in a hallway environment," in *Proceedings of the 38th Southeastern Symposium on System Theory*, pp. 318–322, Cookeville, Tenn, USA, March 2006.

[20] M. Tlich, A. Zeddam, F. Moulin, and F. Gauthier, "Indoor power-line communications channel characterization up to 100 MHz—part I: one-parameter deterministic model," *IEEE Transactions on Power Delivery*, vol. 23, no. 3, pp. 1392–1401, 2008.

[21] M. Tlich, A. Zeddam, F. Moulin, and F. Gauthier, "Indoor power-line communications channel characterization up to 100

MHz-part II: time-frequency analysis," *IEEE Transactions on Power Delivery*, vol. 23, no. 3, pp. 1402–1409, 2008.

[22] A. M. Tonello and F. Versolatto, "Bottom-up statistical PLC channel modeling-part I: random topology model and efficient transfer function computation," *IEEE Transactions on Power Delivery*, vol. 26, no. 2, pp. 891–898, 2011.

[23] A. M. Tonello and F. Versolatto, "Bottom-up statistical PLC channel modeling—part II: inferring the statistics," *IEEE Transactions on Power Delivery*, vol. 25, no. 4, pp. 2356–2363, 2010.

[24] ETSI TR 101 562-1 V2.1.1, "Powerline telecommunications (PLT), MIMO PLT, part 1: measurements methods of MIMO PLT," Tech. Rep., 2012, Chapter 7.1.

[25] HomePlug, "HomePlug AV specification, version 1.1," 2007.

Hindawi Publishing Corporation
Journal of Electrical and Computer Engineering
Volume 2013, Article ID 892628, 20 pages
http://dx.doi.org/10.1155/2013/892628

Research Article

An Overview of the HomePlug AV2 Technology

Larry Yonge,[1] Jose Abad,[2] Kaywan Afkhamie,[1] Lorenzo Guerrieri,[3] Srinivas Katar,[1] Hidayat Lioe,[4] Pascal Pagani,[5] Raffaele Riva,[6] Daniel M. Schneider,[7] and Andreas Schwager[7]

[1] *Qualcomm Atheros, 203 East Silver Springs Boulevard, Ocala, FL 34470, USA*
[2] *Broadcom Corporation, Llacuna 56–70, 8th Floor, Building A, 08005 Barcelona, Spain*
[3] *DORA S.p.A., STMicroelectronics Group, Via Lavoratori Vittime del Col Du Mont 28, 11100 Aosta, Italy*
[4] *Marvell Semiconductors, 5488 Marvell lane, Santa Clara, CA 95054, USA*
[5] *Orange Labs Networks, 2 Avenue Pierre Marzin, 22300 Lannion, France*
[6] *STMicroelectronics S.r.l., Via Olivetti 2, 20864 Agrate Brianza, Italy*
[7] *Sony, Hedelfinger Straße 61, 70327 Stuttgart, Germany*

Correspondence should be addressed to Pascal Pagani; pascal.pagani@ieee.org

Received 3 August 2012; Accepted 21 November 2012

Academic Editor: Andrea M. Tonello

HomePlug AV2 is the solution identified by the HomePlug Alliance to achieve the improved data rate performance required by the new generation of multimedia applications without the need to install extra wires. Developed by industry-leading participants in the HomePlug AV Technical Working Group, the HomePlug AV2 technology provides Gigabit-class connection speeds over the existing AC wires within home. It is designed to meet the market demands for the full set of future in-home networking connectivity. Moreover, HomePlug AV2 guarantees backward interoperability with other HomePlug systems. In this paper, the HomePlug AV2 system architecture is introduced and the technical details of the key features at both the PHY and MAC layers are described. The HomePlug AV2 performance is assessed, through simulations reproducing real home scenarios.

1. Introduction

The convergence of voice, video, and data within a variety of multifunction devices, along with the evolution of High Definition (HD) and 3-Dimensional (3D) video, are today driving the demands for home connectivity solutions. Home networks are required to support high throughput connectivity guaranteeing at the same time a high level of reliability and coverage (the percentage of links that are able to sustain a given throughput in two-node or multinode networks). Applications such as HD Television (HDTV), Internet Protocol Television (IPTV), interactive gaming, whole-home audio, security monitoring, and Smart Grid management have to be supported by the new home networks.

During the last decade, in-home power line communication (PLC) has received increasing attention from both the industry and research communities. The reuse of existing wires to deploy wide band services is the main source of attractiveness of the in-home PLC technologies. Another major advantage of PLC is the ubiquity of the power lines which can be used to provide whole-home connectivity solutions. However, the power line medium has not been originally designed for data communication; the frequency selectivity of the channel and different types of noise (background noise, impulsive noise, and narrow band interferers) make the power line a very challenging environment and require state of the art design solutions.

In 2000, the HomePlug Alliance [1], an industry-led organization, was formed with the scope to promote power line networking through the adoption of HomePlug specifications. In 2001, the HomePlug Alliance released the HomePlug 1.0.1 specification followed in 2005 by a second release named HomePlug AV [2]. The letters "AV" abbreviate "Audio, Video". HPAV rapidly became the most widespread adopted solution

for in-home power line communication. To meet the future market needs, in January 2012 the HomePlug Alliance published the HomePlug AV2 specification [3]. HomePlug AV2 enables Gigabit-class connection speeds by leveraging on the existing power line wires while remaining fully interoperable with other technologies for in-home connectivity (HomePlug AV [2], HomePlug Green PHY [4], and IEEE 1901 [5]). The Alliance's AV Technical Working Group (AV TWG) defined new features at both the PHY and MAC layers. These have been introduced in the HomePlug AV2 specification based on extensive field tests conducted in real home scenarios across different countries. The field results obtained by the AV TWG validated the HomePlug AV2 claimed performance both in terms of achievable data rate and coverage.

In this paper, we highlight the key differentiating HomePlug AV2 features compared to the HomePlug AV technology. At the physical (PHY) layer HomePlug AV2 includes the following. (i) *Multiple-Input Multiple-Output* (MIMO) signaling with Beamforming to offer the benefit of improved coverage throughout the home, especially on highly attenuated channels. MIMO enables HomePlug AV2 devices to transmit on any two-wire pairs within three-wire configurations comprising Line (L), Neutral (N) and Protective Earth (PE) (the coupling is done in the MIMO Analog Front End (AFE) blocks in Figure 1). (ii) *Extended Frequency Band* up to 86 MHz to increase the throughput especially at the low to mid coverage percentages (part of IFFT/FFT (1024, 8192) and Mapper blocks in Figure 1). (iii) *Efficient Notching* allows transmitters to create extremely sharp frequency notches. If Electromagnetic Compatibility (EMC) regulation will require a fragmented communication spectrum, the throughput loss by excluded frequencies can be minimized (part of Power Allocation and Window and Overlap blocks in Figure 1). (iv) *Power back-off* to increase the HomePlug AV2 data rate while reducing the electromagnetic emissions (part of Power Allocation blocks and the AFEs in Figure 1). (v) *EMC Friendly Power Boost* to optimize the transmit power by monitoring the input port reflection coefficient (known as the S_{11} parameter) at the transmitting modem. (vi) *Additional PHY Improvements*, comprising higher order Quadrature Amplitude Modulation (4096-QAM) (part of Mapper and Demodulator blocks in Figure 1), higher Code Rates (8/9 code rate) (part of Turbo Convolutional Encoder in Figure 1) and smaller guard intervals (part of Cyclic Prefix blocks in Figure 1), to assist better peak data rates. At the Medium Access Control (MAC) layer, HomePlug AV2 includes the following. (i) *Power Save mode* to improve energy efficiency when the device is in standby. (ii) *Short Delimiter* to reduce the overhead of the transmission shortening the Preamble and Frame Control symbols. (iii) *Delayed Acknowledgements* to increase the overall transmission efficiency by reducing the Inter Frame Spacings. (iv) *Immediate Repeating* to expand the coverage by repeating the signal on paths with better Signal to Noise Ratio (SNR) characteristics.

All the features listed above improve the Quality of Service of AV2 power line modems, by improving coverage and robustness of communication links.

The following sections provide technical details for all the above mentioned features. Moreover, the AV TWG evaluated the performance of the HomePlug AV2 system. The adoption of all the above listed features provides a significant gain of HomePlug AV2 compared to HomePlug AV. The remainder of this paper is organized as follows. Section 2 presents the overall HomePlug AV2 system architecture preceded by a brief overview of the HomePlug AV technology. The new PHY and MAC layer technical features are detailed in Sections 3 and 4, respectively. Section 5 explains how the technology coexistence is dealt with. Section 6 summarizes the performance gain of HomePlug AV2 compared to HomePlug AV and Section 7 concludes this introduction to the HomePlug AV2 technology.

2. System Architecture

2.1. A Brief Overview of HomePlug AV. HomePlug AV employs PHY and MAC technology that provides a 200-Mbps class power line networking capability. The PHY operates in the frequency range of 2–28 MHz, uses windowed Orthogonal Frequency Division Multiplexing (OFDM) and a powerful Turbo Convolutional Code (TCC) that provides robust performance within 0.5 dB of Shannon's limit. Windowed OFDM provides more than 30 dB spectrum notching. OFDM symbols with 917 usable carriers (tones) are used in conjunction with a flexible guard interval. Modulation densities from BPSK to 1024 QAM are adaptively applied to each carrier based on the channel characteristic between the transmitter (Tx) and the receiver (Rx).

On the MAC layer, HomePlug AV provides a Quality of Service (QoS) connection oriented, contention-free service on a periodic Time Division Multiple Access (TDMA) allocation, and a connectionless, prioritized contention-based service on a Carrier Sense Multiple Access/Collision Avoidance (CSMA/CA) allocation. The MAC receives MAC Service Data Units (MSDUs) and encapsulates them with a header, optional Arrival Time Stamp (ATS), and a checksum to create a stream of MAC frames. The stream is then divided into 512-octet segments, encrypted and encapsulated into serialized PHY Blocks (PBs), and packed as MAC Protocol Data Units (MPDUs) to the PHY unit which then generates the final PHY Protocol Data Unit (PPDU) to be transmitted onto the power line [2].

HomePlug AV2 enhances significantly the capability above to accommodate new generation of multimedia applications with Gigabit performance.

2.2. The HomePlug AV2 Technology. The HomePlug system is specified for in-home communication adapted to the power line channel. The in-home communications are established with Time Division Duplexing (TDD) mechanism to allow for symmetric communication between peers, as opposed to the classical access system in ADSL with two different downstream and upstream throughputs.

The PHY layer employs OFDM modulation scheme for better efficiency and adaptability to the channel impairments (such as being frequency selective and suffering from narrowband interference and impulsive noise). The HomePlug AV2 OFDM parameters correspond to a system with 4096 carriers

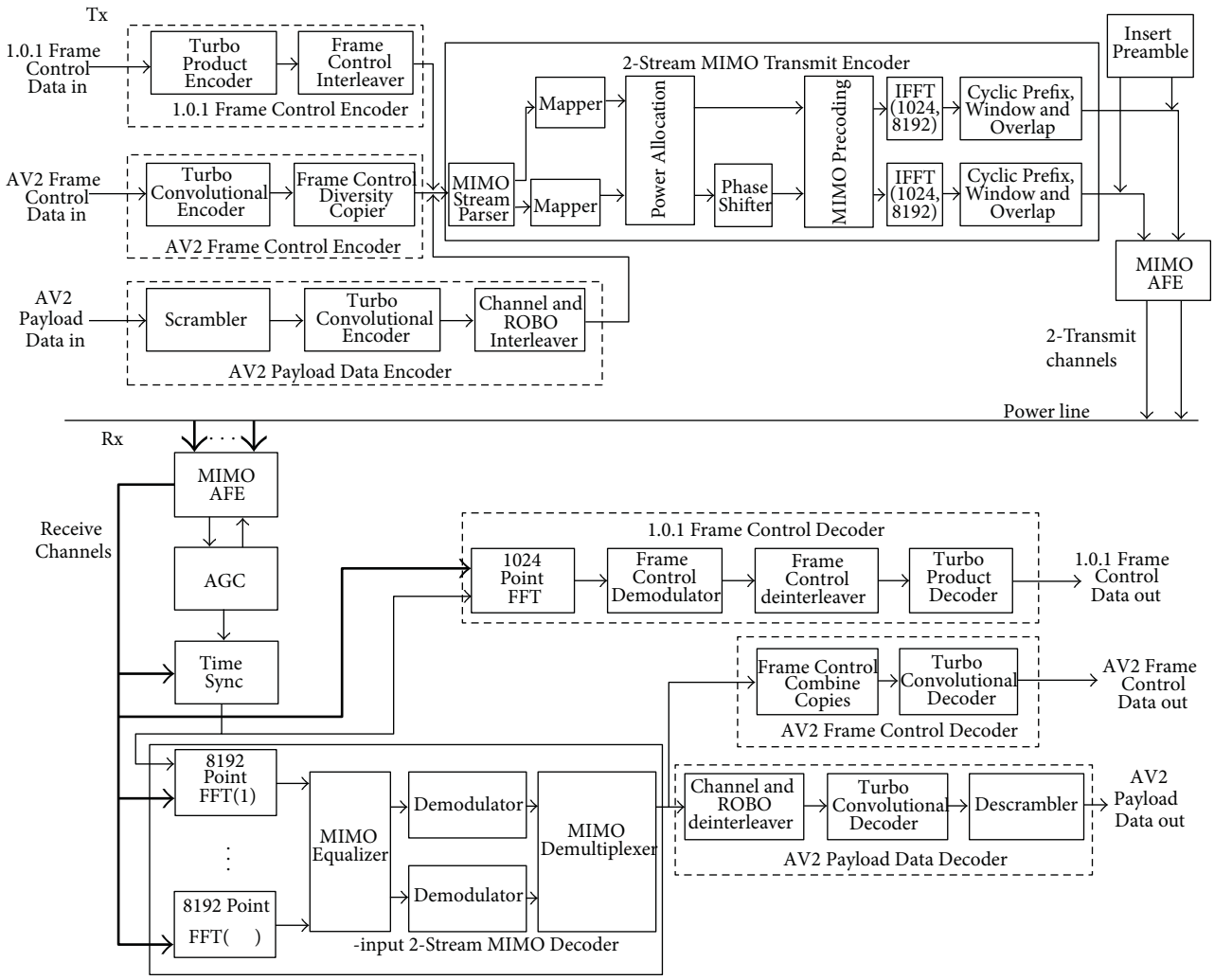

Figure 1: HomePlug AV2 transmitter and receiver PHY layer.

in 100 MHz, but only carriers from 1.8 to 86.13 MHz are supported for communication (3455 carriers). The subcarrier spacing of 24.414 kHz was chosen in the HomePlug AV system according to the power line coherence bandwidth characteristic and is maintained in HomePlug AV2 for interoperability.

More significantly, HomePlug AV2 incorporates MIMO capability (see details in the next sections) to improve throughput and coverage.

A block diagram of the PHY layer is shown in Figure 1. The HomePlug AV2 system is capable of supporting two network operating modes: AV-only mode and Hybrid mode (1.0.1 Frame Control Encoder in Figure 1). Hybrid mode is used for coexistence with HomePlug 1.0.1 stations. For that purpose, a 1.0.1 Frame Control Encoder is included for Hybrid modes and an AV2 Frame Control Encoder for both Hybrid and AV-only modes. The AV-only mode is used for communications in networks where only HomePlug AV and HomePlug AV2 stations are involved.

Besides, two OFDM paths are shown in order to implement the MIMO capabilities with 2 transmission ports.

Apart from the Hybrid or AV-only Frame Control symbols, the payload data can be sent using adaptive bit loading per carrier or robust modes (ROBO) with fixed Quadrature Phase Shift Keying (QPSK) constellation and several copies of data interleaved in both time and frequency.

Looking at the data path details in the block diagram (Figure 1), the following can be seen: at the transmitter side, the PHY layer receives its inputs from the MAC layer. Three separate processing chains are shown because of the different encoding for HomePlug 1.0.1 Frame Control (FC) data, HomePlug AV2 FC data, and HomePlug AV2 payload data. AV2 Frame Control data is processed by the AV2 Frame Control Encoder, which has a Turbo Convolutional Encoder and Frame Control Diversity Copier, while the HomePlug AV2 payload data stream passes through a Scrambler, a Turbo Convolutional Encoder, and an Interleaver. The HomePlug

1.0.1 Frame Control data passes through a separate HomePlug 1.0.1 Frame Control Encoder.

The outputs of the FC Encoders and Payload Encoder lead into a common MIMO OFDM modulation structure, consisting of a MIMO Stream Parser that provides up to two independent data streams to two transmit paths which include two Mappers, a phase shifter that applies a 90-degree phase shift to one of the two streams (to reduce the coherent addition of the two signals), a MIMO precoder to apply transmitter Beamforming operations, two Inverse Fast Fourier Transform (IFFT) processors, preamble and Cyclic Prefix insertion, and symbol Window and Overlap blocks, which eventually feed the AFE module with one or two transmit ports that couple the signal to the power line medium.

At the receiver, an AFE with one, two, three, or four (N_R) receive ports operates with individual Automatic Gain Control (AGC) modules and one or more time-synchronization modules to feed separate Frame Control and payload data recovery circuits. Receivers plugged to power outlets which are connected to the three wires Line, Neutral, and Protective Earth might utilize up to three differential mode Rx ports and one common mode Rx port.

The Frame Control data is recovered by processing the received signals through a 1024-point FFT (for HomePlug 1.0.1 delimiters) and multiple 8192-point FFTs, and through separate Frame Control Decoders for the HomePlug AV2/AV and HomePlug 1.0.1 modes. The payload portion of the sampled time domain waveform, which contains only HomePlug AV2 formatted symbols, is processed through the multiple 8192-point FFT (one for each receive port), a MIMO Equalizer that receives N_R signals, performs receive Beamforming, and recovers the two transmit streams, two Demodulators, a Demultiplexer to combine the two MIMO streams, and a channel deinterleaver followed by a Turbo Convolutional Decoder and a Descrambler to recover the AV2 payload data.

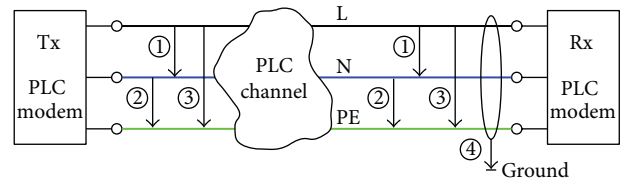

Figure 2: MIMO-PLC channel: different feeding and receiving options.

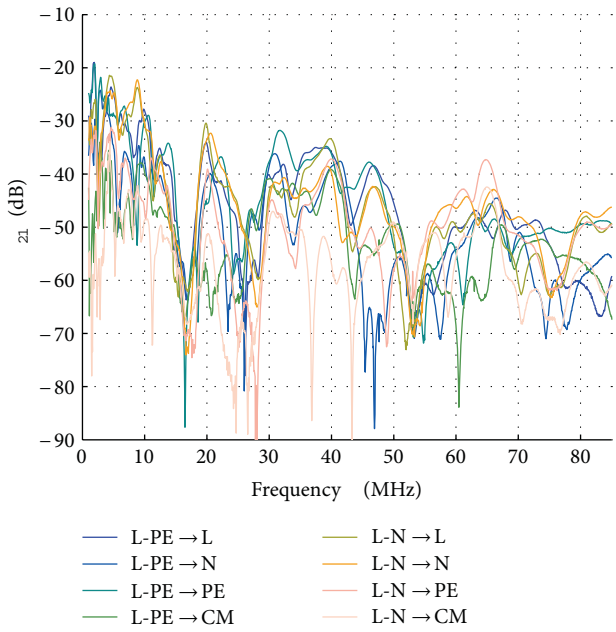

Figure 3: Magnitude of the transfer functions (S_{21}, forward scattering parameter) of all MIMO paths of a 2 × 4 MIMO configuration.

3. PHY Layer Improvements of HomePlug AV2

3.1. Multiple-Input Multiple-Output (MIMO) Capabilities with Beamforming. The HomePlug AV2 specification incorporates Multiple-Input Multiple-Output (MIMO) capabilities with Beamforming, which offers the benefit of improved coverage throughout the home, particularly for hard to reach outlets. MIMO technology enables HomePlug AV2 devices to transmit and receive on any two-wire pairs within a three-wire configuration. Figure 2 shows a three-wire configuration with Line (L), Neutral (N), and Protective Earth (PE). Whereas HomePlug AV always transmits and receives on the Line-Neutral pair (port 1 in Figure 2), HomePlug AV2 modems can transmit and receive signals on the other pairs as well. Any two pairs formed by the Line, Neutral, or Protective Earth wires (i.e., L-N, L-PE, and N-PE) can be used at the transmitter. At the receiver, up to four receive ports may be used according to Figure 2. The common mode (CM) signal—indicated as port 4 in Figure 2—is the voltage difference between the sum of the three wires and the ground.

The numbers of used transmit ports N_T and used receive ports N_R define the MIMO configuration, which is called $N_T \times N_R$ MIMO. For example, using L-N and L-PE to feed and receive signals results in a 2 × 2 MIMO configuration. HomePlug AV2 specification supports MIMO configurations with up to 2 Tx ports and up to N_R Rx ports.

Some regions and maybe homes with older electrical installations do not have the third wire installed in the private buildings. In this scenario, HomePlug AV2 automatically switches to Single-Input Single-Output (SISO) operating mode. HomePlug AV2 incorporates also selection diversity in SISO mode. The ports used for feeding and receiving might be different from the traditional L-N feeding. If, for example, the path from L-PE to L-N offers better channel characteristics than L-N to L-N, the transmitter can choose to use the L-PE port for feeding.

Figure 3 shows the magnitude of several transfer functions of a typical MIMO-PLC channel. The figure illustrates all eight possible paths of a 2 × 4 MIMO configuration where L-N and L-PE pairs are used as feeding and all four receive ports are used as receiving. The example shows that the signal

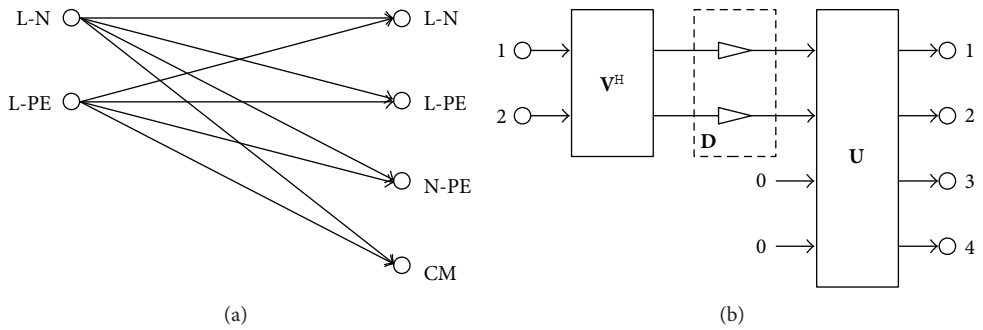

FIGURE 4: Schematic MIMO channel and decomposition into parallel and independent *MIMO streams*.

fed into one port is visible at all receive ports. Crosstalk caused by the coupling of the wires results in the presence of all possible MIMO paths. At most frequencies the S_{21} (forward scattering parameter of the network analyzer) curves are quite independent. As less correlation the S_{21} curves show, as higher is the gain by MIMO. For some frequencies, for example in the region of the fading degradation around 16 MHz, the shapes of the transfer functions are similar due to the same underlying topology of the different MIMO paths. Usually, the wires are located in parallel within the walls facing a similar multipath propagation. This results in a higher spatial correlation of the MIMO-PLC channel than compared to radio MIMO channels.

More information about the MIMO-PLC channel characteristics and channel modeling may be found in [6–18].

The channels presented in Figure 3 were recorded with a delta coupler at the transmitter (L-PE, L-N) and a star coupler at the receiver (L, N, PE, CM). This coupler combination allows 2×4 MIMO [19].

The MIMO-PLC channel is described by a $N_R \times N_T$ channel matrix for each OFDM subcarrier c:

$$\mathbf{H}(c) = \begin{bmatrix} h_{11}(c) & \cdots & h_{1N_T}(c) \\ \vdots & \ddots & \vdots \\ h_{N_R1}(c) & \cdots & h_{N_RN_T}(c) \end{bmatrix} \quad (1)$$

with c belonging to the set of used subcarriers (depending, e.g., on the frequency band and tone mask).

Figure 4(a) shows the schematic MIMO channel for a 2×4 MIMO configuration with the overall 8 MIMO paths. HomePlug AV2 supports 1 or 2 streams (see Section 3.1.1). As HomePlug AV2 supports MIMO configurations with up to 2 Tx ports and up to N_R Rx ports, the maximum number of supported *streams* in AV2 is 2. The number of the underlying *MIMO streams* depends on the rank of the channel matrix. If the channel matrix has full rank, the number of *MIMO streams* is $= \min(N_T, N_R)$. The underlying *MIMO streams* are obtained by a Singular Value Decomposition (SVD) of the channel matrix [20]:

$$\mathbf{H}(c) = \mathbf{U}(c)\,\mathbf{D}(c)\,\mathbf{V}(c)^H, \quad (2)$$

where $\mathbf{V}$ and $\mathbf{U}$ are unitary matrices, that is, $\mathbf{V}^{-1} = \mathbf{V}^H$ and $\mathbf{U}^{-1} = \mathbf{U}^H$ (with H the Hermitian operator) and $\mathbf{D}$ is a diagonal matrix containing the singular values of $\mathbf{H}$. Figure 4(b) illustrates this decomposition.

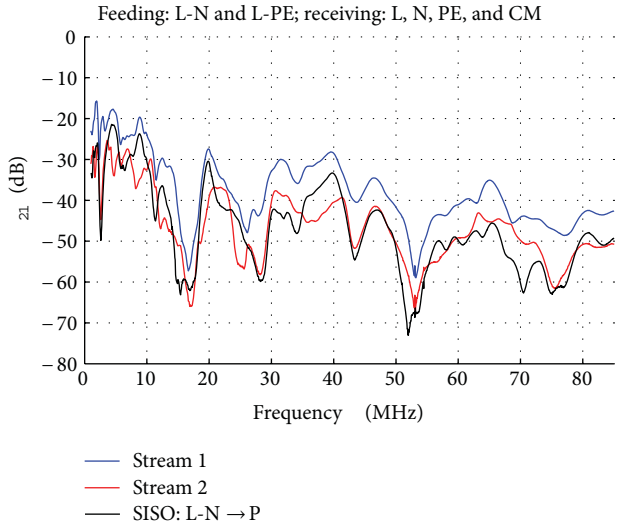

FIGURE 5: Attenuation of the decomposed PLC-MIMO channel of Figure 3.

Figure 5 shows the decomposition of the two *streams* of the MIMO-PLC channel shown in Figure 3. As a comparison, the attenuation of the SISO channel is also depicted.

The decomposition into parallel and independent *streams* by means of the SVD illustrates the MIMO gain; instead of having one spatial stream in SISO, two independent spatial *streams* are available in a $2 \times N_R$ MIMO configuration with $N_R \geq 2$ doubling in average the MIMO capacity [9, 12, 13, 21]. This fact is also verified by means of Figure 5; the first spatial stream shows less attenuation compared to the SISO channel; the second stream is slightly higher attenuated compared to SISO. Hence, in this example, the MIMO link would result in more than twice the capacity of the SISO link.

3.1.1. MIMO Stream Parser. Depending on how many *streams* are used in the transmission, the payload bits have to be split into different spatial *streams*. This task is performed by the MIMO Stream Parser (MSP). The MSP splits the incoming

bits into one or two streams based on the MIMO mode of operation and the Tone Map information (see Figure 1). To transmit a single-stream payload with Spot-Beamforming (see Section 3.1.3) or for SISO transmissions, the MSP sends all the data at its input to the first Mapper. In this case, the MSP operates as if it had only one output and it was connected to the first mapper in Figure 1. To transmit a two-stream payload with Eigen-Beamforming (see Section 3.1.3), the MSP allocates the bits to the two streams.

3.1.2. Precoding. Precoded Spatial Multiplexing or Beamforming was chosen as the MIMO scheme as it offers the best performance by adapting the transmission in an optimum way to the underlying Eigen modes of the MIMO-PLC channel. The best performance is achieved for various channel conditions. On the one hand, the full spatial diversity gain is achieved in highly attenuated and correlated channels when each symbol is transmitted via each available MIMO path. On the other hand, a maximum bit rate gain is achieved for channels with low attenuation when all available spatial streams are utilized. Beamforming also offers flexibility with respect to the receiver configuration. Only one spatial stream may be activated by the transmitter when only one receive port is available, that is, if the outlet is not equipped with the 3rd wire or if a simplified receiver implementation is used that supports only one spatial stream. Since Beamforming aims to maximize one MIMO stream, the performance loss of not utilizing the second stream is relatively small compared to the Spatial Multiplexing schemes without precoding. This is especially true for highly attenuated and correlated channels, where the second MIMO stream carries only a small amount of information. These channels are most critical for PLC and adequate MIMO schemes are important. A comparison and analysis of different MIMO schemes may be found in [14, 21, 22].

Beamforming requires knowledge about the channel state information at the transmitter to apply the optimum precoding. Usually, only the receiver has channel state information, for example, by channel estimation. Thus, the information about the precoding has to be fed back from the receiver to the transmitter. The HomePlug AV2 specification supports adaptive modulation [23, 24]. The application of adaptive modulation also requires feedback about the constellation of each subcarrier (Tone Map); that is, the feedback path is required anyway. The information about the Tone Maps and the precoding are updated simultaneously upon a change in the PLC channel (realized by a channel estimation indication message). The information about the precoding is quantized very efficiently and the amount required for the precoding information is in the same order of magnitude as the information about the Tone Maps. Thus, the overhead in terms of management messages and required memory can be kept low.

The optimum linear precoding matrix $\mathbf{F}$ for a precoded Spatial Multiplexing system can be factored into the two matrices $\mathbf{V}$ and $\mathbf{P}$ [25]:

$$\mathbf{F} = \mathbf{VP}. \tag{3}$$

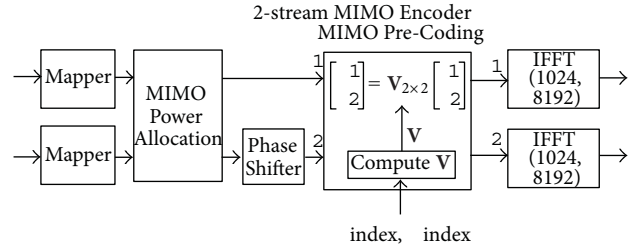

Figure 6: Precoding at the transmitter.

Note that the subcarrier index is omitted in (3) and in the following section to simplify the notation and to allow better legibility. However, it has to be kept in mind that the following vector and matrix operations are applied to each subcarrier separately if not stated otherwise.

$\mathbf{P}$ is a diagonal matrix that describes the power allocation of the total transmit power to each of the transmit streams. Power allocation is considered in more detail in Section 3.1.4. $\mathbf{V}$ is the right hand unitary matrix of the SVD of the channel matrix (see (2)). Precoding by the unitary matrix $\mathbf{V}$ is often referred to as unitary precoding or Eigen-Beamforming.

Figure 6 shows the basic MIMO blocks of the transmitter. The Mappers of the two streams follow the MIMO stream parser (see Figure 1). The two symbols of the two streams are then weighted by the power allocation coefficients and multiplied by the matrix $\mathbf{V}$ (the computation of $\mathbf{V}$ is explained in Section 3.1.3 in more detail). Finally, each stream is OFDM modulated separately.

3.1.3. Beamforming and Quantization of the Beamforming Matrix. The precoding matrix $\mathbf{V}$ is derived by means of the SVD (see (2)) from the channel matrix $\mathbf{H}$.

There are two possible modes of operation. If only one spatial stream is utilized, single-stream Beamforming (or Spot-Beamforming) is applied. In this case, the precoding is described by the first column vector of $\mathbf{V}$; that is, the precoding simplifies to a column vector multiplication. Note that despite the fact that only one spatial stream is used, both transmit ports are active as the precoding vector splits the signal to two transmit ports. If both spatial streams are used, two-stream Beamforming (or Eigen-Beamforming) is used and the full precoding matrix $\mathbf{V}$ is applied in the MIMO precoding block in Figure 6.

Since the information about the precoding matrix has to be fed back from the receiver to the transmitter, an adequate quantization is required. To achieve this goal, the special properties of $\mathbf{V}$ are utilized.

The unitary property of $\mathbf{V}$ consequences that the columns $\mathbf{v}_i$ $(i = 1, 2)$ of $\mathbf{V}$ are orthonormal; that is, the column vectors are orthogonal and the norm of each column vector is equal to 1 [26]. There is more than one unique solution to the SVD; the column vectors of $\mathbf{V}$ are phase invariant; that is, multiplying each column vector of $\mathbf{V}$ by an arbitrary phase rotation results in another valid precoding matrix.

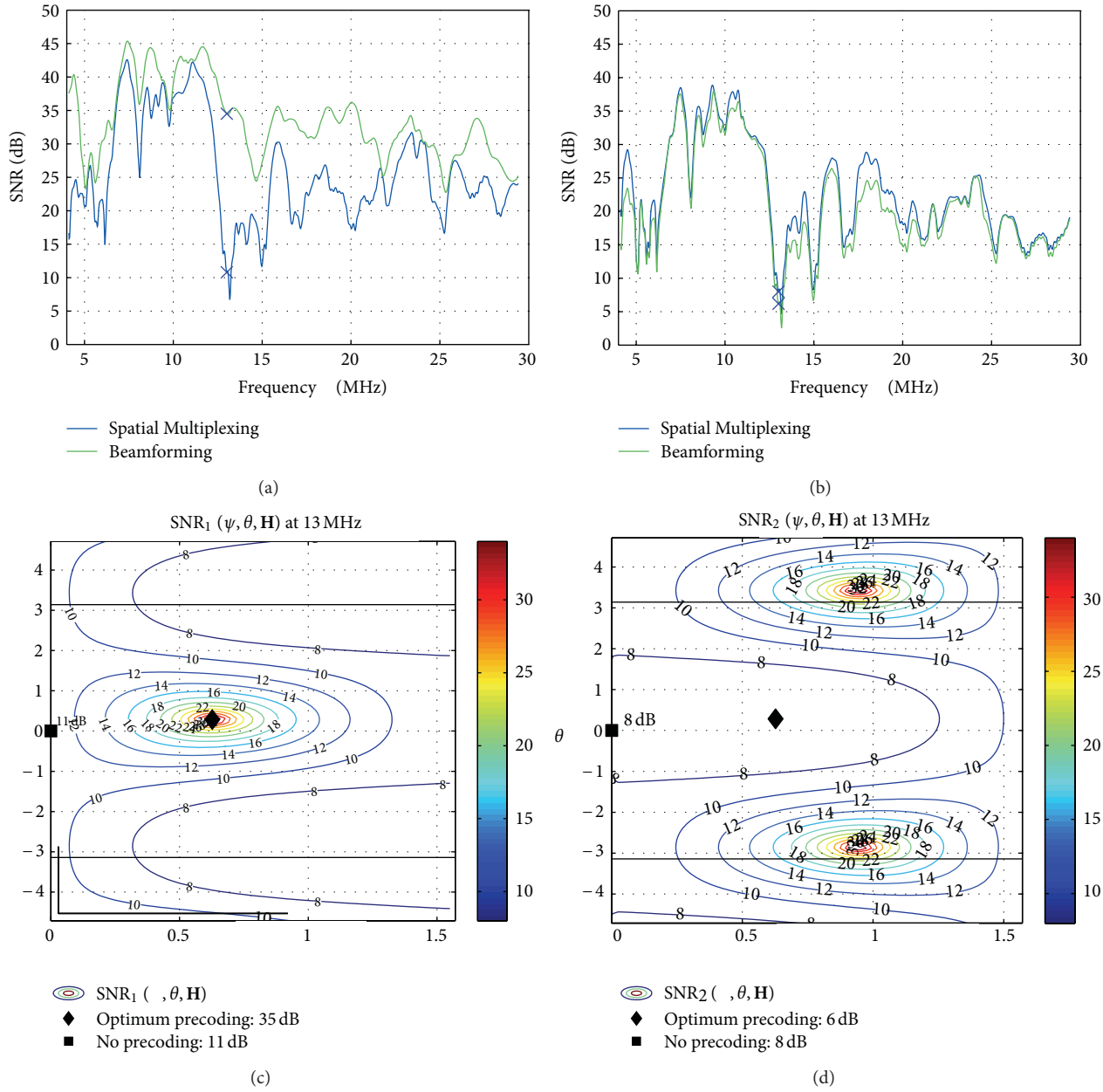

FIGURE 7: Influence of precoding on the SNR: SNR of the first (a) and second (b) streams with and without precoding, transmit power to noise power of $\rho = 65$ dB, 40 dB average channel attenuation; SNR depending on the precoding matrix at 13 MHz of the first (c) and second (d) streams.

These properties allow to represent the complex 2×2 matrix $\mathbf{V}$ by only the two angles θ and ψ:

$$\mathbf{V} = \begin{bmatrix} \mathbf{v}_1 & \mathbf{v}_2 \end{bmatrix} = \begin{bmatrix} v_{11} & v_{12} \\ v_{21} & v_{22} \end{bmatrix} = \begin{bmatrix} \cos\psi & \sin\psi \\ -e^{j\theta}\sin\psi & e^{j\theta}\cos\psi \end{bmatrix}, \quad (4)$$

where the range of θ and ψ to represent all possible Beamforming matrices is $0 \leq \psi \leq \pi/2$ and $-\pi \leq \theta \leq \pi$.

According to the phase-invariance property, the first entry of each column (v_{11}, v_{12}) may be set to be real without loss of generality, as defined in (4). It is easy to prove that the properties of the unitary precoding matrix are fulfilled. The norm of the column vectors is one: $|v_{11}|^2 + |v_{21}|^2 = |v_{12}|^2 + |v_{22}|^2 = \sin^2(\psi) + \cos^2(\psi) = 1$. Also, the two columns are orthogonal:

$$\mathbf{v}_1^H \mathbf{v}_2 = \sin(\psi)\cos(\psi) - \sin(\psi)\cos(\psi)\, e^{-j\theta} e^{j\theta} = 0. \quad (5)$$

In both modes, Spot-Beamforming and Eigen-Beamforming, the Beamforming vector or Beamforming matrix, respectively, is described by both angles θ and ψ. Thus, the signaling of θ and ψ is the same in both modes.

If the MIMO Equalizer is based on zero-forcing (ZF) detection, the detection matrix

$$\mathbf{W} = \mathbf{H}^{p} = \left(\mathbf{H}^{H}\mathbf{H}\right)^{-1}\mathbf{H}^{H} \tag{6}$$

is the pseudo inverse $\mathbf{H}^{\mathrm{P}}$ of the channel matrix $\mathbf{H}$. In case of Eigen-Beamforming with the precoding matrix $\mathbf{V}$, $\mathbf{H}$ can be replaced by the equivalent channel $\mathbf{HV}$ in (6) and the detection matrix can be expressed by

$$\mathbf{W} = \mathbf{V}^{H}\mathbf{H}^{p} = \mathbf{D}^{-1}\mathbf{U}^{H}. \tag{7}$$

The SNR of the MIMO streams after detection is calculated as

$$\mathrm{SNR}_1 = \rho\frac{1}{\left\|\mathbf{w}_1\right\|^2}, \qquad \mathrm{SNR}_2 = \rho\frac{1}{\left\|\mathbf{w}_2\right\|^2}, \tag{8}$$

with ρ being the ratio of transmit power to noise power and $\|w_i\|$ the norm of the ith row of the detection matrix $\mathbf{W}$.

Figure 7(a) shows the SNR of the first stream of a MIMO-PLC channel. The median attenuation of this link is 40 dB. The ratio of the transmit power to noise power is $\rho = 65$ dB. The blue line represents the SNR of Spatial Multiplexing without precoding and the green line represents the Eigen-Beamforming. The SNR of the 2nd stream is displayed in Figure 7(b).

The two markers X in Figure 7(a) mark a frequency (13 MHz) where good Beamforming conditions are found. Different precoding matrices influence the SNR of the two MIMO streams according to (6) and (8).

Figures 7(c) and 7(d) show the level of the gain or signal elimination due to Beamforming for the frequency marked by X in Figures 7(a) and 7(b). The color lines in Figures 7(c) and 7(d) indicate the SNR. Depending on the precoding matrix the SNR varies between 6 dB and 35 dB. No Beamforming ($\psi = 0$ and $\theta = 0$) would result in a SNR of 11 dB. As seen in Figure 7(c), there is one SNR maximum in the area spanned by ψ and θ. Due to both streams being orthogonal one shows an SNR minimum at the location where the other one has its maximum. The SNR plot in Figures 7(c) and 7(d) is 2π periodic in θ, where the black horizontal lines indicate $\theta = \pm\pi$.

The Beamforming matrix is quantized efficiently to reduce the amount of feedback required to signal $\mathbf{V}$. This quantization is chosen such that the loss of the SNR after detection (refer also to (6) and (8)) is within 0.2 dB compared to optimum Beamforming without quantization.

3.1.4. Power Allocation. MIMO power allocation is applied to two-stream MIMO transmissions. The power allocation adjusts the power of a carrier on one stream relative to the other stream. For SISO transmissions and MIMO Spot-Beamforming transmissions, MIMO power allocation can be bypassed since there is only one transmit stream. In this case, the only available option is to allocate all the power to the single stream. The power allocation module is located between the Mapper and the precoding block (see Figure 1) and performs on the two MIMO streams before Eigen-Beamforming. The power allocation in AV2 is designed in a way not to feed back additional information from the receiver to the transmitter. The power allocation evaluates the Tone Maps of the two streams to set the power allocation coefficients of the two streams. It was shown that the performance is very close to the optimum power allocation (mercury water filling [27]). Power allocation improves especially highly attenuated channels at the high coverage point.

3.1.5. Precoding Grouping. HomePlug AV2 devices support an expanded frequency spectrum (up to 86.13 MHz, see Section 3.2) and one additional stream (utilizing MIMO) compared to the 30 MHz for HomePlug AV devices. Thus, HomePlug AV2 devices need to store two Tone Maps (one for each stream) and one precoding matrix (PCM) per carrier. This significantly increases the memory requirements for an AV2 modem. In order to save memory, HomePlug AV2 devices transmit and store the PCM only on a subset of carriers called precoding pilot carriers. At the transmitter, the PCMs for the carriers between two adjacent precoding pilot carriers are obtained via interpolation. The spacing between the precoding pilot carriers is selected out of a set of predefined values and may be adjusted depending on the memory capabilities or channel conditions. The more memory is embedded in the modems, the finer the granularity is. The performance loss of precoding grouping compared to the quantization of each subcarrier separately is marginal due to the high correlation of the precoding matrices of neighbored subcarriers. An investigation about different precoding grouping algorithms for MIMO-PLC may be found in [14].

3.2. Extended Frequency Band up to 86 MHz. During the specification development, the AV TWG realized a measurement campaign, where power line channel and noise measurements were performed in 30 homes located in different countries, from Europe to USA. Such variability was a key ingredient to obtain insight into the power line at frequencies above those used in HomePlug AV (1.8–30 MHz). In particular, in every home, all the possible links among at least 5 different nodes were measured.

Examples of recorded channel attenuation and noise PSD are reported in Figures 8 and 9, respectively.

Based upon the results of the measurement campaign, the present EMC regulations, coverage, and complexity targets, the final outcome of the analysis was the selection of the 30–86 MHz band for the following reasons.

(i) The FM band region 87.5–108 MHz shall be avoided. In fact this frequency region presents higher attenuation and higher noise compared to the 30–86 MHz band (see also Figures 8 and 9). Since, probably, lower transmit level requirements will be needed in order to not interfere with the FM radio service, very low operating SNRs are obtained in this band with negligible coverage increase;

(ii) The 30–86 MHz frequency band appears to offer a throughput increase especially at the low to mid coverage percentages; the reason is that while the

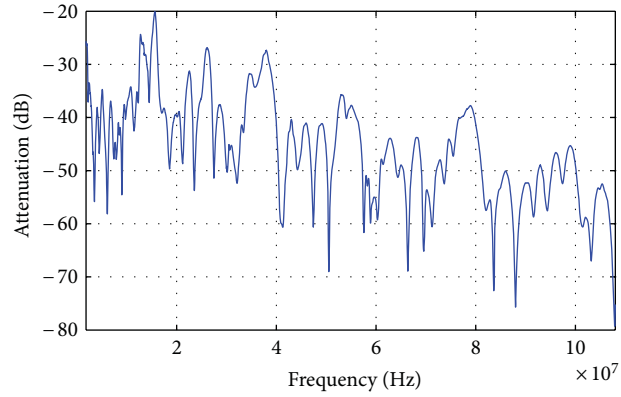

Figure 8: HomePlug AV2 measurement campaign. Example of channel measurement.

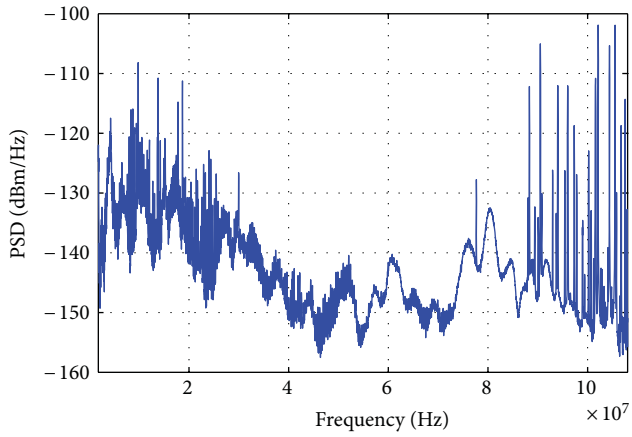

Figure 9: HomePlug AV2 measurement campaign. Example of noise measurement.

attenuation is greater compared to the 1.8–30 MHz band, noise is lower. A concern derives from the fact that EMC requirements for the 30–86 MHz frequency band are generally tighter than in the 1.8–30 MHz band. However, this observation could be mitigated in view of the fact that, for instance, the upcoming standard FprEN 50561-1 appears to be more restrictive in the 1.8–30 MHz frequency band.

(iii) Within the HomePlug AV2 specification it has been possible to provide flexibility in choosing the stop frequency in the 30–86 MHz interval. In particular, an AV2 device implementing a frequency band 1.8-X MHz band (with $30 < X < 86$) will be interoperable with a device implementing a frequency band 1.8-Y MHz (with $30 < Y < 86$, $X \neq Y$).

(iv) The 30–86 MHz frequency band extension allows devices to be fully interoperable with the IEEE 1901 devices that use the 1.8–50 MHz frequency band. In fact, HomePlug AV2 devices that implement a frequency band extension shall support at least the IEEE 1901 bandwidth.

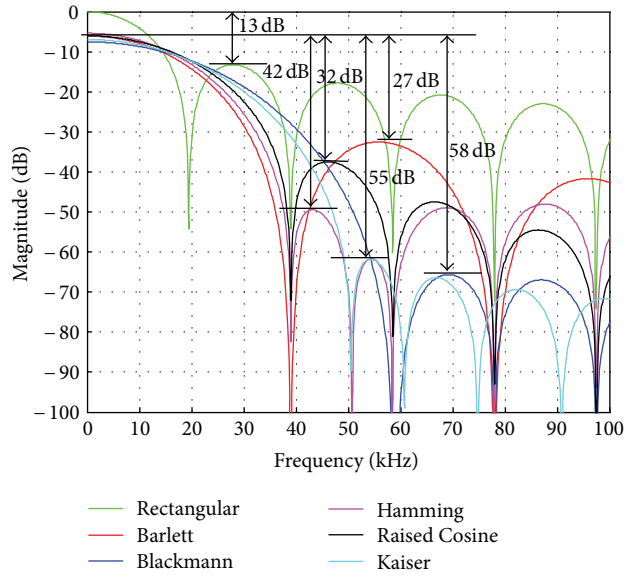

Figure 10: OFDM side lobes of a single carrier. Comparison of various window functions.

3.3. Efficient Notching. HomePlug AV2 increases throughput by allowing devices to minimize the overhead incurred due to EMC notching requirements. While in HomePlug AV the mechanism ("windowed OFDM") for creating the PSD notches is fixed and relatively conservative, HomePlug AV2 devices may gain up to 20% in efficiency if they implement additional techniques to accommodate sharper PSD notches. The 20% includes the gain of guard carriers which were excluded by HomePlug AV modems and the reduced Transition Interval in time domain. Such devices gain additional carriers at the band edges and may utilize shorter cyclic extensions, which reduces the duration of the OFDM symbols.

3.3.1. Influence of Windowing on Spectrum and Notch Shape. The FFT process uses a rectangular window to cut data out of a continuous stream to convert them from time to frequency domain. The FFT of a rectangular function in the time domain is a $\sin(x)/x$ function in the frequency domain. The $\sin(x)/x$ becomes 0 at integer multiples of π. Some parts of the signal remain in-between the zeros, which results in the unwanted side lobes of an FFT OFDM system. Figure 10 shows a $\sin(x)/x$ function as green curve. The frequency axis is shown horizontally. The level in a logarithmic view is presented on the vertical axis.

The process of multiplying a window with an OFDM symbol (see Figure 11) in the time domain aims to suppress the sharp corners at the beginning and the end of the OFDM symbol in order to get smooth transitions. This affects the shape and distances of the side lobes in the frequency domain [28]. There are numerous types of window functions available for implementation such as Hamming, Barlett (triangular), Kaiser, Blackman, Raised Cosine (Hann), and so forth. A comparison of various window waveforms with the achieved side lobe attenuation is shown in Figure 10 which also serves

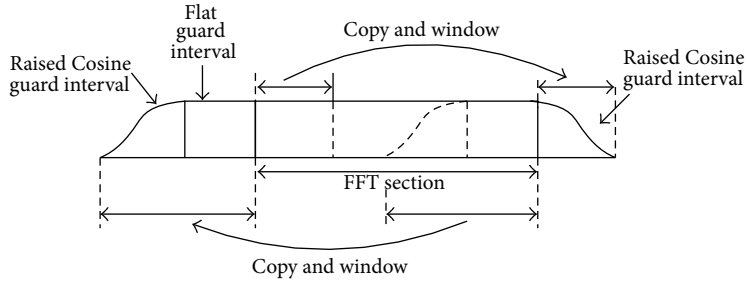

Figure 11: OFDM symbol with GI and window.

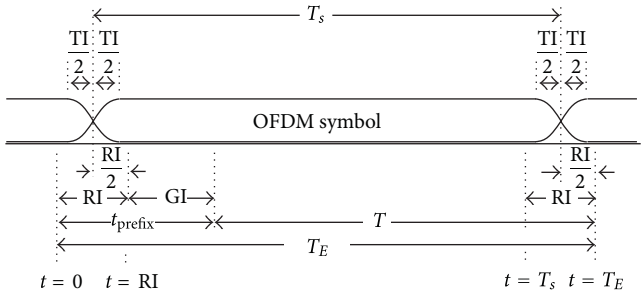

Figure 12: Consecutive OFDM symbols, guard interval (GI), roll-off interval (RI), and windowing.

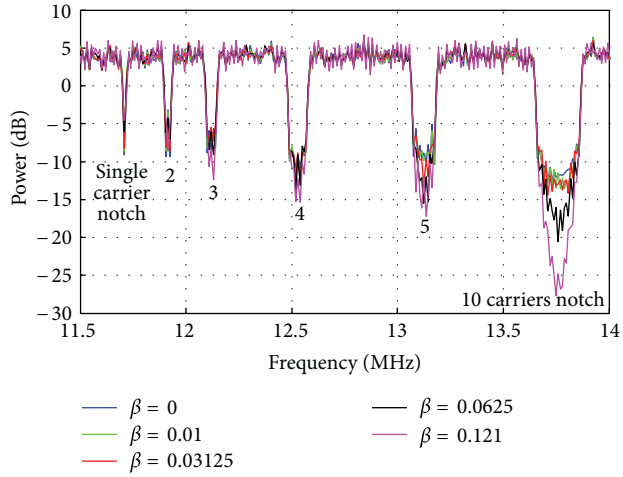

Figure 13: OFDM spectra with different notch widths and depths achieved with different roll-off factors.

to illustrate the disadvantage of windowing. The side lobes are suppressed, but the main lobe stays wider. The first time the spectrum reaches zero, the distance for all windows is at least twice the frequency of the rectangular window used by the pure FFT. Windowing is considered to be state of the art in signal processing [29].

The process of how a window is applied is shown in Figure 11. The original OFDM symbol or the output of the IFFT at the transmitter is marked with "FFT section." As described above, the guard interval is copied from the tail samples to the beginning of the symbol. In order to create a window, the symbol has to be expanded further at the beginning and at the end by copying the bits as done for the Guard Interval (GI). This expansion is multiplied with the smoothly descending window. The more smoothly the signal approaches zero in the time domain, the lower the side lobes in the frequency domain. Of course, this expansion of a symbol is a waste of communication resources as it does not carry useful information and has to be cut by the receiver.

The two descending slopes in the time domain could overlap, to save communication resources at consecutive OFDM symbols, as shown in Figure 12. The new symbol time T_s is measured between the middles of the roll-offs before and after the symbol. The overlap region is the roll-off interval (RI) (see in Figure 12) which is related to the OFDM symbol duration T_s via the parameter β:

$$\mathrm{RI} = \beta T_s \tag{9}$$

and the total symbol length T_E:

$$T_E = (1 + \beta) \cdot T_s. \tag{10}$$

The HomePlug AV specification allows the usage of several Guard intervals [30, 31]. If the shortest guard interval is selected, HomePlug AV uses a β of RI/(T + GI) = 4.96 μs/(40.96 μs + 5.56 μs) = 0.1066.

With HomePlug AV2, the Transition Interval TI is introduced. The shape of the windowing is transmitter implementation dependent; it does not affect interoperability. The pulse shaping window and Guard interval might be reduced even to zero to minimize overhead in time domain and to notch efficiently. In order to guarantee backward compatibility with previous HomePlug versions the definition and timings of the parameter RI as shown in Figure 12 have to stay stable. In contrast to RI, the new parameter TI might be reduced to zero.

There is a balance between this intervals and obtaining a better side lobe attenuation.

Figure 13 shows the notch of any OFDM system spectrum which could be obtained by varying the roll-off factors (the β values) of the Raised Cosine window. Increasing the roll-off factor directly increases the amount of attenuation achieved inside the notches. However, this has the drawback of increased symbol length.

To create notches in the OFDM spectrum, a model is implemented using QAM modulation and notches of omitting a various number of carriers: 1, 2, 3, 4, 5, and 10. A max-hold function is implemented in order to create these

figures. The 10 carrier notch shows the spectral benefit of windowing. The influence of windowing is hardly visible up to the point of the 5-carrier notch. At the 5-carrier notch, the difference between no window and the highest simulated β is around 5 dB. The trade-off for this β is a 27% longer symbol time. At the 10-carrier notch, the center frequency is suppressed by more than 15 dB without windowing, but the adjacent side slopes of the used corner carriers are only improved by 5 dB.

The additional overhead in the time domain is extremely large compared to the improved notch depth. Windowing with a small roll-off factor is sufficient in order to suppress the side lobes outside the used spectrum, but it is not recommended to increase the depth of a single carrier notch.

In the case of the HomePlug AV specification using a β of 0.1066, some guard carriers on the left and right side of a protected frequency range have to be omitted to guarantee the depth of the notch. The North American Carrier Mask requests 10 notches in-between 1.7 MHz and 30 MHz. The first carriers as well the last carriers of this spectrum are notched. These two notches have only one slope to the carriers allocated for communications. All other notches have two slopes resulting in 18 notch slopes in total. The spectrum loses almost 6% of communication resources in frequency domain. Additionally the β causes almost 13% of wasted resources in time domain. Assuming an ideal implementation with maximal sharpness in time as well as frequency domain, it would be possible to regain these communication resources when applying the North American Carrier Mask. If the frequency spectrum becomes more fragmented because of additional notches like requested by the newly upcoming European regulations [32] these losses become even more obvious.

3.3.2. Digital, Adaptive Band Stop Filters Improve the Notch's Depth and Slopes. Of course an ideal implementation as described above is not possible, but digital band stop filters increase the sharpness of the notches as well the implementation efforts in hardware. Shrinking the semiconductor manufacturing process to smaller structures, allowing to integrate additional functions on the same die size, shifts the balance towards hardware implementation efforts.

HomePlug AV2 specification gives maximum freedom to the chip implementer. Filter algorithm, order, and structure are implementation dependent. An example is documented in [19]. As higher the filtering efforts, as better is the sharpness of the notch slopes, as shorter might be GI, as higher the resources available for communication. A reduction of the Guard Interval down to zero (see Section 3.5.1) is possible at short PLC channels without multipath reflections or intersymbol interference.

3.4. HomePlug AV2 Power Optimization Techniques. The HomePlug AV2 standard introduces two novel techniques that can be used to optimize the use of transmit power. The first one, named "transmit power back-off", is a technique that reduces the transmitted power spectral density for a selected set of carriers when this can be done without adversely affecting performance. Conversely, the second technique, called "EMC Friendly Power Boost" is a technique that allows the transmitter to increase the power on some carriers with the knowledge that this can be done without exceeding regulatory limits.

3.4.1. Power Back-Off. In power line communications the transmit power limit is typically defined as a power spectral density (PSD) mask applicable over the range of frequencies used in the standard. And since power line modems are directly connected to the electrical wiring, they are traditionally designed to transmit with the maximum allowed transmit PSD on each frequency (i.e., they do not need to be sensitive to a limited battery supply). In many cases maximizing transmit power leads to the best performance; however, certain definitions of PSD masks combined with certain channel conditions can produce cases where modems can benefit from transmitting at less than the maximum allowed power level.

We illustrate the benefits of transmit power control using the North American regulatory limits as an example. FCC regulations that are applicable to power line devices in North America are commonly interpreted to allow a transmit PSD of −50 dBm/Hz from 1.8 to 30 MHz, and −80 dBm/Hz from 30 MHz up to 86 MHz. This 30 dB drop in the PSD (at 30 MHz) causes the signal from the higher frequency carriers (above 30 MHz) to have much smaller amplitude than the signal for the low band carriers (up to 30 MHz). Consequently, when the overall signal is represented in a quantized digital domain, the high band signal has lower resolution than the signal in the lower band and will therefore also have a limited SNR. This will be evident at the transmitter where the 30 dB drop will result in a reduction of 5 bits of resolution for the high band signal. If the transmit power is backed off in the low band, so that the PSD drop is reduced, then the high band signal will be represented with an increased number of bits of resolution and enjoy increased SNRs out of the transmitter.

Another limiting factor is the limited dynamic range of the analog to digital converter (ADC). We illustrate its impact using once again the example of the North American PSD limits. For the sake of simplicity, we assume a flat power line channel, and flat noise spectrum in Figure 14. For convenience, the power line channel (cyan curves labeled Rx signal: the transmitted signal after channel attenuation) and noise (green curves labeled Rx noise) contributions to the received signal are shown separately. Moreover, the different signals are shown before (dashed line curves) and after (continuous line curves) the analog amplifier. On the left of Figure 14 the scenario without power back-off is shown; the transmitted signal is 30 dB greater in the 1.8–30 MHz band compared to the 30–86 MHz band. The analog amplifier brings the received signal to a level A tailored to optimize the ADC conversion. Since the dominating noise is the ADC noise (black curve), after the ADC converter SNRs of 35 dB and 5 dB are found below and above 30 MHz, respectively. On the right of Figure 14 the scenario with power back-off is shown: the transmitted signal is reduced by 10 dB

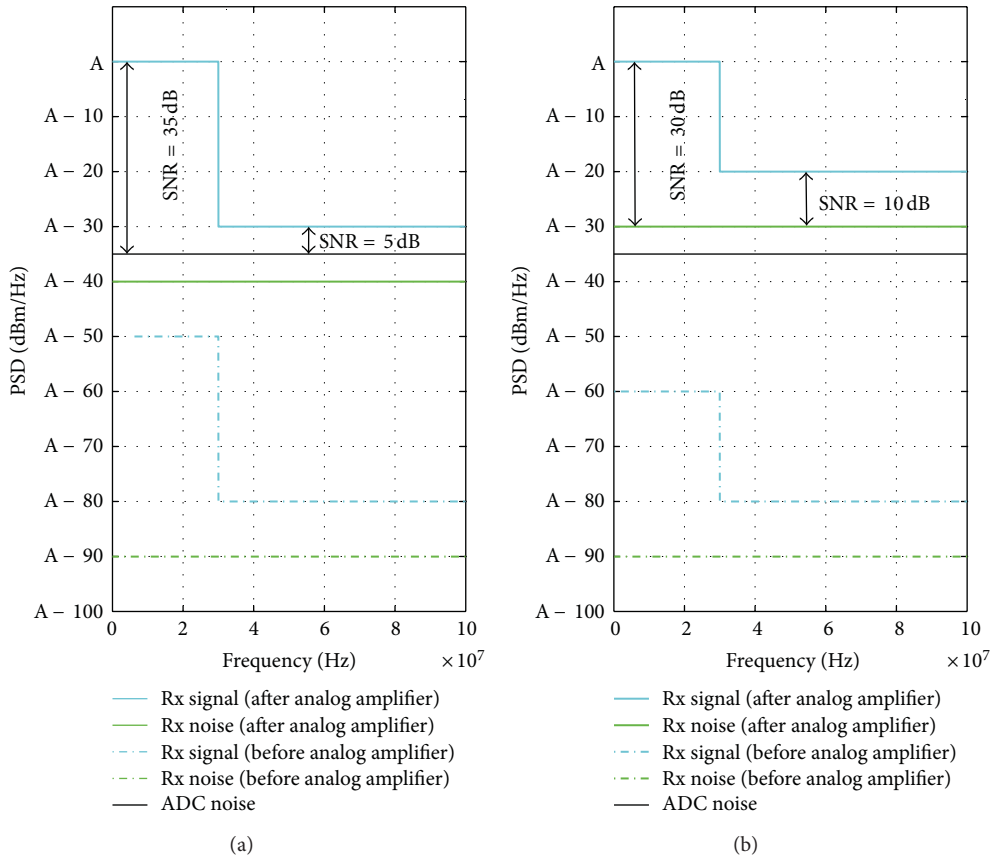

Figure 14: Benefits of power back-off. (a) No power back-off, (b) 10 dB power back-off.

in the 1.8–30 MHz frequency band so that it is only 20 dB greater compared to the 1.8–86 MHz band. Again, the analog amplifier brings the received signal to the A level. However in this case, the dominating noise is no longer the ADC noise and the obtained SNRs are 30 dB and 10 dB in the 1.8–30 MHz and 30–86 MHz, respectively.

In this example, the power back-off technique results in a 5 dB SNR reduction for the carriers in the lower frequency band, and a 5 dB SNR increase for the carriers in the upper frequency band. Given the larger bandwidth of the upper frequency band there will be an overall throughput gain due to transmit power back-off.

Transmit power back-off is also an effective interference mitigation technique. For instance, in Europe, the ability of a PLC transmitter to reduce the transmit power depending on the attenuation link is a possible requirement considered in [32], though the procedure described in [32] does not consider Quality of Service (QoS) requirements of PLC modems.

3.4.2. EMC Friendly Power Boost Using S_{11} Parameter. The EMC Friendly Power Boost is a mechanism introduced in the HomePlug AV2 specification to optimize the transmit power by monitoring the input port reflection coefficient at the transmitting modem. This coefficient is known as the S_{11} parameter. PSD limits as proposed in the HomePlug AV2 specification are based on representative statistics of the impedance match at the interface between the device port and the power line network. In practice, the input impedance of the power line network is frequency selective and varies for different network configurations. This leads to part of the transmit power being dissipated within the transmitter. The input port reflection coefficient, or input return loss, is characterized by the S-parameter S_{11}, and the part of transmit power dissipated at the transmitter is given by the amount $20 \cdot \log 10(|S_{11}|)$ in dB. In situations where the impedance mismatch is large (and thus the S_{11} parameter is large), only a small part of the input power is effectively transferred to the power lines. In those cases, the Electromagnetic Interference (EMI) induced by the PLC modem is reduced and can be much lower than the values recommended by EMC regulation limits.

In order to compensate for the frequency selective impedance mismatch at the interface between the device port and the power line network, HomePlug AV2 modems adapt their transmission mask, upon measurement of the S_{11} parameter at the transmitter. The transmitted signal power is increased by an Impedance Mismatch Compensation (IMC) factor, leading a more effective power transmission to the power line medium. While increasing the Tx power leads to

an increase of the radiated EMI, the design of the IMC factor ensures that the resulting EMI continuously falls below the targeted EMC regulation limits.

A statistical analysis was conducted on the practical values of the S_{11} parameter and the effectiveness of the EMC Friendly Power Boost technique based on a series of measurements performed by the ETSI Specialist Task Force 410 [6–10, 33]. S_{11} parameter and EMI measurements were taken over the 1 MHz–100 MHz range in 6 countries: Germany, Switzerland, Belgium, UK, France, and Spain. The modem used for measurements is described in [6–8].

The S_{11} measurements considered in this study consist of 3 differential feeding possibilities (L-N, N-PE, and PE-L), and 1 common mode feeding (CM). For the EMI measurements, we consider the measurements taken with different feeding possibilities, that is, differential feeding with the other differential ports being unterminated or terminated with 50 Ohm, and CM feeding.

The measurement set used in this analysis consists of 478 frequency sweeps, that can be categorized as follows:

(i) 6 different locations in Germany and 3 different locations in France.

(ii) 264 measurements outdoor at 10 m, 43 measurements outdoor at 3 m, and 171 measurements indoors.

Statistical analysis of this experimental data allowed designing the practical implementation of the EMC Friendly Power Boost technique. In the following, we define the Impedance Mismatch Compensation (IMC) factor as (in dB)

$$\mathrm{IMC}(k) = \min\left(\max\left(10\cdot\log_{10}\left(\frac{1}{1-\left|S_{11}(k)\right|^2}\right) - M(k), 0\right), \mathrm{IMC}_{\max}\right), \tag{11}$$

where $S_{11}(k)$ is the carrier dependent estimate of the S_{11} parameter, M is a margin accounting for possible estimate uncertainties in the measurement of parameter S_{11}, and $\mathrm{IMC}_{\max}$ is the maximum allowed value of the IMC factor in dB.

Figures 15 and 16 represent the statistical CDF of the S_{11} parameter as well as the corresponding IMC_0 factor, computed with a margin M of 0 dB. These statistics are based on the experimental data collected during the ETSI STF 410 measurement campaign.

On Figure 15, one can read that the S_{11} parameter is larger than −10 dB for 80% of the cases. This means that for 80% of the records, more than 10% of the energy is reflected back towards the transmitter.

More interestingly, Figure 16 gives an idea of the potential power increase offered by the EMC Friendly Power Boost technique.

(i) For 40% of the records, the Tx power could be increased by more than 2 dB to compensate for the impedance mismatch.

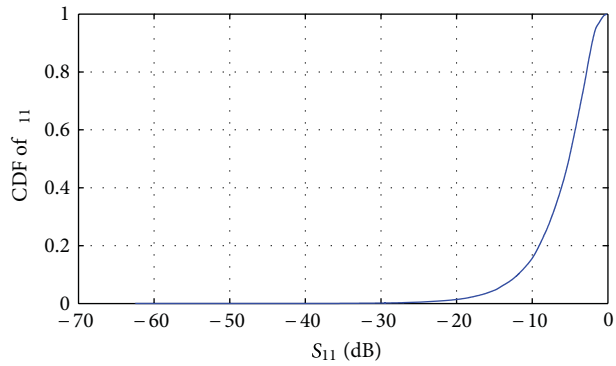

Figure 15: CDF of S_{11} parameter.

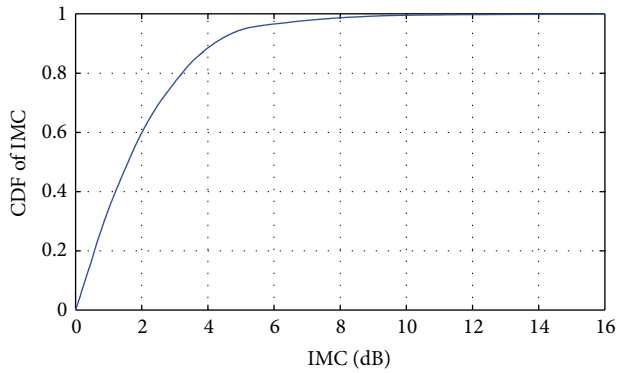

Figure 16: CDF of IMC parameter.

(ii) For 10% of the records, the Tx power could be increased by more than 4 dB to compensate for the impedance mismatch.

We then focused on the effect of the EMC Friendly Power Boost technique on the radiated EMI statistics. The recorded values allowed the computation of two statistics:

(i) the statistical CDF of the recorded EMI in terms of E-field for all frequencies and feeding possibilities without applying any power boost,

(ii) the statistical CDF of the recorded EMI in terms of E-field for all frequencies and feeding possibilities when applying the EMC Friendly Power Boost.

Figure 17 presents, for each percentile of the CDF, the difference in dB between the E-Field CDFs for the two methods of transmission.

Different observations can be made from this figure. First, the application of the EMC Friendly Power Boost leads to an increase of the radiated field CDF comprised between 0 and 6 dB. Note that the extreme value of 6 dB arises for one of the lowest values of radiated field, and, hence, is not relevant. Secondly, in general, the application of the EMC Friendly Power Boost increases the radiated power CDF by about 2 dB. More importantly, the increase of the radiated power CDF is lower than 2 dB for the 25% most radiating cases. This practically means that in the worst case scenarios where the

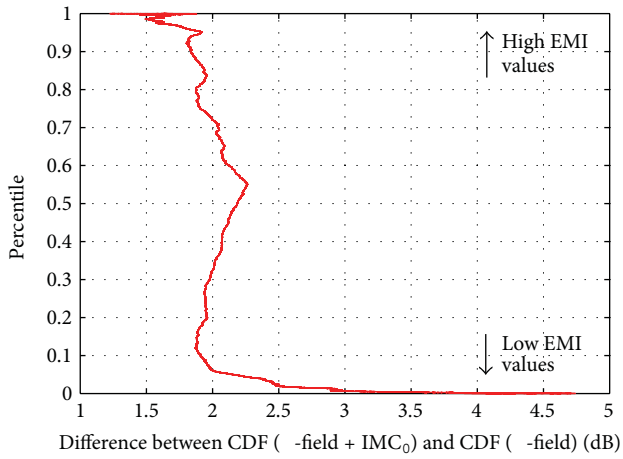

Figure 17: Difference in dB between the CDFs of the radiated EMI before and after applying the EMC Friendly Power Boost.

modems produce the largest EMI, the application of the IMC factor does not increase the EMI by more than 2 dB. This value can be compared with the CDF of the IMC factor given in Figure 16. Although the IMC factor is larger than 2 dB in 40% of the cases and larger than 4 dB in 10% of the cases, the application of the EMC Friendly Power Boost techniques does not increase the radiated power CDF extreme values by more than 2 dB. Of course, even an increase of the EMI by 2 dB is not acceptable. Therefore, a margin M of 2 dB is applied when increasing the Tx power using the IMC factor.

Based on this study, we conclude that the application of the EMC Friendly Power Boost technique provides a significant gain in terms of transmit power increase for a large number of configurations, where the impedance mismatch causes the dissipation of the signal at the transmitter. In addition, the statistical analysis shows that this technique will not lead to an increase of the undesirable radiated interference, in particular in the worst EMI scenarios, as long as a margin M of 2 dB is used in the computation of the IMC factor, as specified in (11). Finally, a recommended limit for the maximum allowed value of the IMC factor is $\text{IMC}_{\text{max}} = 6$ dB.

3.5. Additional PHY Improvements. In addition to the MIMO technology, the frequency band extension, the Efficient Notching, and power optimization techniques such as the power back-off and the EMC friendly power boost, other elements of the PHY layer were modified as presented in the paragraphs below.

3.5.1. New Time Domain Parameters. In the HomePlug AV2 specification, a number of time domain parameters were refined. As the sampling frequency has increased from 75 MHz to 200 MHz, the number of time samples for a given symbol duration is increased by a factor 8/3; the IFFT interval is 8192 samples in length, and the number of samples in the HomePlug AV Guard Interval has increased accordingly. In addition, new features have been added:

(i) The Transition Interval defines the part of the Roll-off Interval dedicated to the transition window, allowing more flexibility in the choice of the window (see Section 3.3)

(ii) A new Guard Interval has been defined for the HomePlug AV2 Short Delimiter (see Section 4.2.1)

(iii) The payload symbol Guard Interval has been made variable and can be as short as 0 μs. It can also be increased up to 19.56 μs. This allows adaptation to a wide range of channel conditions and removes the overhead of the Guard Interval for channels that have either very low multipath dispersion, or that are completely limited by the receive noise and not by ISI.

3.5.2. Additional Constellations. In HomePlug AV, the maximum constellation size is 1024-QAM, corresponding to 10 coded bits per carrier. HomePlug AV2 also provides support for 4096-QAM, which corresponds to 12 bits per carrier. The higher constellation size increases the peak PHY rates by 20%. Practically, the increased throughput will be available mostly on average to very good channels, but even some of the poorer channels sometimes have frequency bands in which high SNRs can be achieved, and the increased constellation size can be used.

3.5.3. Forward Error Correction (FEC) Coding. HomePlug AV2 uses the same duobinary Turbo Code as HomePlug AV. In addition to the code rates of 1/2 and 16/21, HomePlug AV2 also provides support for a 16/18 code rate. This allows more granularity in the compromise between robustness and throughput degradation. For this new code rate, a new puncturing structure is defined, as well as a new channel interleaver. In addition, a new Physical Block size of 32 octets is defined, which includes specification of a new termination matrix for the FEC as well as a new interleaver seed table. The 32-byte octet PBs are used in the PHY level acknowledgements and allow for the acknowledgement of much larger packet sizes that are supported with the increased PHY rates possible in HomePlug AV2.

3.5.4. Line Cycle Synchronization. The HomePlug AV2 specification describes also the device operation in scenarios where there is no alternating current (AC) line cycle (e.g., a direct current (DC) power line) or when the AC line cycle is different from 50 Hz or 60 Hz. In this case, the Central Coordinator is preconfigured to select a Beacon Period matching either 50 Hz (i.e., Beacon Period is 40 msec) or 60 Hz (i.e., Beacon Period is 33.33 msec). One key use case where this feature is useful is the transfer of data towards a multimedia equipped electrical vehicle during the electrical charging phase (using DC power).

4. MAC Layer Improvements of HomePlug AV2

4.1. Power Save Modes. HomePlug AV2 stations improve their energy efficiency in standby mode through the adoption

of the specific Power Save Mode already defined in the HomePlug Green PHY [4] specification. In Power Save mode stations reduce their average power consumption by periodically transitioning between Awake and Sleep states. Stations in the Awake state can transmit and receive packets over the power line. In contrast, stations in Sleep state temporarily suspend transmission and reception of packets over the power line.

We introduce some basic terms useful to describe the Power Save Mode.

(i) Awake Window: period of time during which the station is capable of transmitting and receiving frames. The Awake Window has a range from a few milliseconds to several Beacon Periods (a Beacon Period is two times the AC line cycle: 40 ms for a 50 Hz AC line and 33.3 ms for a 60 Hz AC).

(ii) Sleep Window: period of time during which the station is not capable of transmitting or receiving frames.

(iii) Power Save Period (PSP): interval from the beginning of one Awake Window to the beginning of the next Awake Window. Power Save Period is restricted to $2k$ multiples of Beacon Periods (i.e., 1 Beacon Period, 2 Beacon Periods, 4 Beacon Periods, ...).

(iv) Power Save Schedule (PSS): the combination of the values of the PSP and of the Awake Widow duration. To communicate with a station in Power Save mode, other stations in the logical network (AVLN) need to know its PSS.

Potentially, the specification allows aggressive PSSs constituted by an Awake Window duration of 1.5 ms and a PSP of 1024 Beacon Periods, that will cause over 99% energy saving compared to HomePlug AV. In practice, some in-home applications will require lower latency and response time, and a balance will take place reducing the mentioned gain. This is particular appealing for applications that foresee a PLC utilization that is variable during the day (for instance large utilization in daylight time and small utilization during night period). It is worth highlighting that the HomePlug AV2 specification is flexible in allowing each station in a network to have a different PSS. Given these remarks, in order to enable efficient Power Save operation without causing difficulties to regular communication, all the stations in a network need to know the PSSs of the other stations. The network Central Coordinator (CCo) has a key role since it grants the requests of the different stations to enter and exit from Power Save mode operation. Moreover, it distributes the different PSSs to all the stations in the network. When needed a CCo can

(i) optionally disable Power Save mode for all stations of the AVLN,

(ii) optionally wake up a station in Power Save mode.

The shared knowledge of the PSS allows stations communicating during the common Awake Windows (the HomePlug AV2 and HomePlug Green PHY specifications have

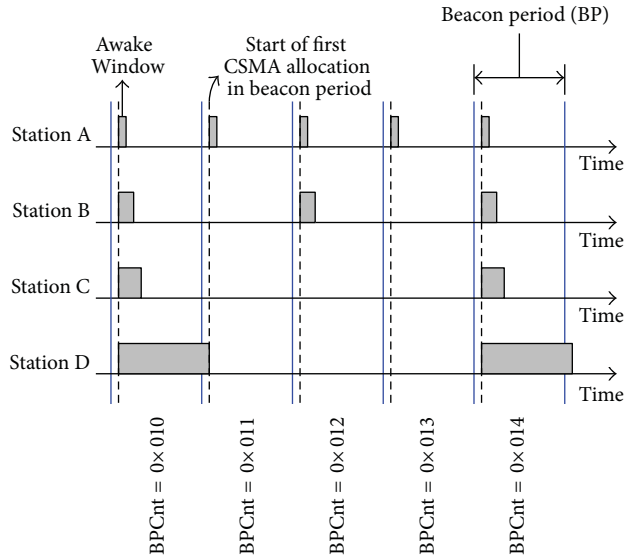

Figure 18: Example of Power Save operation in HomePlug AV2 and HomePlug Green PHY.

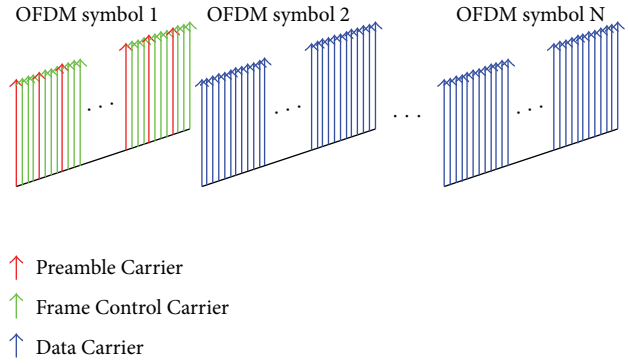

Figure 19: Short Delimiter.

structured the protocol insuring that at least one superposition of all the Awake Windows occurs). This overlap interval can also be used for transmission of information that needs to be received by all stations within the AVLN.

Figure 18 shows an example of Power Save Schedule of the four stations {A, B, C, and D}. All stations save more than 75% energy compared to HomePlug AV. Note that in this example, stations A and B can communicate once every 2 Beacon Periods. Moreover, all the stations are always awake at the same time once every 4 Beacon Periods thus preserving communication possibility.

4.2. Short Delimiter and Delayed Acknowledgement. The Short Delimiter and Delayed Acknowledgement features were added to HomePlug AV2 to improve efficiency by reducing the overhead associated with transmitting payloads over the power line channel. In HomePlug AV, this overhead results in relatively poor efficiency for transmission control protocol (TCP) payloads. One goal that was achieved with

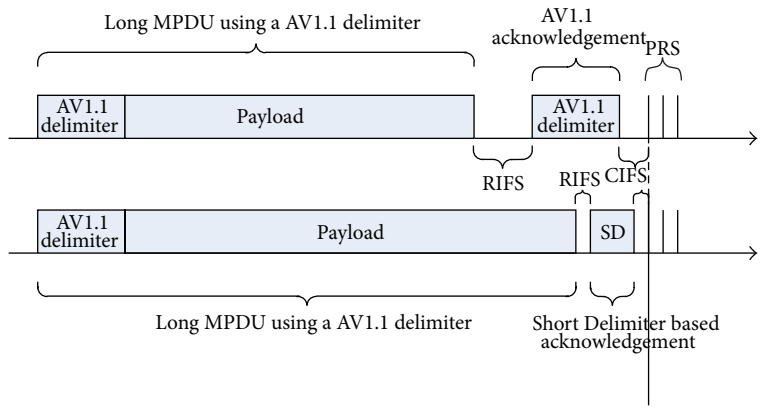

Figure 20: Short delimiter efficiency improvement.

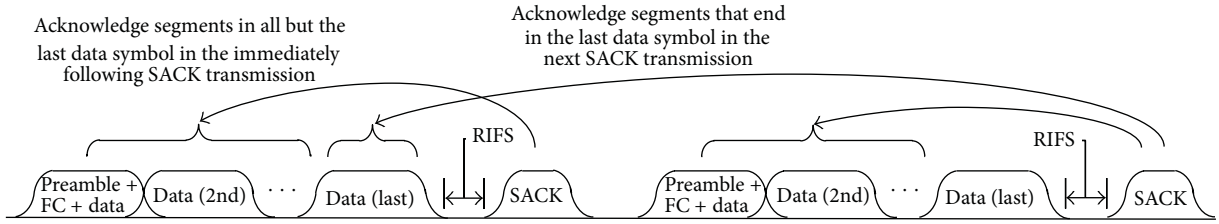

Figure 21: Delayed Acknowledgement.

these new features was TCP efficiency that improved to be relatively close to that of UDP.

In order to send a packet carrying payload data over a noisy channel, signaling is required for a receiver to detect the beginning of the packet and to estimate the channel so that the payload can be decoded, and additional signaling is needed to acknowledge the payload was received successfully. Interframe spaces are also required between the payload transmission and the acknowledgement for the processing time at the receiver to decode and check the payload for accurate reception and to encode the acknowledgement. This overhead is even more significant for TCP payload since the TCP acknowledgement payload must be transmitted in the reverse direction.

4.2.1. Short Delimiter. The delimiter specified in HomePlug AV contains the Preamble and Frame Control symbols and is used for the beginning of data PPDUs as well as for immediate acknowledgements. The length of the HomePlug AV delimiter is 110.5 μs and can represent a significant amount of overhead for each channel access. A new single OFDM symbol delimiter is specified in HomePlug AV2 to reduce the overhead associated with delimiters by reducing the length to 55.5 μs. Figure 19 shows that every fourth carrier in the first OFDM symbol is assigned as a Preamble Carrier, and the remaining carriers encode the Frame Control. The following OFDM symbols encode data the same as in HomePlug AV.

Figure 20 demonstrates the efficiency improvement when the HomePlug AV2 Short Delimiter is used for the acknowledgement of a CSMA Long MPDU (MAC Protocol Data Unit) compared to the HomePlug AV delimiter. Not only is the length of the delimiter reduced from 110.5 to 55.5 μs, the Response Inter-Frame Space (RIFS) and Contention Inter-Frame Space (CIFS) can also be reduced to 5 μs and 10 μs, respectively. Reduction of RIFS requires Delayed Acknowledgement, which is described in Section 4.2.2. Backward compatibility when contending with HomePlug AV devices is maintained by indicating the same length field for virtual carrier sense in both cases so that the position of the priority resolution symbols (PRS) contention remains the same. A field in the Frame Control of the Long MPDU indicates the Short Delimiter format to a HomePlug AV2 device so that it can correctly determine the length of the payload.

4.2.2. Delayed Acknowledgement. The processing time to decode the last OFDM symbol and encode the acknowledgement can be quite high, thus requiring a rather large Response Inter-Frame Space (RIFS). In HomePlug AV, since the preamble is a fixed signal, the preamble portions of the acknowledgement can be transmitted while the receiver is still decoding the last OFDM symbol and encoding the payload for the acknowledgement. With the Short Delimiter, the preamble is encoded in the same OFDM symbol as the Frame Control for the acknowledgement, so the RIFS would need to be larger than for HomePlug AV, eliminating much of the gain the Short Delimiter provides.

Delayed Acknowledgement solves this problem by acknowledging the segments ending in the last OFDM symbol in the acknowledgement transmission of the next PPDU, as shown in Figure 21. This permits practical implementations with a very small RIFS, reducing the RIFS overhead close to zero. HomePlug AV2 also allows the

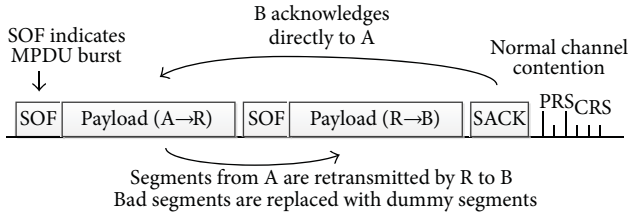

Figure 22: Immediate repeating channel access for CSMA.

option of delaying acknowledgement for segments ending in the second to last OFDM symbol to provide flexibility for implementers.

4.3. Immediate Repeating. HomePlug AV2 supports repeating and routing of traffic to not only handle hidden nodes but also to improve coverage (i.e., performance on the worst channels).

With HomePlug AV2, hidden nodes are extremely rare. However, some links may not support the data rate required for some applications such as a 3D HD video stream. In a network where there are multiple HomePlug AV2 devices, the connection through a repeater typically provides a higher data rate than the direct path for the poorest 5% of channels.

Immediate Repeating is a new feature in HomePlug AV2 that enables high efficient repeating. Immediate Repeating provides a mechanism to use a repeater with a single channel access, and the acknowledgement does not involve the repeater. As shown in Figure 22, station A transmits to the repeater R. In the same channel access, repeater R transmits all payload received from station A to station B. B sends an acknowledgement directly to A. With this approach, latency is actually reduced with repeating, assuming the resulting data rate is higher, the obvious criteria for using repeating in the first place. Also, resources required by the repeater are minimized since the repeater uses and immediately frees memory it would require for receiving payload destined for it. Also the receiver has no retransmission responsibility for failed segments.

5. Coexistence with Other PLC Technologies

5.1. Inter System Protocol. Intersystem Protocol (ISP) allows coexistence between noninteroperable devices sharing the same power line medium. Using the current ISP protocol, noninteroperable devices are able to coexist. The HomePlug AV2 will operate in a 1901-FFT mode [5] in order to coexist with the other systems, in this case the TDM slot allocated for the 1901-FFT is to be used by the HomePlug AV2 system.

The ISP protocol allows a TDM scheme to be implemented between coexisting in-home systems and between coexisting in-home and access systems. Each of the PLC system categories is allocated a particular ISP window in a round-robin fashion. The allocation is determined by (1) the number of systems on the power line, (2) the type of the systems present, and (3) the access system bandwidth request, as defined in the 1901 standard [34].

The TDM synchronization period for the in-home and access systems is defined with the parameter T_H in Figure 23. There are four ISP windows within a single T_H period. Each ISP window is further divided into three TDM units (TDMU), so there are a total of twelve TDMUs in each T_H period, labeled TDMU#0 through TDMU#11. Each TDMU is further divided into eight TDM slots (TDMS), labeled TDMS#0 through TDMS#7.

Figure 23 illustrates the TDM partitioning relative to the AC line cycles. The ISP window is used to generate and detect the ISP signal that is allocated within the first TDMS#0 in TMDU#0, TMDU#3, TMDU#6, and TDMU#9. The purpose and nature of the ISP signals will be described later. Note: the term Beacon Period in the HomePlug AV2 specification is similar to the 2 AC line cycles of the TDMU.

5.2. ISP Signals. Coexistence signaling is carried out by the use of periodically repeating ISP signals within the ISP windows. The signals are used to convey information on coexisting system presence, resource requirements, and resynchronization request. Each PLC system category is allocated a particular ISP window in a round-robin fashion, as illustrated in Figure 23.

The ISP signal is transmitted using a range of designated phases that convey a range of information to be used by the system. This set of instantaneous information is termed the Network Status that defines the allocation of resources to each coexisting system.

The ISP signal is merely detected. By monitoring the ISP signal transmitted within the ISP windows allocated to other systems, a coexisting system is able to determine the number and type of coexisting systems present on the line and their resource requirements. Similarly, by monitoring the signal within its own ISP window, a coexisting system is able to detect a resynchronization request from one of the other coexisting systems.

The ISP signal consists of 16 consecutive OFDM symbols. Each OFDM symbol is formed by a set of "all-one" binary phase shift keying (BPSK), modulated onto the carrier waveforms using IFFT, and multiplied by a window function to reduce out-of-band energy complying with the transmit spectrum requirement. Since all devices send the signal simultaneously, the ISP signal must be sent with 8 dB less power than the normal transmission.

Timing parameter that is used for generating an ISP signal is described in Figure 24.

5.3. Startup and Resynchronization Procedures. The TDM synchronization scheme mentioned above is used such that each PLC system shares the medium without interfering with one another. However, it is possible that two or more systems are synchronized to two or more different, mutually visible ISP sequences [35]. In such cases, in order to prevent mutual interference, it is important that they resynchronize to the same ISP sequence.

In other words, whenever a HomePlug AV2 device starts up or restarts, it needs to be aware of the presence of any other systems with which it is able to coexist. Accordingly, a startup

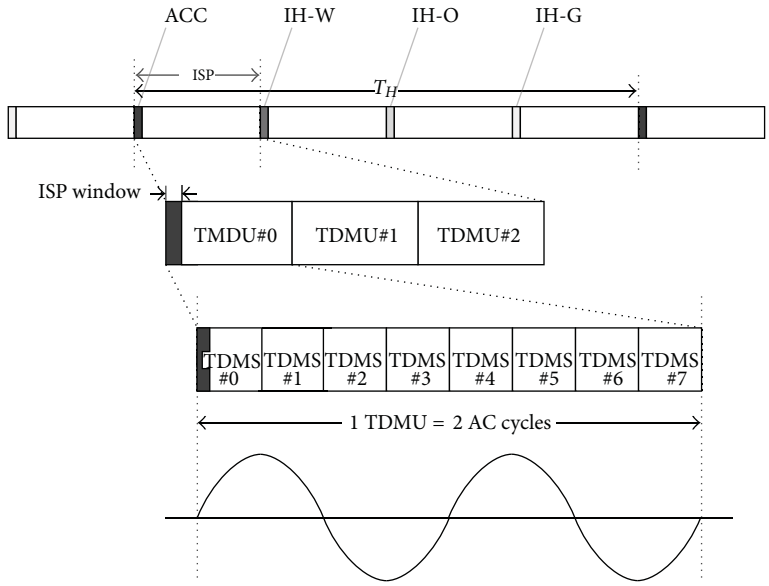

Figure 23: Time Division Multiplexing on ISP.

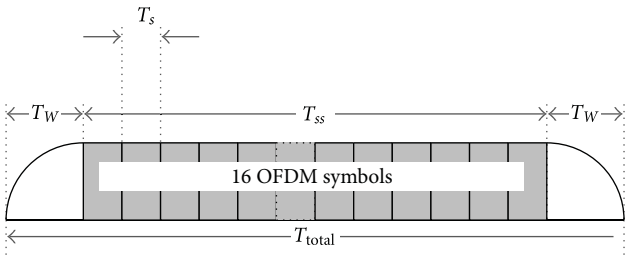

Timing Parameters	Description	Time (μs)
T_s	IFFT interval	5.12
T_{ss}	OFDM symbols duration	$T_{\text{total}} - 2\times T_W$
T_W	Windowing duration	≤ 10.24
T_{total}	ISP signal interval	81.92

Figure 24: ISP Signal Timing Parameter.

and resynchronization procedure is defined within the ISP protocol that allows the starting system to synchronize with an existing system.

6. Gain of HomePlug AV2 Compared to HomePlug AV

The AV TWG has evaluated the performance of the HomePlug AV2 specification; this activity has been fundamental in order to see if the produced specification meets the requirements of all the stakeholders. The following tables show the performance improvement as compared to HomePlug AV in terms of coverage. These preliminary results are based on a 6-home field test in Florida, home sizes 1900–3300 sq. ft.

Table 1 presents the results in a 2-node network scenario; 95% of nodes experiment a throughput improvement greater than 136% compared to HomePlug AV (which means a performance enhancement by a factor nearly equal to 2.4!). Benefits are even higher when considering the most favorable connections (see the improvement at the 5% coverage value). Table 2 considers a 4-node scenario where 3 streams carrying different data are transmitted from one source (e.g., a Set-Top Box) to 3 different destinations (e.g., TVs). In this case, the improvement in the aggregate throughput is relevant for the 99% of networks compared to HomePlug AV (more than 131%).

Table 1: Improvement of HomePlug AV2 in a 2-node network.

Coverage based on UDP throughput	Percentage of throughput improvement of HomePlug AV2 compared to HomePlug AV
95%	>136%
5%	>220%

Table 2: Improvement of HomePlug AV2 in a 4-node network.

Coverage based on UDP throughput	Percentage of throughput improvement of HomePlug AV2 compared to HomePlug AV
99%	>131%
5%	>173%

Note that the benefits of the HomePlug AV2 technology are expected to be greater (which explains the ">" symbol) than the ones shown in Tables 1 and 2 since, for instance, a 2×2 MIMO was tested in Florida; 2×3 or 2×4 MIMO would likely provide better performance.

Another interesting figure is the theoretical maximum PHY throughput for the system, for different options of the standard (Table 3). This number represents the throughput of transmitted bits on the PHY layer for optimum channel

Table 3: Maximum PHY rate computation.

System configuration (North American tone mask)	Max PHY rate
HomePlug AV (1.8–30 MHz) (917 carriers, 10 bits/carr, 5.56 μs GI)	197 Mbps
IEEE 1901 (1.8–50 MHz) (1974 carriers, 12 bits/carr, 1.6 μs GI)	556 Mbps
HomePlug AV2 SISO (1.8–86.13 MHz) (3455 carriers, 12 bits/carr, 0.0 μs GI)	1012 Mbps
HomePlug AV2 MIMO (1.8–86.13 MHz) (3455 carriers, 12 bits/carr, 0.0 μs GI, 2 streams)	2024 Mbps

conditions and gives an idea of the benefits of different features. It can be seen that if the full frequency range is used, HomePlug AV2 provides a 1 Gbps throughput in SISO configuration and 2 Gbps in a MIMO configuration.

7. Conclusion

In this paper, an overview of HomePlug AV2 has been presented. The overall system architecture and the key technical HomePlug AV2 improvements introduced at PHY and MAC layers have been described. It has been also shown the related performance improvements were achieved by HomePlug AV2 while ensuring both backward compatibility versus HomePlug AV and the coexistence with other power line technologies.

The HomePlug AV2 performance presented in this work has been assessed by AV TWG through simulations based on field measurements.

The results show the significant benefits introduced by the new set of HomePlug AV2 features, both in terms of achievable data rate and coverage.

References

[1] HomePlug Alliance, http://www.homeplug.org/.

[2] HomePlug Alliance, HomePlug AV White Paper, http://www.homeplug.org/.

[3] HomePlug Alliance, HomePlug AV Specification Version 2.0, January 2012.

[4] HomePlug Alliance, HomePlug GreenPHY, the Standard for In-Home Smart Grid Powerline Communications, http://www.homeplug.org/.

[5] IEEE Standard 1901-2010, IEEE Standard for Broadband over Power Line Networks: Medium Access Control and Physical Layer Specifications, http://standards.ieee.org/findstds/standard/1901-2010.html, 2010.

[6] ETSI TR 101 562, PowerLine Telecommunications (PLT); 19 MIMO PLT; Part 1: Measurement Methods of MIMO PLT, http://www.etsi.org/deliver/etsi_tr/101500_101599/10156201/01.03.01_60/tr_10156201v010301p.pdf, 2012.

[7] ETSI TR 101 562, PowerLine Telecommunications (PLT); MIMO PLT; Part 2: Setup and Statistical Results of MIMO PLT EMI Measurements, http://www.etsi.org/deliver/etsi_tr/101500_101599/10156202/01.02.01_60/tr_10156202v010201p.pdf, 2012.

[8] ETSI TR 101 562, PowerLine Telecommunications (PLT); MIMO PLT; Part 3: Setup and Statistical Results of MIMO PLT Channel and Noise Measurements, http://www.etsi.org/deliver/etsi_tr/101500_101599/10156203/01.01.01_60/tr_10156203v010101p.pdf, 2012.

[9] D. Schneider, A. Schwager, W. Bäschlin, and P. Pagani, "European MIMO PLC field measurements: channel analysis," in *Proceedings of the IEEE International Symposium on Power Line Communications and its Applications (ISPLC '12)*, Beijing, China, March 2012.

[10] P. Pagani, R. Hashmat, A. Schwager, D. Schneider, and W. Bäschlin, "European MIMO PLC field measurements: noise analysis," in *Proceedings of the IEEE International Symposium on Power Line Communications and its Applications (ISPLC '12)*, Beijing, China, March 2012.

[11] D. Veronesi, R. Riva, P. Bisaglia et al., "Characterization of in-home MIMO power line channels," in *Proceedings of the IEEE International Symposium on Power Line Communications and Its Applications (ISPLC '11)*, pp. 42–47, Udine, Italy, April 2011.

[12] D. Rende, A. Nayagam, K. Afkhamie et al., "Noise correlation and its effect on capacity of inhome MIMO power line channels," in *Proceedings of the IEEE International Symposium on Power Line Communications and Its Applications (ISPLC '11)*, pp. 60–65, Udine, Italy, April 2011.

[13] R. Hashmat, P. Pagani, A. Zeddam, and T. Chonavel, "MIMO communications for inhome PLC Networks: measurements and results up to 100 MHz," in *Proceedings of the 14th IEEE International Symposium on Power Line Communications and its Applications (ISPLC '10)*, pp. 120–124, Rio de Janeiro, Brazil, March 2010.

[14] D. Schneider, *Inhome power line communications using multiple input multiple output principles [Doctoral thesis]*, University of Stuttgart, Stuttgart, Germany, 2012.

[15] R. Hashmat, P. Pagani, A. Zeddam, and T. Chonavel, "A channel model for multiple input multiple output in-home power line networks," in *Proceedings of the IEEE International Symposium on Power Line Communications and Its Applications (ISPLC '11)*, pp. 35–41, Udine, Italy, April 2011.

[16] R. Hashmat, P. Pagani, A. Zeddam, and T. Chonavel, "Analysis and modeling of background noise for inhome MIMO PLC channels," in *Proceedings of the 14th IEEE International Symposium on Power Line Communications and its Applications (ISPLC '12)*, pp. 120–124, Beijing, China, March 2012.

[17] F. Versolatto and A. M. Tonello, "A MIMO PLC random channel generator and capacity analysis," in *Proceedings of the IEEE International Symposium on Power Line Communications and Its Applications (ISPLC '11)*, pp. 66–71, Udine, Italy, April 2011.

[18] R. Hashmat, P. Pagani, T. Chonavel, and A. Zeddam, "A time domain model of background noise for In-home MIMO PLC networks," *IEEE Transactions on Power Delivery*, vol. 27, no. 4, pp. 2082–2089, 2012.

[19] A. Schwager, *Powerline communications: significant technologies to become ready for integration [Doctoral thesis]*, University of Duisburg-Essen, Essen, Germany, 2010.

[20] A. Paulraj, R. Nabar, and D. Gore, *Introduction To Space-Time Wireless Communications*, Cambridge University Press, New York, NY, USA, 2003.

[21] L. Stadelmeier, D. Schneider, D. Schill, A. Schwager, and J. Speidel, "MIMO for inhome power line communications," in *Proceedings of the 7th International ITG Conference on Source and Channel Coding (SCC '08)*, Ulm, Germany, January 2008.

[22] A. Canova, N. Benvenuto, and P. Bisaglia, "Receivers for MIMO-PLC channels: throughput comparison," in *Proceedings of the 14th IEEE International Symposium on Power Line Communications and its Applications (ISPLC '10)*, pp. 114–119, Rio de Janeiro, Brazil, March 2010.

[23] S. Katar, B. Mashburn, K. Afkhamie, H. Latchman, and R. Newman, "Channel adaptation based on cyclo-stationary noise characteristics in PLC systems," in *Proceedings of the IEEE International Symposium on Power Line Communications and Its Applications (ISPLC '06)*, pp. 16–21, Orlando, Fla, USA, March 2006.

[24] A. M. Tonello, J. A. Cortes, and S. D'Alessandro, "Optimal time slot design in an OFDM-TDMA system over power-line time-variant channels," in *Proceedings of the IEEE International Symposium on Power Line Communications and its Applications (ISPLC '09)*, pp. 41–46, Dresden, Germany, April 2009.

[25] A. Scaglione, P. Stoica, S. Barbarossa, G. B. Giannakis, and H. Sampath, "Optimal designs for space-time linear precoders and decoders," *IEEE Transactions on Signal Processing*, vol. 50, no. 5, pp. 1051–1064, 2002.

[26] A. R. Horn and R. C. Johnson, *Matrix Analysis*, Cambridge University Press, New York, NY, USA, 1985.

[27] A. Lozano, A. M. Tulino, and S. Verdú, "Optimum power allocation for parallel gaussian channels with arbitrary input distributions," *IEEE Transactions on Information Theory*, vol. 52, no. 7, pp. 3033–3051, 2006.

[28] S. D. 'Alessandro, A. M. Tonello, and L. Lampe, "Adaptive pulse-shaped OFDM with application to in-home power line communications," *Telecommunication Systems Journal*, vol. 51, no. 1, pp. 31–1311, 2011.

[29] F. J. Harris, "On the use of windows for harmonic analysis with the discrete Fourier transform," *Proceedings of the IEEE*, vol. 66, no. 1, pp. 51–83, 1978.

[30] K. H. Afkhamie, H. Latchman, L. Yonge, T. Davidson, and R. Newman, "Joint optimization of transmit pulse shaping, guard interval length, and receiver side narrow-band interference mitigation in the HomePlugAV OFDM system," in *Proceedings of the IEEE 6th Workshop on Signal Processing Advances in Wireless Communications (SPAWC '05)*, pp. 996–1000, New York, NY, USA, June 2005.

[31] A. M. Tonello, S. D'Alessandro, and L. Lampe, "Cyclic prefix design and allocation in bit-loaded OFDM over power line communication channels," *IEEE Transactions on Communications*, vol. 58, no. 11, pp. 3265–3276, 2010.

[32] CENELEC, "Power line communication apparatus used in low voltage installations—radio disturbance characteristics—limits andmethods of measurement—part 1: apparatus for inhome use," Final Draft European Standard FprEN 50561-1, 2011.

[33] A. Schwager, W. Bäschlin, J. L. Gonzalez Moreno et al., "European MIMO PLC field measurements: overview of the ETSI STF410 campaign & EMI analysis," in *Proceedings of the IEEE International Symposium on Power Line Communications and its Applications (ISPLC '12)*, Beijing, China, March 2012.

[34] IEEE Standard 1901-2010, IEEE Standard for Broadband over Power Line Networks: Medium Access Control and Physical Layer Specifications, Chapter 16, "Inter System Protocol (ISP)", 2010.

[35] IEEE Standard 1901-2010, IEEE Standard for Broadband over Power Line Networks: Medium Access Control and Physical Layer Specifications, Annex R, "Resynchronization example", 2010.

Hindawi Publishing Corporation
Journal of Electrical and Computer Engineering
Volume 2013, Article ID 635086, 11 pages
http://dx.doi.org/10.1155/2013/635086

Research Article

A Study on the Optimal Receiver Impedance for SNR Maximization in Broadband PLC

Massimo Antoniali, Andrea M. Tonello, and Fabio Versolatto

Dipartimento di Ingegneria Elettrica Gestionale e Meccanica (DIEGM), Università di Udine, 33100 Udine, Italy

Correspondence should be addressed to Andrea M. Tonello; tonello@uniud.it

Received 27 July 2012; Revised 31 October 2012; Accepted 13 December 2012

Academic Editor: Moises V. Ribeiro

We consider the design of the front-end receiver for broadband power line communications. We focus on the design of the input impedance that maximizes the signal-to-noise ratio (SNR) at the receiver. We show that the amplitude, rather than the power, of the received signal is important for communication purposes. Furthermore, we show that the receiver impedance impacts the amplitude of the noise term. We focus on the background noise, and we propose a novel description of the noise experienced at the receiver port of a PLC network. We model the noise as the sum of four uncorrelated contributions, that is, the active, resistive, receiver, and coupled noise components. We study the optimal impedance design problem for real in-home grids that we assessed with experimental measurements. We describe the results of the measurement campaign, and we report the statistics of the optimal impedance. Hence, we study the best attainable performance when the optimal receiver impedance is deployed. We focus on the SNR and the maximum achievable rate, and we show that power matching is suboptimal with respect to the proposed impedance design approach.

1. Introduction

The communication technology that exploits the power delivery network to convey data is commonly referred to as power line communication (PLC). PLC is broadly deployed and, recently, it has been recognized as a key technology to enable the communication within the smart grid. The last node of the smart grid is the home, where PLC is suitable for both home entertainment, with datarates of about 200 Mbps, and home-automation, with lower data-rates but higher robustness and reliability.

The design of the PLC transceiver is a challenging task due to the severe attenuation, fading effects, and noise impairments that characterize the communication media. In other application scenarios, as wireless, the transceivers are designed to fulfill the maximum power transfer condition. Basically, the maximum power transfer is achieved under complex matching conditions, that is, when the internal impedance of the transmitter and the input impedance of the receiver are the complex conjugate of the characteristic impedance of the transmission medium. In wireless, this corresponds to the input impedance of the antenna. Indeed, the absence of reflections and stationary waves is obtained under simple (not complex) matching conditions, that is, when the impedance of the transmitter and the receiver are equal to the characteristic impedance of the transmission medium. Reflections and stationary waves are not desired. The reflected waves yield to multiple delayed echoes in the channel impulse response and they can be either due to the multipath nature of the channel or due to the unmatched termination nodes. Matching ensures the absence of the latter type of reflections. The stationary waves yield to voltage values along the line that are higher than necessary and that may damage the transmission medium, especially in wireline communications as, for instance, over coaxial cables.

When the characteristic impedance of the medium is real, the maximum power transfer and the absence of reflections are ensured by the same matching conditions. In the following, we simply indicate with impedance matching the receiver design that enables the maximum power transfer. In wireless, impedance matching can be easily satisfied by letting the characteristic impedance of the antenna and the

cables, the internal impedance of the transmitter and the input impedance of the receiver be equal to the reference value of 50 Ω.

In PLC, impedance matching is typically achieved through the use of impedance matching networks, so that the received signal power is maximized. Basically, the matching network is a loss-less network of lumped elements whose input impedance is matched to that of the power delivery network. The latter is frequency dependent and it varies significantly from outlet to outlet. Furthermore, it may exhibit a time-varying behavior [1]. Several matching networks were presented in the literature for PLC, and their use was demonstrated to be beneficial in terms of an increase of the received signal power [2, Ch. 4] [3, 4]. However, from a data transmission point of view, it is important to maximize the signal-to-noise ratio (SNR) and not only the signal power.

The effective formulation of the SNR is in signal amplitude rather than in power terms. The reason is that the analog front-end of the PLC receiver is designed to convert the analog amplitude of the received signal into a digital sample stream. In this respect, the amplitude of the received signal is more important than its power, though the two quantities are related once the receiver impedance is given.

In PLC, the maximum power transfer condition does not imply the maximization of the SNR in amplitude terms because power matching may turn into a higher noise contribution. Concerning an in-home network, the noise injected by the household devices is attenuated by the insertion loss of the path followed to reach the receiver outlet. In general, the latter is different from that followed by the communication signal. The receiver impedance affects the insertion loss, and common impedance matching techniques do not take into account the impact of the receiver impedance on the insertion loss experienced by the noise. It follows that impedance matching may reduce the attenuation of the noise path, thus increasing the noise amplitude at the receiver port. Furthermore, the receiver impedance itself contributes to the increase of the amplitude of the noise.

In this work, we discuss the optimal design of the receiver impedance that enables achieving the maximum SNR in broadband PLC. We formulate the SNR in terms of amplitude and we focus on in-home networks.

Firstly, we propose an analytic description of the noise as the sum of multiple contributions. We consider the resistive noise of the network by itself, the noise injected by the household devices, and the noise introduced by the receiver impedance. From the experimental evidence, we show that the noise injected by the household devices, namely, the active noise, dominates among all noise contributions.

Then, we formulate the SNR as a function of the receiver impedance. To this aim, we assume the transmitter impedance to be constant and known. We study the convexity of the optimization problem and we derive the optimal receiver impedance that maximizes the SNR at each single frequency.

Finally, we validate the results for real-life in-home networks. We exploit the results of an experimental measurement campaign that we carried out in Italy, where we collected more than 1200 channel responses in different premises. For each site, we performed measurements between all couples of available outlets in the 1.5–100 MHz frequency range. The measured database is useful to provide a realistic description of the frequency response and the line impedance that characterizes the signal paths.

In this work, we focus on the time invariant description of the network because, from the experimental evidence, we observed that very little (or inexistent) time variation was present in the sites that we considered, namely, in the order of few dBs. More in general, the PLC channel can be periodically time variant. In such a case, an extension of our analysis can be obtained under the assumption that both the channel and the noise exhibit a slow periodic variation that is synchronous with the mains. Thus, the mains period can be divided into short time intervals (slots) during which we can reasonably assume both the channel and the noise to be time invariant. Hence, we can apply the analysis that we propose in this work to each single slot.

We study the attainable SNR improvement when the optimal receiver impedance is used. We compare the results to the case of impedance matching, when the receiver impedance is constant and equal to the reference value of 50 Ω, and when it is constant and equal to 1 kΩ. The latter case is representative of a receiver with high input impedance.

The remainder of the work is as follows. In Section 2, we describe the model of the power delivery network. In Section 3, we overview the transceiver design, with emphasis on the receiver side. Then, in Section 4, we formulate the optimization problem, and, in Section 5, we study its convexity. In Section 6, we present several numerical results. Basically, we study the optimal receiver impedance for a real scenario. Furthermore, we provide some details on the measurements. Then, we study the performance in terms of SNR and achievable rate and we compare the results to the ones that we would obtain for the other receiver impedance designs. Finally, the conclusions follow.

2. Power Delivery Network Model

PLC experiences high attenuation and deep fading effects that are a function of the loads and the layout of the network. We focus on in-home networks. In [5], we presented an accurate model of the in-home power delivery network. Basically, in-home networks exhibit a treelike structure and the outlets are the termination nodes. The outlets are fed by the power line cables which resemble the branches of the network. Between any pair of outlets, only one electrical path is possible.

From a data transmission perspective, we can abstract the power delivery network to obtain an equivalent representation that is suitable for the SNR analysis of the following sections. In Figure 1, we show the model. We represent the power delivery network as an $\mathcal{O}$-port network, where $\mathcal{O}$ is the number of outlets. The transmitter and the receiver are connected to two ports of the network, namely, ports t and r. We model the transmitter as a real voltage source with its own internal impedance, and the receiver as a passive load. The household appliances are connected to the remaining ports of the network. They inject noise, and we model them as

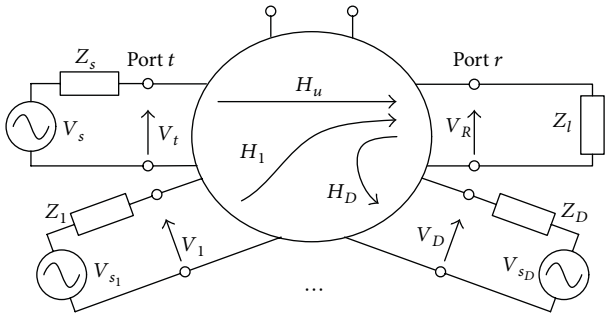

Figure 1: Equivalent model of the power delivery network.

noise sources, namely, real voltage generators with their own internal impedance. In general, the number of household appliances is $D \leq \mathcal{O}$ because some outlets may be not in use, as shown in the uppermost part of Figure 1.

The signal path between two ports of the network is characterized by the channel frequency response (CFR). We refer to the CFR as the ratio, in the frequency domain, between the voltage at the output and input ports.

We introduce the following notation. We denote the complex amplitude of the source signal, the internal impedance of the transmitter, the complex amplitude of the voltage at the transmitter port, the complex amplitude of the voltage at the receiver port, and the input impedance of the receiver with $V_s(f)$, $Z_s(f)$, $V_t(f)$, $V_R(f)$, and $Z_\ell(f)$, respectively. All the quantities are defined in the frequency domain, at frequency f. Concerning the noise, we use the subscript $\{\cdot\}_d$ to denote the dth source of noise, where $d = 1, \ldots, D$, and we denote the complex amplitude of the dth noise source and its internal impedance with $V_{s_d}(f)$ and $Z_d(f)$, respectively, and the voltage amplitude at the port where the dth noise source is connected with $V_d(f)$. Furthermore, we note that all impedances are, in general, noisy and thus they generate a thermal noise contribution. Finally, we denote the CFR between the transmitter and the receiver port with $H_u(f)$, and between the port where the dth noise source is connected and the receiver port with $H_d(f)$.

3. PLC Transceiver Design

We consider the analog front-end (AFE) of the transceiver. At the transmitter side, the AFE amplifies the signal. The final amplification stage is the line driver. In this work, we do not consider the impairments related to the design of the line driver and we model it as a real voltage generator with an internal impedance Z_s. To obtain the numerical results of Section 6, we simply neglect it; that is, we let $Z_s = 0\,\Omega$. The assumption is validated by the fact that the output impedance of the transmitter stage of commercially available broadband PLC transceivers is typically low, for example, $3\,\Omega$ [6].

At the receiver side, the AFE processes the received signal to make it suitable for the analog-to-digital (AD) conversion. The final goal is to convert the (analog) amplitude of the received signal into a digital sample stream. Thus, the focus is on the amplitude of the received signal, rather than its power, and this motivates the formulation of the SNR in amplitude terms. Furthermore, to preserve the signal amplitude, the input impedance of the analog-to-digital converter (ADC) circuit is typically high [7].

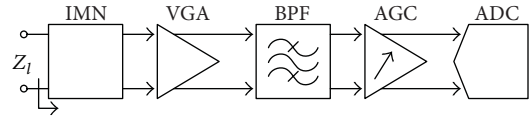

Figure 2: Block diagram of the PLC receiver AFE [6].

At the receiver, the AFE consists of several blocks. In Figure 2, we show the schematic diagram [6]. The variable gain amplifier (VGA) is followed by a band-pass filter (BPF) and an adaptive gain control (AGC). A low-noise amplifier (LNA) can be used to substitute the VGA, and an additional ad hoc amplifier can be deployed to drive the AD converter instead of the AGC [8]. The gain of the AGC is adjusted dynamically to ensure always the optimum signal level for AD conversion and the maximum dynamic range [6].

Practical receiver schemes adopt matching techniques to interface the blocks of the AFE. In wireless, where the communications are in the range of GHz, the reference impedance value is $50\,\Omega$ [9], and the advantages provided by impedance matching are the following. Firstly, since the reference impedance is real, matching enables both the maximum transfer of power and the absence of reflections at the receiver port. The latter condition is desired to avoid multipath fading exceeding that amenable closely to the channel. Secondly, matching simplifies the design of the LNA and the BPF. The noise figure (NF) of the LNA is a function of the impedance that is seen at the input and output port of the amplifier [10]. By letting the impedance be equal to a reference value, the LNA can be optimized to exhibit the lowest NF. Similarly, the behavior of the BPF is a function of the impedance seen by the filter at the input and output ports. The BPF is designed to operate in matching conditions, and its frequency behavior, that is, the pass-band and the stop-bands, may vary significantly otherwise [9].

In PLC, the transmission interests the frequency range below 100 MHz, where the presence of reflected waves can be tolerated to preserve the amplitude of the received signal. Therefore, the interface between the blocks can be designed in high-impedance mode.

The use of an impedance matching network (IMN) before the AFE provides some benefits. Strictly, the matching network allows the receiver to be matched to the complex and frequency-dependent impedance of the power delivery network, regardless of the input impedance of the first stage of the AFE. In the literature, the design of the matching network was aimed at obtaining the maximum transfer of power from the network [3, 4]. Alternative solutions are possible. In this respect, we propose the use of the matching network to obtain the optimal receiver impedance that lets the SNR be maximum, as we describe in the following sections. Basically, we model the IMN as an impedance Z_ℓ in parallel with the first stage of the AFE, and we assume the first stage to exhibit

an infinite input impedance. Therefore, the resultant input impedance of the transceiver is equal to Z_ℓ.

4. SNR Formulation

We follow the notation of Figure 1. We study the SNR at the receiver port r when the transmitter is connected to port t, and D noise sources are connected to the remaining ports of the network. At the receiver port, $V_R(f)$ is the sum of the signal of interest $V_u(f)$ and the noise $V_n(f)$, that is, $V_R(f) = V_u(f) + V_n(f)$. We formulate the SNR in amplitude terms, as the power spectral density (PSD) of $V_u(f)$ divided by the PSD of $V_n(f)$. It reads

$$\Gamma(f) = \frac{P_{V_uV_u}(f)}{P_{V_nV_n}(f)}. \tag{1}$$

To obtain (1), we assume the signals to be stationary and continuous in time, and we note that the PSD of the generic signal $x(t)$, limited in power, can be computed as [11]

$$P_{XX}(f) = \lim_{T\to\infty} \frac{\overline{\left(|X_T(f)|^2\right)}}{T} \left[\mathrm{V}^2/\mathrm{Hz}\right], \tag{2}$$

where $X_T(f)$ is the Fourier transform of $x(t)$ on a finite time interval of length T, and $\overline{(\cdot)}$ denotes the statistical expectation.

Now, we study the terms in (1). Firstly, let us consider the signal of interest. According to the notation of Figure 1, we explicit it as

$$P_{V_uV_u}(f) = |H_u(Z_\ell, f)|^2 P_{V_tV_t}(f) \left[\mathrm{V}^2/\mathrm{Hz}\right]. \tag{3}$$

Hence, let us focus on the noise term. In this work, we limit the study to the stationary noise components, and we explicit the PSD of the noise at the receiver port, namely, $P_{V_nV_n}(f)$ as the sum of contributions due to four noise terms. They are the active noise $V_a(f)$, the resistive noise $V_r(f)$, the receiver noise $V_\ell(f)$, and the coupled noise $V_c(f)$. The latter component models the radio disturbances that are captured by the wiring through coupling. We assume the coupled noise to be independent from the receiver impedance. Thus, we can neglect the impact of the coupled noise on the design of the optimal receiver impedance, and we let $P_{V_cV_c}(f) = 0$. Furthermore, we assume the noise terms to be uncorrelated with zero mean. It follows

$$P_{V_nV_n}(f) = P_{V_aV_a}(f) + P_{V_rV_r}(f) + P_{V_\ell V_\ell}(f) \left[\mathrm{V}^2/\mathrm{Hz}\right]. \tag{4}$$

In the next sections, we describe the noise terms in (4) and we propose an analytical expression to model them, we introduce and motivate the approximations that allow us to formulate and solve the SNR maximization problem and, finally, we present the final SNR expression.

4.1. Active Noise. The active noise is generated by the power-supply circuitry of the household appliances that are connected to the power delivery network. We model the household appliances as real and independent voltage generators.

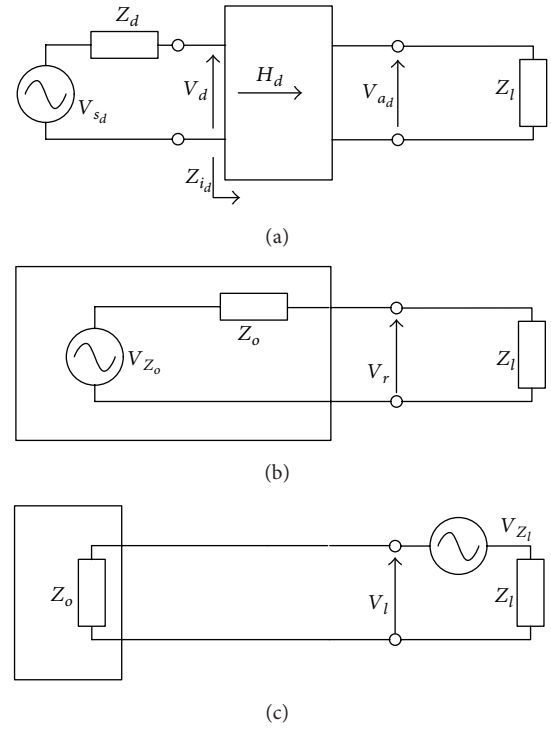

Figure 3: Equivalent models for the active, resistive, and receiver noise terms.

We show the equivalent model in Figure 3(a). The active noise at the receiver port reads

$$\begin{aligned} P_{V_aV_a}(f) &= \sum_{d=1}^{D} P_{V_{a_d}V_{a_d}}(f) \\ &= \sum_{d=1}^{D} |H_d(Z_\ell, f)|^2 \\ &\quad \times \left| \frac{Z_{i_d}(Z_\ell, f)}{Z_{i_d}(Z_\ell, f) + Z_d(f)} \right|^2 P_{V_{s_d}V_{s_d}}(f) \left[\mathrm{V}^2/\mathrm{Hz}\right], \end{aligned} \tag{5}$$

where $Z_{i_d}(Z_\ell, f)$ is the input impedance of the power delivery network at the port where the dth appliance is connected. All other quantities in (5) are consistent with the notation of Figure 1. Furthermore, we note that we account for the thermal noise contribution due to the real part of $Z_d(f)$ in the resistive noise term. Toward the receiver, the active noise injected by the dth device is attenuated by $H_d(Z_\ell, f)$ and, further, by an attenuation factor that is a function of the input impedance $Z_{i_d}(Z_\ell, f)$. Both $H_d(Z_\ell, f)$ and $Z_{i_d}(Z_\ell, f)$ depend on the load impedance $Z_\ell(f)$. It follows that the design of the load impedance has an impact on the received active noise.

Now, we introduce the following approximations. We assume that $P_{V_{s_d}V_{s_d}}(f)$ is identical for all appliances, that is, $P_{V_{s_d}V_{s_d}}(f) = P_{V_wV_w}(f)$ for all $d \in \{1, \ldots, D\}$, and we neglect the source impedance, that is, we let $Z_d(f) = 0$. In this respect, we point out that by letting $Z_d = 0$, we follow a

conservative approach because, in such a case, we experience the highest level of noise at the receiver.

In Section 5, we show that the optimal receiver impedance is independent from $P_{V_wV_w}(f)$. However, the value of $P_{V_wV_w}(f)$ is fundamental to obtain realistic values of SNR. To determine $P_{V_wV_w}(f)$, we explicit the quantity as follows:

$$P_{V_wV_w}(f) = \frac{P_{V_nV_n}(f) - P_{V_rV_r}(f) - P_{V_\ell V_\ell}(f)}{\sum_{d=1}^{D} \left|H_d(Z_\ell, f)\right|^2} \left[\mathrm{V}^2/\mathrm{Hz}\right], \tag{6}$$

and we exploit the experimental results in [12]. Basically, $P_{V_nV_n}$ is the total additive background noise experienced at the receiver port. In [12], the total additive background noise experienced at the receiver port was measured and modeled in power terms for the reference load of 50 Ω. The model reads

$$P_{\mathrm{bck}}(f) = \frac{1}{f^2} + 10^{-15.5} \ [\mathrm{mW/Hz}]. \tag{7}$$

To be consistent with the measurement setup in [12], in (6), we let Z_ℓ be constant and equal to 50 Ω and we substitute $P_{V_nV_n}$ with

$$P_{V_nV_n}(f) = 0.05 \cdot P_{\mathrm{bck}}(f) \left[\mathrm{V}^2/\mathrm{Hz}\right], \tag{8}$$

that is, the V^2/Hz-representation of the measured noise PSD in (7), where the coefficient 0.05 allows for the conversion from dBm/Hz to V^2/Hz. Furthermore, in (6), we compute $P_{V_rV_r}(f)$ and $P_{V_\ell V_\ell}(f)$ as described in Sections 4.2 and 4.3, respectively.

4.2. Resistive Noise. Resistive elements introduce thermal noise [13]. The noisy impedance $Z(f)$ can be modeled as a thermal noise voltage source and a noiseless impedance. The PSD of the amplitude of the thermal noise reads

$$P_{V_ZV_Z}(f) = 4kT\mathscr{R}\{Z(f)\} \left[\mathrm{V}^2/Hz\right], \tag{9}$$

where $k = 1.38 \cdot 10^{-23}$ J/K is the Boltzmann constant, $T = 290$ K is the absolute temperature, and $\mathscr{R}\{\cdot\}$ denotes the real operator. The branches and the nodes of the power delivery network are not ideal and they show a resistive component that contributes to the thermal noise at the receiver. Further sources of thermal noise are the internal impedance of both the transmitter and the household appliances. Now, we point out that the power delivery network between the transmitter and the receiver port can be modeled as a passive two-port network. We can gather the thermal noise contributions into the resistive noise PSD that can be obtained from the network impedance at the receiver port $Z_o(f)$. In this respect, we point out that an alternative description of the noise generated by the network can be obtained in terms of noise figure. For further details, we refer to [14]. In Figure 3(b), we show the equivalent network model from which we obtain

$$P_{V_rV_r}(f) = \left|\frac{Z_\ell(f)}{Z_\ell(f) + Z_o(f)}\right|^2 4kT\mathscr{R}\{Z_o(f)\} \left[\mathrm{V}^2/\mathrm{Hz}\right] \tag{10}$$

and we remark that $Z_o(f)$ is a function of the internal impedance of the transmitter and the loads.

4.3. Receiver Noise. We isolate the thermal noise due to the receiver from the contribution due to the rest of the network and we refer to it as receiver noise, namely, $V_\ell(f)$. The receiver noise is due to the parallel impedance that we propose to use as IMN before the first amplification stage of the front-end, that is, the VGA. The parallel impedance provides an SNR improvement as shown in Section 6, but it can be, in general, resistive and thus it may increase the thermal noise contribution.

We do not account for the noise contribution due to the VGA because the input impedance of the VGA is modeled as noiseless. In fact, all noise contributions due to the amplification stage are described by the noise figure of the AFE [15].

In Figure 3(c), we show the equivalent model of the noisy receiver impedance. We model the PSD of $V_\ell(f)$ as

$$P_{V_\ell V_\ell}(f) = \left|\frac{Z_o(f)}{Z_o(f) + Z_\ell(f)}\right|^2 4kT \cdot \mathscr{R}\{Z_\ell(f)\} \left[V^2/Hz\right]. \tag{11}$$

From (11), we note that the PSD of the amplitude of the receiver noise is lower than the actual noise generated by the impedance $Z_\ell(f)$ due to the presence of the voltage divider term.

4.4. Final Model. We now explicit the dependencies of the SNR from the impedance of the receiver. To this aim, we proceed as follows. Firstly, we formulate the CFR and the output impedance of the power delivery network as a function of the chain-matrix parameters, that is, [16]

$$H_i(Z_\ell, f) = \left(A_i(f) + \frac{B_i(f)}{Z_\ell(f)}\right)^{-1}, \tag{12}$$

$$Z_o(f) = \frac{B_u(f) + D_u(f) Z_s(f)}{A_u(f) + C_u(f) Z_s(f)} \ [\Omega], \tag{13}$$

$$\Gamma\left(Z_\ell\right) = \frac{\left|\left(A_u + \dfrac{B_u}{Z_\ell}\right)^{-1}\right|^2 P_{V_tV_t}}{\underbrace{\sum_{d=1}^{D}\left|\left(A_d + \dfrac{B_d}{Z_\ell}\right)^{-1}\right|^2 P_{V_wV_w}}_{\text{active noise}} + \underbrace{\left|\dfrac{Z_\ell}{\dfrac{B_u + D_uZ_s}{A_u + C_uZ_s} + Z_\ell}\right|^2 4kT\mathscr{R}\left\{\dfrac{B_u + D_uZ_s}{A_u + C_uZ_s}\right\}}_{\text{resistive noise}} + \underbrace{\left|\dfrac{\dfrac{B_u + D_uZ_s}{A_u + C_uZ_s}}{\dfrac{B_u + D_uZ_s}{A_u + C_uZ_s} + Z_\ell}\right|^2 4kT\mathscr{R}\left\{Z_\ell\right\}}_{\text{receiver noise}}}, \tag{14}$$

where $i = u, d$, and A_i, B_i, C_i and D_i are the parameters of the transmission matrix that describes the link i. Then, we substitute (3), (4), and (12) in (1), and we replace the PSD of the noise terms with the correspondent expressions (5), (10) and (11), where we explicit $Z_o(f)$ according to (13). In (14), we report the resultant SNR expression. We neglect the frequency dependency for notation simplicity.

5. SNR Optimization Problem

We formulate the SNR optimization problem as follows:

$$\begin{aligned} Z_{\text{opt}}\left(f\right) &= \underset{Z_\ell(f)}{\text{argmax}}\left\{\Gamma\left(Z_\ell, f\right)\right\} \\ \text{s.t.} \quad & x\left(f\right) \geq 0, \\ & y\left(f\right) \in \mathbb{R}, \end{aligned} \tag{15}$$

where $\mathbb{R}$ denotes the set of real numbers, and we introduce the notation $x(f) = \mathscr{R}\{Z_\ell(f)\}$ and $y(f) = \mathscr{I}\{Z_\ell(f)\}$, with $\mathscr{I}\{\cdot\}$ being the imaginary operator. We also highlight that the SNR is dependent on Z_ℓ and f. We start from (14) and, according to the derivations that we report in the Appendix, we obtain

$$\Gamma\left(x, y\right) = \frac{P_{V_tV_t}}{P_a\left(x, y\right) + P_r\left(x, y\right)}, \tag{16}$$

where

$$P_a\left(x, y\right) = \sum_{d=1}^{D}\frac{f_u\left(x, y\right)}{f_d\left(x, y\right)}P_{V_wV_w}, \tag{17}$$

$$P_r\left(x, y\right) = 4kT\left(\zeta_u + \frac{\left|B_u\right|^2}{x^2 + y^2}x\right), \tag{18}$$

$$f_i\left(x, y\right) = \left|A_i\right|^2\left(x^2 + y^2\right) + 2\zeta_i x + 2\varsigma_i y + \left|B_i\right|^2, \tag{19}$$

$$\zeta_i = \mathscr{R}\left\{B_iA_i^*\right\}, \tag{20}$$

$$\varsigma_i = \mathscr{I}\left\{B_iA_i^*\right\}, \tag{21}$$

and $i = u, d$. Furthermore, we remark that all quantities in (16)–(21) are a function of the frequency and we neglect the dependence only for notation simplicity. Experimentally, we have observed that $\zeta_i \geq 0$, while ς_i can be either positive or negative.

Now, we focus on the denominator in (16) and we note the following. Firstly, the active noise is described by the first term, while the contributions of the resistive and receiver noise are gathered in the second term. Secondly, the receiver noise contribution in $P_r(x, y)$ does not increase monotonically as a function of x. Furthermore, $P_r(x, y)$ can be neglected because it is always significantly lower than $P_a(x, y)$ for realistic noise scenarios. In fact, $P_r(x, y)$ is dominated by the Boltzmann constant k, and it assumes values in the order of 10^{-23}. Indeed, $P_{V_aV_a}$ assumes values in the order of 10^{-17}, according to the derivations of Section 4.1. Therefore, we can approximate the SNR as

$$\Gamma\left(x, y\right) \approx \frac{1}{\sum_{d=1}^{D} f_u\left(x, y\right)/f_d\left(x, y\right)} \cdot \frac{P_{V_tV_t}}{P_{V_wV_w}}. \tag{22}$$

We substitute (22) into (15) and we study the concavity of the maximization problem. In general, the expression in (22) is not concave in the domain of x and y that we consider. In detail, the functions $f_i(x, y)$ are convex. The ratio of convex functions is, in general, not convex. Similarly, the sum of nonconvex functions is, in general, not convex. Therefore, the denominator term in (22) is, in general, not convex. It follows that the maximization problem is not concave [17].

Consequently, we performed the exhaustive search to identify the optimal pair (x, y) for each frequency bin, as described in Section 6. From simulation results, we obtained that the optimal receiver resistance is identically null in the entire frequency range, that is, $x = 0$. Therefore, by letting $x = 0$ in (15), we note that the domain of the maximization problem can be limited to the set of values $y = \{\widehat{y}\}$ for which

$$\frac{\partial\Gamma\left(x = 0, y\right)}{\partial y} = 0. \tag{23}$$

6. Numerical Results

We have studied the optimal receiver impedance in real networks. To this aim, we carried out a measurement campaign in Italy and we collected more than 1200 channel responses. We considered three sites, with 11, 23, and 26 outlets, respectively. We followed an exhaustive approach. For each site, we performed measurements between all pairs of available outlets, where no loads were connected.

We performed measurements in the frequency domain. We deployed a vector network analyzer (VNA) in combination with broadband couplers and extension cables. We removed the effect of the couplers and the cables from the measures to obtain the actual scattering parameters of the

PLC channel. We connected the VNA to the network through coaxial cables and broadband couplers. Couplers protect the equipment from the mains and they show an attenuation of 50 dB at the mains frequency, and lower than 5 dB up to 100 MHz.

We calibrated the VNA when only the cables were connected and we removed the effect of the couplers by exploiting the chain rule of the ABCD matrices. To this aim, we characterized the couplers in terms of ABCD matrices. The procedure proved to be the most reliable.

From the measured scattering parameters, we computed the CFR. In Figure 4, we provide the results. In different subplots, we show the channels from the three sites. Furthermore, we report the average profile (dashed line). In all cases the CFR exhibits a frequency decreasing behavior. In sites 2 and 3, that is, the largest premises, the average attenuation is greater than in site 1, that is, a small urban flat. For the statistical characterization of the channels, we refer to [18], where we describe the channels in terms of the main metrics, and we study the probability density function of the CFR as a function of frequency. Furthermore, we point out that herein we consider a restricted set of the measurements in [18].

From the measured scattering parameters, we also computed the output impedance. We define it as in (13), and we note that it can be interpreted as the network impedance at the receiver port when the impedance Z_s is connected to the transmitter port [18]. Hence, Z_o is a function of the source impedance Z_s. In our case, $Z_s = 0\,\Omega$. We denote the real and imaginary component of $Z_o(f)$ with $R_o(f)$ and $X_o(f)$, respectively. To analyze the results, in Figure 5, we report the statistics in quantile terms. We focus on three probability values, that is, $\alpha = 10, 50$, and 90%, and we plot the quantiles $q_{\Lambda,\alpha}(f)$ that corresponds to $\Pr[\Lambda(f) \leq q_{\Lambda,\alpha}(f)] = \alpha$, where $\Lambda \in \{R_o, X_o\}$ and $\Pr[\cdot]$ denotes the probability. Interestingly, we can note that the resistive component is more spread in the lower frequency range, while the reactive component exhibits statistically an inductive-like behavior; that is, it increases with frequency.

The measured values of H_d, H_u, and Z_o have been substituted in (14). By exploiting measurements, we obtain realistic results, although we introduced the following approximations. We neglected the impact of the internal impedance of the noise sources on H_u and H_d, and the impact of the internal impedance of the transmitter on H_d. In fact, when we performed measurements, no loads were connected to the available outlets. The household appliances were connected to the remaining outlets. Hence, according to the model of Figure 1, the measures resemble the case of no loads connected to the transmitter and the D noise ports. Similar considerations hold true for the measurements of the output impedance.

For the analysis of the effect of the optimal impedance, we focus on the 1.5–100 MHz frequency range and the resolution of the measurements is $\Delta = 500$ kHz. In the following, we adopt the discrete frequency representation, and we denote with l the frequency sample $f = l\Delta$. Furthermore, $f_1 = N_1\Delta = 1.5$ MHz and $f_2 = N_2\Delta = 100$ MHz.

We carried out an exhaustive search of the optimal receiver impedance for the measured channels. We limited

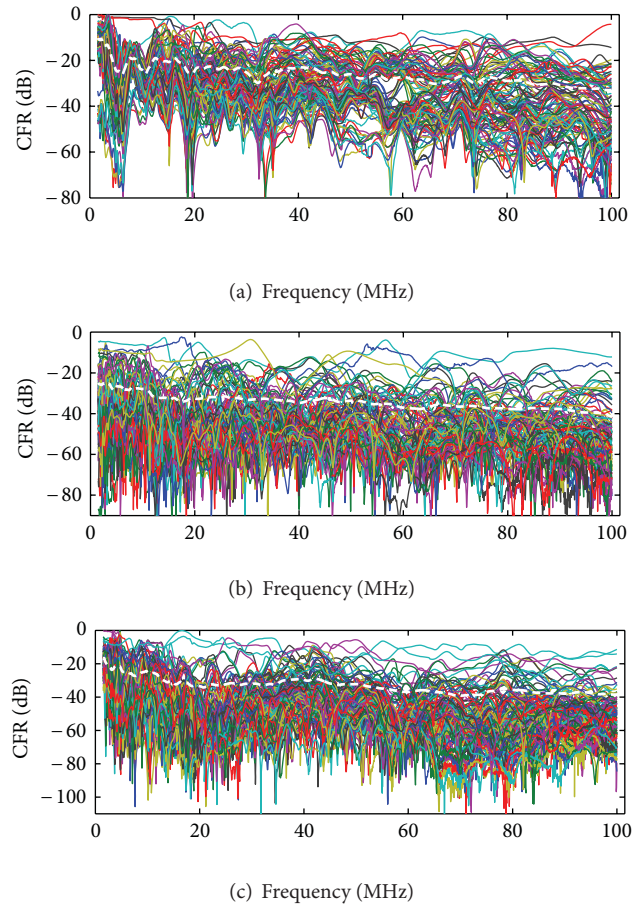

Figure 4: Measured channel frequency responses. From top to bottom, sites 1, 2, and 3. In all cases, the mean profile is also shown (dashed line).

the search domain to $\{0, 1\,\text{k}\Omega\}$ and to $\{-1\,\text{k}\Omega, 1\,\text{k}\Omega\}$ for the resistive and the reactive component, respectively. In both cases, the resolution is $1\,\Omega$. In Figures 6 and 7, we show the quantiles of the components of $Z_{\text{opt}}(f)$ as a function of the frequency. We limit the plot to three probability values, that is, $\alpha = 20, 50$, and 80%. Figure 6 shows that the resistive component of the optimal receiver impedance is equal to 0 for all realizations and frequencies. We speculate that this result is determined by the nonnegative behavior of the coefficients ζ_i in (18)–(20). Indeed, Figure 7 shows that the reactive component of the optimal receiver impedance exhibits a strong frequency-dependent behavior. Furthermore, the median value of the reactive component is close to 0. It follows that the optimal impedance does not exhibit a prominent inductive-like or capacitive-like behavior.

In Figures 6 and 7, we compare the statistics of the optimal receiver impedance to the statistics of the matched impedance, that is, the impedance that is designed to fulfil the power matching conditions. To this aim, we show the quantiles of the receiver impedance under the power matching assumption, namely, $Z_{\text{pmi}} = Z_o^*$. We focus on the probability values $\alpha = 20, 50$ and 80%. Differently from the optimal case, the resistive component of the matched impedance is nonzero and, by definition, it is equal to the

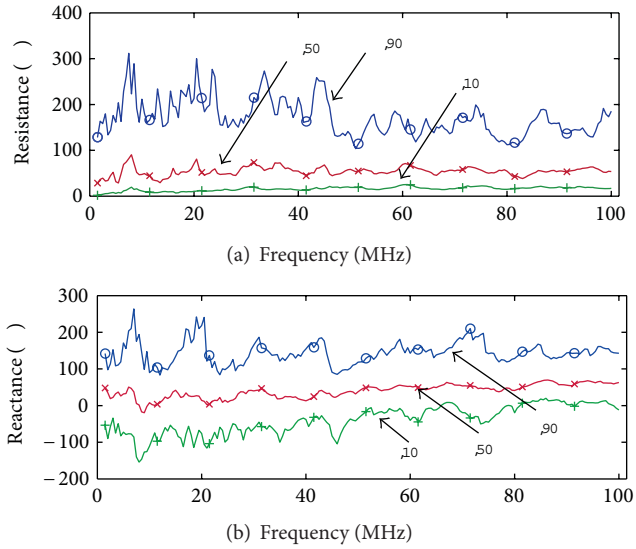

FIGURE 5: Quantiles of the resistive (a) and reactive (b) component of the output impedance. Three probability values are considered, that is, 10, 50 and 90%.

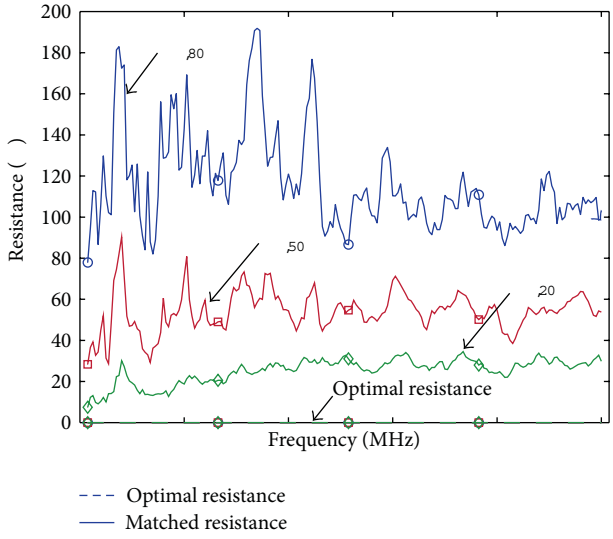

FIGURE 6: Quantiles of the resistive component of the optimal and power matched receiver impedance. Three probability values are considered, that is, 20, 50, and 80%.

resistive component of the output impedance. Indeed, the statistics of the reactive component of Z_{pmi} and Z_{opt} are similar, but, for the matched impedance, the high-probability area is better confined around the median and the profiles of the quantiles associated to probabilities $\alpha = 20$ and 80 are smoother in frequency. Finally, the median of the reactive component of the matched impedance overlaps the median of the reactive component of the optimal impedance.

Now, we study the SNR, namely, $\Gamma(Z_\ell, l)$. We compute it according to (14). We let the transmitted power (in dB terms) be

$$P_{V_t V_t}(l) = \begin{cases} -63\,\text{dBV/Hz} & \text{for } l\Delta \le 30\,\text{MHz} \\ -93\,\text{dBV/Hz} & \text{otherwise} \end{cases} \quad (24)$$

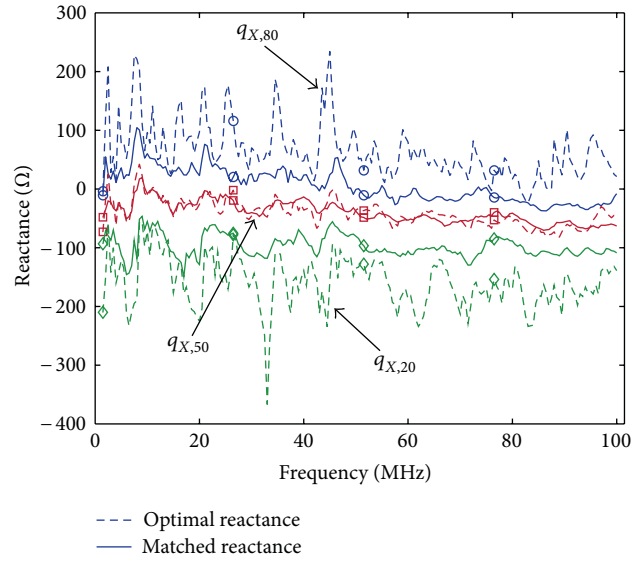

FIGURE 7: Quantiles of the reactive component of the optimal and power matched receiver impedance. Three probability values are considered, that is, 20, 50, and 80%.

that is, the values that yield to a transmitted power of −50 dBm/Hz below 30 MHz, and −80 dBm/Hz beyond 30 MHz on a reference load of 50 Ω. Basically, we shape $P_{V_t V_t}$ as described in [12], and not as directly specified by the EMC norms because the latter do not target the frequency range beyond 30 MHz yet. Furthermore, we determine $P_{V_w V_w}$ as described in Section 4.1.

We compute the SNR when the receiver impedance is optimal, matched in power, or constant in frequency and equal to $Z_{50} = 50\,\Omega$. We assume the latter to be the reference case, and we obtain the SNR improvements provided by the use of Z_{opt} and Z_{pmi} with respect to Z_{50}, that is, $\Delta\Gamma(Z_\kappa, l) = (\Gamma(Z_\kappa, l))_{\text{dB}} - (\Gamma(Z_{50}, l))_{\text{dB}}$ where $\kappa \in \{\text{opt}, \text{pmi}\}$. Note that $\Delta\Gamma$ is formulated as the difference of the SNR in dB terms. Hence, we study the statistics of $\Delta\Gamma(Z_\kappa, l)$. In Figure 8, we show the fitted profiles of the quantiles of $\Delta\Gamma(Z_\kappa, l)$ associated to the probability values 20, 50, and 80%. Impedance adaptation techniques are more beneficial in the lower frequency range, where the optimal impedance and the power matched impedance provide, in half of the cases, up to 4 and 1 dB of improvement, respectively. In the higher frequency range and for half of the cases, the matched impedance does not provide any improvement, while the optimal impedance ensures an SNR gain of approximately 1 dB. Finally, we note that, according to the formulation in (14), the matched impedance can even reduce the SNR with respect to the case of using Z_{50} (see $\Pr[\Delta\Gamma(Z_{\text{pmi}}, l) \le \gamma] = \alpha$ for $\alpha = 20\%$ in Figure 8).

Now, we study the performance in terms of achievable rate. We assume the transmitted signal and the noise to be Gaussian, and we define the achievable rate as follows:

$$C(\nu) = \Delta \sum_{l=N_1}^{N_2} \log_2\left(1 + \Gamma\left(Z_\nu, l\right)\right) \ [\text{bps}], \quad (25)$$

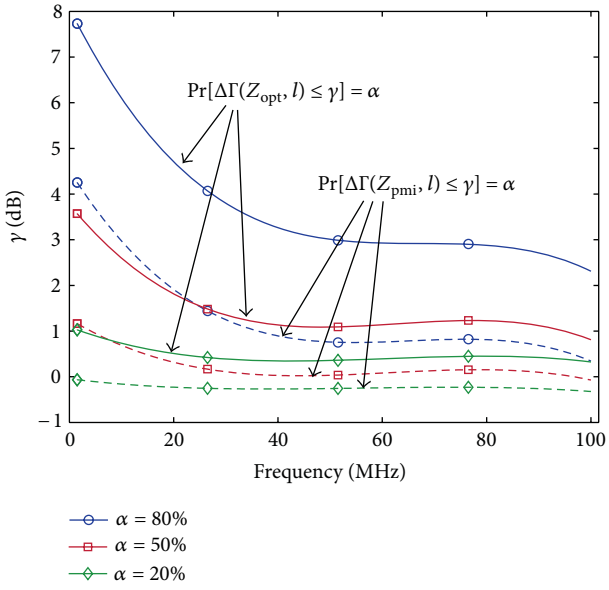

FIGURE 8: Best cubit fit of the SNR quantile profiles associated to the probability values $\alpha = 20, 50$, and 80%.

where $\nu \in \{\text{opt}, \text{pmi}, 50\}$, and we limit the transmitted PSD according to (24). In Figure 9(a), we show the complementary cumulative distribution function (C-CDF) of the achievable rate for the three receiver impedances that we consider. We magnify the plot for the probability values greater than 0.6. As expected, the optimal impedance outperforms the power matched impedance. As an example, $C(\text{opt})$ exceeds 800 Mbps in 83% of the cases, while $C(\text{pmi})$ achieves the same rates in 77% of the cases. In a dual manner, with probability 0.9, $C(\text{opt}) > 745$ Mbps while $C(\text{pmi}) > 695$ Mbps, with an improvement of 7%.

Now we quantify the improvement with respect to Z_{50}. We compute the achievable rate improvement as follows:

$$\Delta C(\kappa) = 100 \frac{C(\kappa) - C(50)}{C(50)} \quad [\%], \tag{26}$$

where $\kappa \in \{\text{opt}, \text{pmi}\}$. In Figure 9(b), we show the cumulative distribution function (CDF) of $\Delta C(\kappa)$. The use of the optimal impedance turns into achievable rate improvements of up to 24%. Interestingly, the power matching approach does not provide significant benefit with respect to Z_{50}. In this case, the improvement is lower than 5% in 90% of the cases. Furthermore, the matched impedance can even reduce the achievable rate. The reason is that the matched impedance maximizes the power of the received signal, but not necessarily the SNR.

6.1. High Receiver Impedance Design. In the previous section, we have shown the performance when the receiver impedance is optimal, matched in power or constant and equal to 50 Ω. It is also interesting to address the performance when the receiver impedance is high. In such case, we denote the receiver impedance with Z_{high} and we let it be purely real and equal to 1 kΩ, that is, the largest value that we admitted for the exhaustive search of the optimal impedance. We limit the study to the achievable rate. We compute it as in (25), and we denote it with $C(\text{high})$. Similarly, we compute the achievable rate improvement as in (26), and we denote it with $\Delta C(\text{high})$. In Figure 9, we show both the C-CDF of $C(\text{high})$ and the CDF of $\Delta C(\text{high})$. As it can be noted, Z_{high} does not provide any benefit with respect to Z_{50} and the two solutions

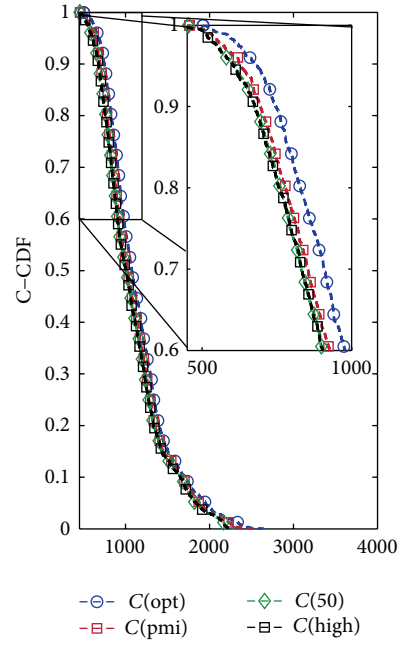

(a) Achievable Rate (Mbps)

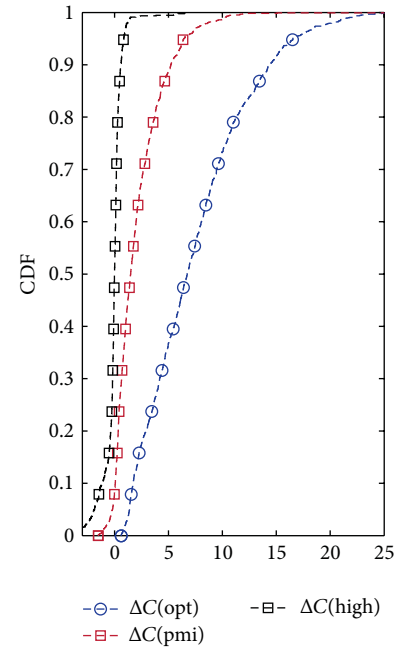

(b) Improvement (%)

FIGURE 9: (a) C-CDF of the achievable rate when the receiver impedance is optimal, matched in power or constant and equal to 50 Ω or 1 kΩ. (b) CDF of the achievable rate improvement with respect to the case of Z_{50}.

are equivalent in terms of achievable rate. Similar results can be obtained by letting Z_{high} be large, and purely imaginary either positive or negative.

As a final remark, we note that the optimal impedance provides the best gain in terms of achievable rate. However, it is rather complex to be implemented in practice. Therefore, more simpler though suboptimal solutions, as $Z_{50}(f)$ and $Z_{\text{high}}(f)$, are often used.

7. Conclusions

We have investigated the optimal design of the receiver input impedance for the maximization of the SNR in broadband PLC. We have firstly presented a comprehensive description of the power delivery network. We have modelled the contribution of the household appliances on the noise at the receiver port. Then, we have discussed the front-end design for broadband PLC transceivers. We have pointed out that the amplitude (and not the power) of the received signal is important for data communication purposes.

Therefore, we have formulated the SNR in amplitude terms, and we have modelled the noise as the sum of four contributions, namely, the active, resistive, receiver, and coupled noise. Basically, the active noise is the noise that is injected by the household appliances, the resistive noise accounts for the thermal noise due to the resistive components of the network, the receiver noise is the thermal noise due to the receiver impedance, and the coupled noise is the noise that couples into the wirings, for example, due to broadcast radios.

We have studied the dependency of the SNR from the receiver impedance and we have highlighted the latter impacts not only on the amplitude of the useful signal, but also on the amplitude of the noise at the receiver port. Hence, we have found the optimal receiver impedance that maximizes the SNR. To this aim, we have exploited the results of an experimental measurement campaign where we have collected the scattering parameters of PLC channels in real home grids. From the measurement results, we have found that the optimal impedance is purely reactive and not equal to that obtained according to the power matching approach, namely, the matched impedance. We have compared the performance of the optimal impedance to that of the matched impedance in terms of SNR and achievable rate for real-life scenarios. We have assumed the performance of a 50-Ω receiver as the reference case and we have found that while the matched impedance can even reduce the performance, the optimal impedance provides improvements up to 24% in terms of achievable rate. Finally, we have shown that when the receiver exhibits a high input impedance, the achievable rate is close to that obtained with a 50-Ω receiver. Therefore, the two solutions are equivalent in performance.

Appendix

SNR Derivations

We aim to simplify the SNR formulation in (14) to obtain (16). We neglect the frequency dependency for notation simplicity, and we proceed as follows. Firstly, we introduce the notation $x = \mathcal{R}\{Z_\ell\}$ and $y = \mathcal{I}\{Z_\ell\}$. Then, we substitute Z_ℓ in (12) with $x + jy$, where j is the imaginary unit, to obtain

$$|H_i(f)|^2 = \frac{x^2 + y^2}{|A_i|^2 (x^2 + y^2) + |B_i|^2 + 2x\zeta_i + 2y\varsigma_i}, \quad \text{(A.1)}$$

where $i = u, d$, ζ_i and ς_i are defined as in (20)-(21), and we exploited the following relations:

$$\zeta_i = \mathcal{R}\{A_i\}\mathcal{R}\{B_i\} + \mathcal{I}\{A_i\}\mathcal{I}\{B_i\}, \quad \text{(A.2)}$$

$$\varsigma_i = \mathcal{R}\{A_i\}\mathcal{I}\{B_i\} - \mathcal{I}\{A_i\}\mathcal{R}\{B_i\}. \quad \text{(A.3)}$$

Now, we focus on the output impedance Z_o. When $Z_s = 0$, the real part of Z_o reads

$$\mathcal{R}\{Z_o(Z_s = 0\,\Omega)\} = \mathcal{R}\left\{\frac{B_u}{A_u}\right\} = \frac{\mathcal{R}\{B_u A_u^*\}}{|A_u|^2}. \quad \text{(A.4)}$$

We exploit (A.4), and we explicit the resistive and the receiver noise in (14) as

$$\begin{aligned} P_{V_r V_r} &= \left|\frac{x + jy}{B_u/A_u + x + jy}\right|^2 \\ &= \frac{|A_u|^2 (x^2 + y^2)}{|A_u|^2 (x^2 + y^2) + |B_u|^2 + 2x\zeta_u + 2y\varsigma_u} \end{aligned} \quad \text{(A.5)}$$

$$\begin{aligned} P_{V_\ell V_\ell} &= \left|\frac{B_u/A_u}{B_u/A_u + x + jy}\right|^2 \\ &= \frac{|B_u|^2}{|A_u|^2 (x^2 + y^2) + |B_u|^2 + 2x\zeta_u + 2y\varsigma_u}, \end{aligned} \quad \text{(A.6)}$$

respectively. Finally, we substitute (A.1) and (A.5)-(A.6) in (14); we divide the numerator and the denominator by (A.1) and we obtain (16).

References

[1] F. J. Cañete, J. A. Cortés, L. Díez, and J. T. Entrambasaguas, "Analysis of the cyclic short-term variation of indoor power line channels," *IEEE Journal on Selected Areas in Communications*, vol. 24, no. 7, pp. 1327–1338, 2006.

[2] H. C. Ferreira, L. Lampe, J. Newbury, and T. G. Swart, *Power Line Communications: Theory and Applications for Narrowband and Broadband Communications over Power Lines*, Wiley & Sons, New York, NY, USA, 2010.

[3] N. Taherinejad, R. Rosales, S. Mirabbasi, and L. Lampe, "On the design of impedance matching circuits for vehicular power line communication systems," in *Proceedings of the IEEE International Symposium on Power Line Communications and Its Applications (ISPLC '12)*, pp. 322–327, March 2012.

[4] P. A. Janse van Rensburg and H. C. Ferreira, "Design of a bidirectional impedance-adapting transformer coupling circuit for low-voltage power-line communications," *IEEE Transactions on Power Delivery*, vol. 20, no. 1, pp. 64–70, 2005.

[5] A. M. Tonello and F. Versolatto, "Bottom-up statistical PLC channel modeling—part I: random topology model and efficient transfer function computation," *IEEE Transactions on Power Delivery*, vol. 26, no. 2, pp. 891–898, 2011.

[6] Maxim, "Integrated powerline communication analog front-end transceiver and line driver," http://www.maximic.com/datasheet/index.mvp/id/6333.

[7] P. G. M. Baltus and R. Dekker, "Optimizing RF front ends for low power," *Proceedings of the IEEE*, vol. 88, no. 10, pp. 1546–1559, 2000.

[8] J. Bauwelinck, E. de Backer, C. Mèlange et al., "A 1024-QAM analog front-end for broadband powerline communication up to 60 MHz," *IEEE Journal of Solid-State Circuits*, vol. 44, no. 5, pp. 1477–1485, 2009.

[9] B. Razavi, *RF Microelectronics*, Prentice Hall, 1998.

[10] C. Bowick, *RF Circuit Design*, Newnes, 1982.

[11] L. W. Couch, *Digital and Analog Communication Systems*, Prentice Hall, 1997.

[12] R. Hashmat, P. Pagani, and T. Chonavel, "MIMO communications for inhome PLC networks: measurements and results up to 100 MHz," in *Proceedings of the IEEE International Symposium on Power Line Communications and Its Applications (ISPLC '10)*, pp. 120–124, March 2010.

[13] A. Papoulis, *Probability, Random Variables, and Stochastic Processes*, McGraw-Hill, 1991.

[14] H. T. Friis, "Noise figures of radio receivers," *Proceedings of the IRE*, vol. 32, no. 7, pp. 419–422, 1944.

[15] W. F. Egan, *Practical RF System Design*, John Wiley & Sons, 2003.

[16] D. M. Pozar, *Microwave Engineering*, Wiley Academy, 2004.

[17] S. Boyd, *Convex Optimization*, Cambridge University Press, 2004.

[18] A. M. Tonello and F. Versolatto, "PLC channel characterization up to 300 MHz: frequency response and access impedance," in *Proceedings of the IEEE Global Communications Conference (GLOBECOM '12)*, December 2012.

Hindawi Publishing Corporation
Journal of Electrical and Computer Engineering
Volume 2013, Article ID 746763, 11 pages
http://dx.doi.org/10.1155/2013/746763

Research Article

Enhancements of G3-PLC Technology for Smart-Home/Building Applications

Luca Di Bert, Salvatore D'Alessandro, and Andrea M. Tonello

Dipartimento di Ingegneria Elettrica, Gestionale e Meccanica (DIEGM), Università di Udine, 33100 Udine, Italy

Correspondence should be addressed to Andrea M. Tonello; tonello@uniud.it

Received 30 September 2012; Accepted 19 December 2012

Academic Editor: Ahmed Zeddam

To enable the smart grid concept, it is fundamental to consider the in-home/building context where, beside the conventional home networking services, home automation and smart energy management services have to be offered. In this paper, we consider the in-home/building scenario, for which we propose a convergent network architecture to enhance the performance of the narrowband power line communication (PLC) G3-PLC technology through its integration with an Ethernet-based network. To this end, we define the protocols characterizing the network modules, namely, switches and routers, which allow for integrating the G3-PLC with Ethernet devices. Since Ethernet represents a convergent standard for many communication devices, by adding this functionality to G3-PLC, interconnectivity with other heterogeneous nodes can be offered. Furthermore, since the G3-PLC medium access control layer is based on a carrier sense multiple access scheme, its performance decreases when the number of network nodes contending for the channel increases. Therefore, we evaluate the network performance when an optimized time division multiple access scheme is adopted. The proposed convergent network architecture has been implemented in the OMNeT++ network simulator.

1. Introduction

Energy efficiency and power saving were identified in 2010 as fundamental objectives to contribute to the sustainable growth specified in the "Europe 2020" strategy [1]. As a consequence, in the near future, the power grid needs to become a distributed large-scale system that has to smartly manage flows of electricity produced by big or small plants, that is, a smart grid (SG). To this respect, demand side and demand response mechanisms have to be implemented, so that prosumers will actively collaborate in the use and delivery of energy [2, 3]. To enable the SG concept, it becomes therefore fundamental to consider the in-home/building context where, beside the conventional home networking services—for example, triple play (high speed internet access, television, telephone), infotainment, and resource sharing in local area networks (LANs)—, home automation and smart energy management services have to be offered.

Differently from home networking services, home automation and energy management services usually involve a large number of nodes (sensors/actuators) that are pervasively deployed within the house/building and transmit a small amount of data. Despite the small amount of data, strict requirements as coverage, latency, delay, and robustness must be fulfilled for some applications, for example, the automation of windows and doors, the control of heating, ventilation and air conditioning (HVAC), the monitoring of presence/temperature/gas/smoke, the management of loads, and so forth.

In this context, power line communication (PLC) is a key technology since (a) the power line grid is pervasively deployed within houses/buildings, and (b) it does not require the use of new wires, which, in turn, reduces deployment costs.

PLC devices are in general grouped into two categories, that is, narrowband (NB) and broadband (BB) devices, according to the bit-rate that they can offer. BB-PLC devices are widely deployed to offer high speed home networking services. They work in the frequency band 2–30 MHz (and beyond) and make use of advanced modulation techniques to offer bit-rates in the order of hundreds of Mbps. On the other hand, NB-PLC devices have been developed to offer low bit-rates for home automation (indoor) and smart metering (outdoor) services. These devices usually work in a frequency

band belonging to the range of 3–490 kHz, depending on the regulations applied in a specific country, for example, CENELEC, ARIB, FCC. Detailed information regarding BB and NB PLC technologies can be found in [4].

Clearly, besides PLC, there is also a broad variety of wireless and wired technologies that can be used for both high and low bit-rate in-home applications [5], for example, WiFi, Zigbee, Bluetooth, Z-Wave, twisted pair Ethernet, MoCA, and so forth.

Despite the existence in the market of this broad variety of communication technologies, the bottleneck to their pervasive deployment, and thus to the joint delivery of different services, is that they often cannot interconnect and interoperate, and in some cases even coexist.

1.1. Smart Home/Building Enabled by a Convergent Network. From the previous discussion, we deem important to realize a convergent communication network in order to integrate a broad variety of communication technologies thus to enable the smart home (SH) concept, that is, the joint delivery of home networking, home automation and energy management services.

The convergent communication network can be obtained by providing a convergent layer where heterogeneous communication technologies can coexist and be interconnected.

Usually, the coexistence, that is, the ability of sharing the same physical medium by two or more devices, is obtained by exploiting different frequency bands at the physical (PHY) layer, or through the use of medium access control (MAC) protocols. The interconnectivity—namely, the capability of devices to exchange data at PHY, data link layer (DLL), and network layer—requires coexistence, and it can be achieved with a convergent layer above the data link layer or at the network layer. Coexistence and connectivity among different technologies, through PHY or data link layer (DLL) mechanisms, have been the focus of many studies. Representative examples are as follows: the inter-PHY protocol developed within the IEEE P1901 working group that allows coexistence among two different broadband PLC devices [6]; the ITU-T G.hn standard that has been conceived with the aim of offering interconnectivity among in-home high speed communication devices working over telephone wires, power lines, and coax [6, 7] (G.hn specifies the PHY layer and the MAC sublayer and addresses the coexistence between protocols that operate on different media); the solution developed within the EU-FP7 OMEGA project, according to which devices belonging to the OMEGA network share the same inter-MAC sublayer and consequently they can coexist and they can be interconnected [8].

Connectivity among heterogeneous devices can be also reached at network layer by exploiting the Internet protocol (IP). The use of the TCP/IP protocol stack to integrate different communication technologies for SH and SG applications is largely advocated. Previous work that follows this approach is described in [3, 9–12] and references therein. Also standardization working groups are considering it, for example, at the end of 2010, IEEE launched the P1905 working group [13] that is focused on the definition of an abstraction layer for multiple home networking technologies. The abstraction layer will provide a common data and control Service Access Point (SAP) for the home networking technologies described in the IEEE P1901, 802.11 [14], 802.3 [15], and MoCA 1.1 specifications [16]. Finally, a number of standard development groups—among which ZigBee [17], HomePlug [18], and Wi-Fi alliances—are working on the development of the ZigBee Smart Energy version 2.0 [19] that will offer IP-based control for advanced metering infrastructures and home area networks allowing for interoperability with 802.11 and HomePlug devices.

1.2. Contribution. In this paper, we consider the in-home scenario where we propose the use of a convergent network to enhance the performance of NB G3-PLC technology [20, 21] through its integration in an Ethernet network. We thus focus on the convergence at the DLL. Clearly, the integration of the proposed network in a TCP/IP network can be easily obtained by adding the corresponding transport/network layers. It should be noted that G3-PLC was mostly designed for outdoor SG applications. Furthermore, it has been used as a baseline technology for the development of the [22] IEEE P1901.2 and the ITU-T G.hnem standard for SG applications. The deployment of G3-PLC in home/buildings is indeed interesting. However, in our previous work [23], we have found, through experimental test campaigns, that the G3-PLC technology can exhibit poor performance within large houses/buildings. Therefore, in this paper, we propose possible enhancements focusing at the MAC DDL sublayer.

The first contribution of this paper is the definition of the protocols characterizing the network modules, namely, switches and routers, which allow the integration of G3-PLC and Ethernet devices in a convergent network architecture. Range extension is achieved by partitioning the overall network into subnetworks, that is, G3-PLC subnetworks. An Ethernet backbone (in particular using cat5 wiring) provides connectivity between the subnetworks.

The second contribution regards the evaluation of the convergent network when adopting a time division multiple access (TDMA) scheme at the MAC sublayer of the G3-PLC nodes. In fact, the G3-PLC MAC sublayer is based on the non-beacon-enabled mode of the IEEE 802.15.4 standard, which is a carrier sense multiple access (CSMA) scheme. As it is known, the performance of CSMA schemes decreases as the number of the network nodes contending for the channel increases. This situation can occur in large houses/buildings where a large number of sensors/actuators is deployed. To cope with this problem, we implement a modified version of the beacon-enabled mode of the IEEE 802.15.4 [24], which is based on a TDMA MAC mechanism, and we show that substantial performance increase can be obtained.

The network performance has been evaluated with the use of the OMNeT++ network simulator [25].

The remainder of the paper is as follows. In Section 2, we briefly describe the G3-PLC and the Ethernet technologies. Then, in Section 3, we present the implementation of the convergent network, and in Section 4, we study its performance. Finally, in Section 5, we consider the TDMA implementation and we compare its performance with CSMA. Conclusions follow in Section 6.

2. Communication Technologies

In this section, we describe the G3-PLC and the Ethernet technologies that will be used to build the convergent in-home network in Section 3.

2.1. G3-PLC. Originally developed for Automatic Metering Management (AMM) applications, G3-PLC is playing a relevant role inasmuch it has been used for the development of the IEEE P1901.2 and the ITU-T G.hnem standard for SG applications [22]. In the following, we discuss its PHY layer and MAC sublayer.

2.1.1. PHY Layer. According to [20], the G3-PLC technology has been designed to support CENELEC, ARIB, and FCC bands in the frequencies range between 10 kHz and 490 kHz. It makes use of pulse shaped—orthogonal frequency division multiplexing (PS-OFDM) carrying DQPSK, or DBPSK symbols in "normal" or "robust" mode. The correspondent maximum data packet is 235 bytes with DQPSK, 235 bytes with DBPSK in "normal" mode, and 133 bytes with DBPSK in "robust" mode. The maximum achievable bit-rate is 33.4 kbps using DQPSK. It should be noted that the differential encoding takes place across the data stream of each subchannel.

The PHY frame format (see Figure 1) is characterized by (i) the preamble, which is a multisymbol field used to perform carrier sense operations, to enable control functions and to synchronize the receiver and the transmitter, (ii) the frame control header (FCH), which carries control information required to correctly demodulate the received signal, (iii) the data payload. The data payload length (n) depends on the transmission mode, that is, normal and robust. In normal mode, the forward error correction (FEC) is performed through a Reed Solomon (RS) encoder and a convolutional encoder, whereas the error check is done with a frame check sequence (FCS). In robust mode, beside RS and convolutional encoding, there is a repetition code (RC) that repeats each bit following the preamble 4 times. At the receiver side, the hard decision Viterbi decoder and the RS decoder are used.

When showing simulation results, we consider G3-PLC working in the CENELEC-A band (despite the fact that CENELEC-A is generally not used for home networking, performance is not significantly affected by the operating band). In this case, it uses PS-OFDM with a raised cosine window, and $M = 256$ subchannels out of which $N_c = 36$ are used in the 35.9–90.6 kHz frequency band. Furthermore, we assume the PHY frame to last $N_s = 40$ OFDM symbols that carry data modulated with DQPSK and robust DBPSK. This assumption, respectively, leads to $n = 163$ or $n = 13$ bytes of data and 16 or 8 RS parity check bytes. Consequently, the maximum achievable bit-rates are 29.6 kbps and 2.4 kbps. Table 1 reports the set of the PHY layer parameters.

2.1.2. MAC Sublayer. According to [21], the MAC sublayer is based on the IEEE 802.15.4-2006 specification for low-rate wireless personal area networks (WPANs) [24]. Basically, the channel access method is based on the CSMA with collision avoidance (CSMA/CA) mechanism and a random backoff time. It is worth noting that G3-PLC does not provide specifications for the higher ISO/OSI layers.

Table 1: G3-PLC system specifications.

Number of PS-OFDM symbols	$N_s = 40$
Number of IFFT/FFT points	$M = 256$
Number of used subchannels	$N_c = 36$
Number of overlapped samples	$N_o = 8$
Number of cyclic prefix samples	$N_{CP} = 30$
Number of FCH symbols	$N_{FCH} = 13$
Sampling frequency (MHz)	$f_s = 0.4$
Number of preamble symbols (without FCH)	$N_{pre} = 9.5$

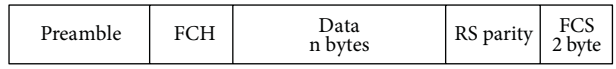

Figure 1: G3-PLC PHY frame format.

The MAC implementation starts from the assumption of a minimum overhead of 8 bytes. Therefore, according to the amount of data bytes defined in the PHY, the maximum MAC payload is 155 bytes in normal mode and 5 bytes in robust mode. For the sake of implementation simplicity, we assume that the transmission does not wait for any current reception acknowledgement (ACK).

2.2. Ethernet. Ethernet is widely deployed on LANs. It offers a convergent logical link control (LLC) sublayer for many different PHY layers and MAC sublayers, for example, coax, twisted pair as well as optical fiber and wireless. Although the Ethernet protocol was originally proposed for use over coax cables, most of today's Ethernet networks make use of twisted pairs and operate in full duplex mode: the network is switched thus the connections are handled point-to-point and cannot be shared by multiple devices. Therefore, the full duplex mode eliminates carrier sense multiple access with collision detection (CSMA/CD) mechanisms because there is no need to determine whether the connection is already being used.

In this perspective, we decided to consider the 100BASE-TX, that is, the predominant form of Fast Ethernet (IEEE 802.3u) over twisted pair cables (cat5), offering bit-rates up to 100 Mbps. Moreover, since 100BASE-TX is full-duplex, it requires the use of switches.

3. Convergent Network Implementation

In this paper, we focus on the integration of G3-PLC technology within an Ethernet network. Since the switched Ethernet network exhibits a star topology and the power line channel can be considered as a bus, we adopt a treelike topology—as a combination of bus and star topologies—to implement the convergent network (see Figure 2). The major benefit deriving from the use of such a topology is its ability to be scalable, extensible, and reliable. The convergence between Ethernet and G3-PLC can be obtained through the definition of a shared common layer that provides interconnectivity among heterogeneous lower layers.

The network convergence is achieved by defining different network devices, that is, *end nodes*, *routers*, and *switches*.

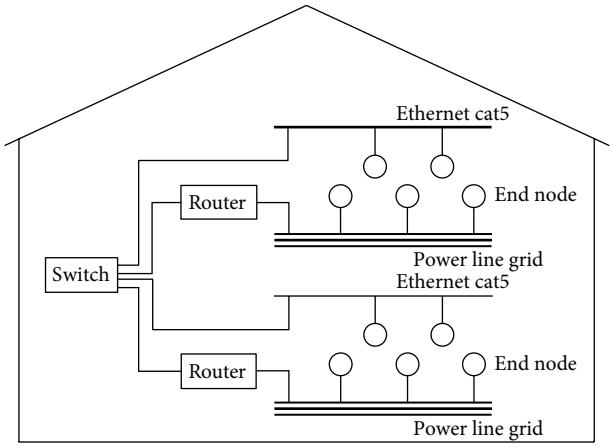

Figure 2: Network topology.

3.1. End Nodes. They represent the devices of the network that directly interact with the surrounding environment, for example, sensors, actuators, switches, meters, and so on. These nodes are grouped into subnetworks according to the same communication technology, that is, G3-PLC. From a logical point of view, the end nodes can be all characterized by the same building blocks, that is, a traffic generator (which is responsible of data packets generation) and the network adapter. The network adapter comprises a PHY, a MAC, and a buffer of data packets coming from the traffic generator.

3.2. Router. Since G3-PLC does not provide any specification for the integration in a switched Ethernet network, we need a network device that groups G3-PLC nodes into a subnetwork and integrates the subnetwork with the rest of the Ethernet network. To do that, we define a router that offers network adapters towards both Ethernet and G3-PLC. Beside the network adapters, the Router has a routing module that is responsible of translating and forwarding packets from one network adapter to the other and vice versa: this module is responsible of interconnectivity between Ethernet and G3-PLC. It is worth noting that since the maximum allowed G3-PLC PHY frame size is 251 bytes (corresponding to a payload of 235 data bytes both in DQPSK and DBPSK normal mode), the router encapsulates each G3-PLC frame into one Ethernet frame, whose maximum payload dimension is 1500 bytes. On the other side, Ethernet frames exceeding 251 bytes are fragmented by the router in order to fulfill G3-PLC constraints. However, this assumption is not necessarily optimal.

As depicted in Figure 3, the routing module keeps trace of packets received from its subnetwork nodes, and it generates a forwarding table with *source address*, *insertion time*, and *link quality*. In this perspective, the router dynamically learns about the existence of nodes during reception of packets and modifies its table updating the link quality or removing aged entries, according to the insertion time. It is worth noting that a given subnetwork can be managed by two (or more) routers in order to ensure a more reliable communication on harsh power line channels, or equally, to increase the network coverage. Furthermore, in order to prevent loops, the router is able to recognize and discard packets directly arrived from other routers.

3.3. Switch. The switch is a well-known network device. As depicted in Figure 4, the switch has been modified in order to work seamlessly with the routers. In particular, it is able to build and update a forwarding table exploiting nodes information harvested by each router. A forwarding table entry is composed of *source address*, *insertion time*, *link quality*, and arrival *port number*. Therefore, the switch compares the information carried by a packet with the correspondent table entries and forwards the packet to the correct port (or broadcast if the destination address has no correspondence in the table). In this case, the insertion time parameter is exploited to remove aged entries from the table and thus increasing the system fault tolerance. Again, the switch is able to prevent packet loops. We also point out that since link quality is updated periodically, the switch is able to dynamically handle the network changes. It is now clear that the combination of the router and switch procedures enables the integration of heterogeneous communication technologies leading to a convergent network. Moreover, this combination provides the basis for satisfying quality of service (QoS) constraints.

It should be finally noted that the integration of G3-PLC with Ethernet easily allows for integrating the G3-PLC technology in IP networks.

4. Simulation Setup and Results

The convergent network has been implemented using the OMNeT++ simulator and its extension INET-Framework [26]. OMNet++ is an open source, component-based simulation library, and framework that is primarily thought for building network simulators. Basic components, that is, *simple modules*, are programmed in C++ and then combined into larger components, that is, *compound modules*, using a network description (NED) language. NED language is also used to connect compound modules and assemble the whole network. A screenshot of the simulated network is shown in Figure 5 where we assume a cat5 cable propagation delay of 500 ns.

In order to quantify the convergent network performance, we define a representative metric, namely, the aggregate network throughput (THR). It is evaluated as

$$\mathrm{THR} = \sum_{u=1}^{N} \mathrm{THR}^{(u)} \ [\mathrm{bps}], \tag{1}$$

where N is the number of network nodes and $\mathrm{THR}^{(u)}$ is the average throughput achieved by the uth node, which is obtained as

$$\mathrm{THR}^{(u)} = 8nN_g^{(u)} \ [\mathrm{bps}], \tag{2}$$

where n are the data bytes encapsulated in the PHY frame, $N_g^{(u)}$ is the number of correct received PHY frames per second by the uth node, which are detected exploiting either

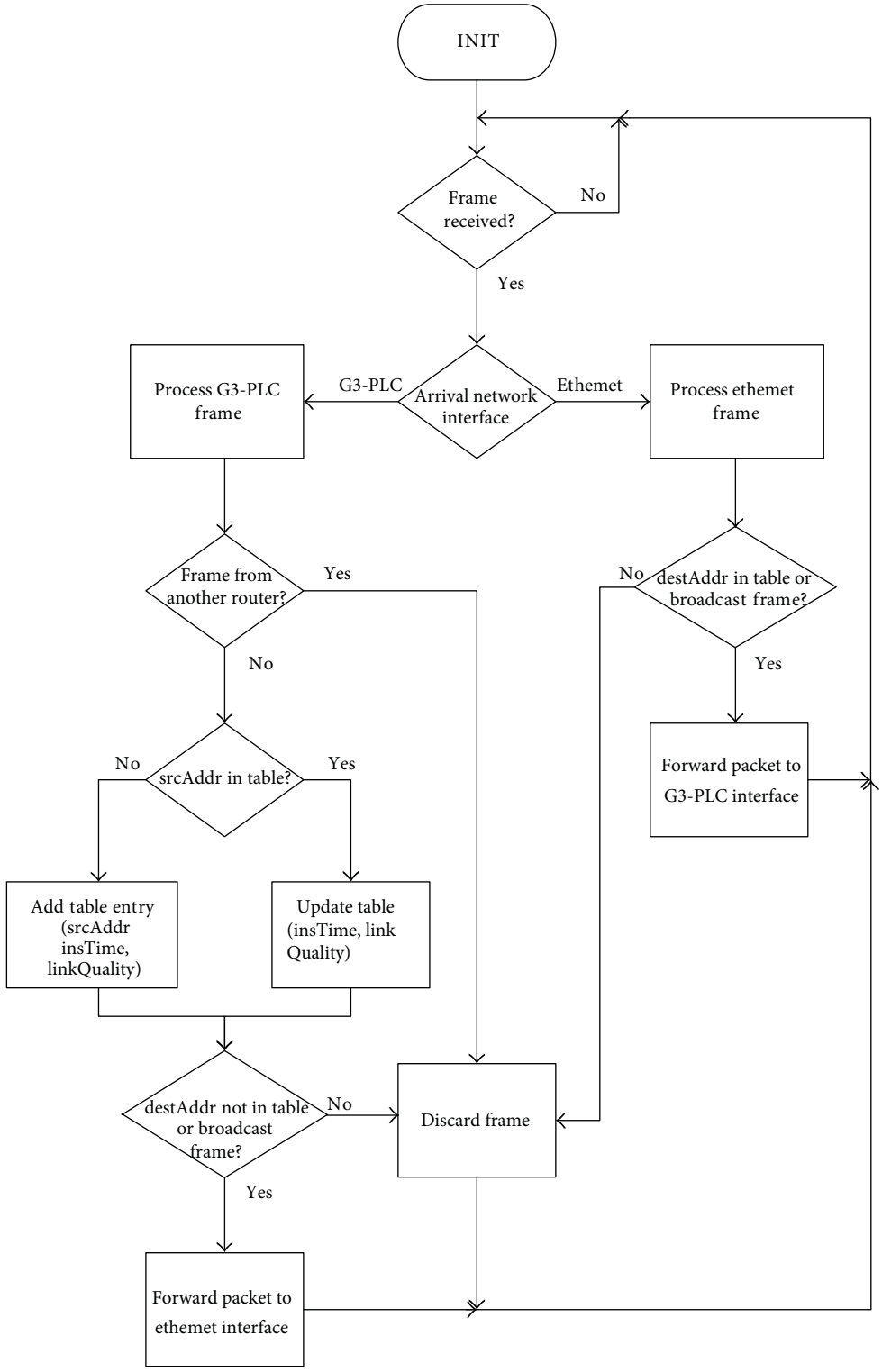

Figure 3: Router flow chart.

the knowledge of the transmitted frame or the FCS field. Furthermore, we define the frame error rate (FER) as follows:

$$\mathrm{FER}^{(u)} = \frac{\left(N_t^{(u)} - N_g^{(u)}\right)}{N_t^{(u)}}, \tag{3}$$

where $N_t^{(u)}$ is the total number of transmitted frames destined to uth user. It is worth noting that the FER takes into account corrupted frames as well as missed frames.

In order to model the power line channel in the OMNeT++ implementation, we make use of the hardware

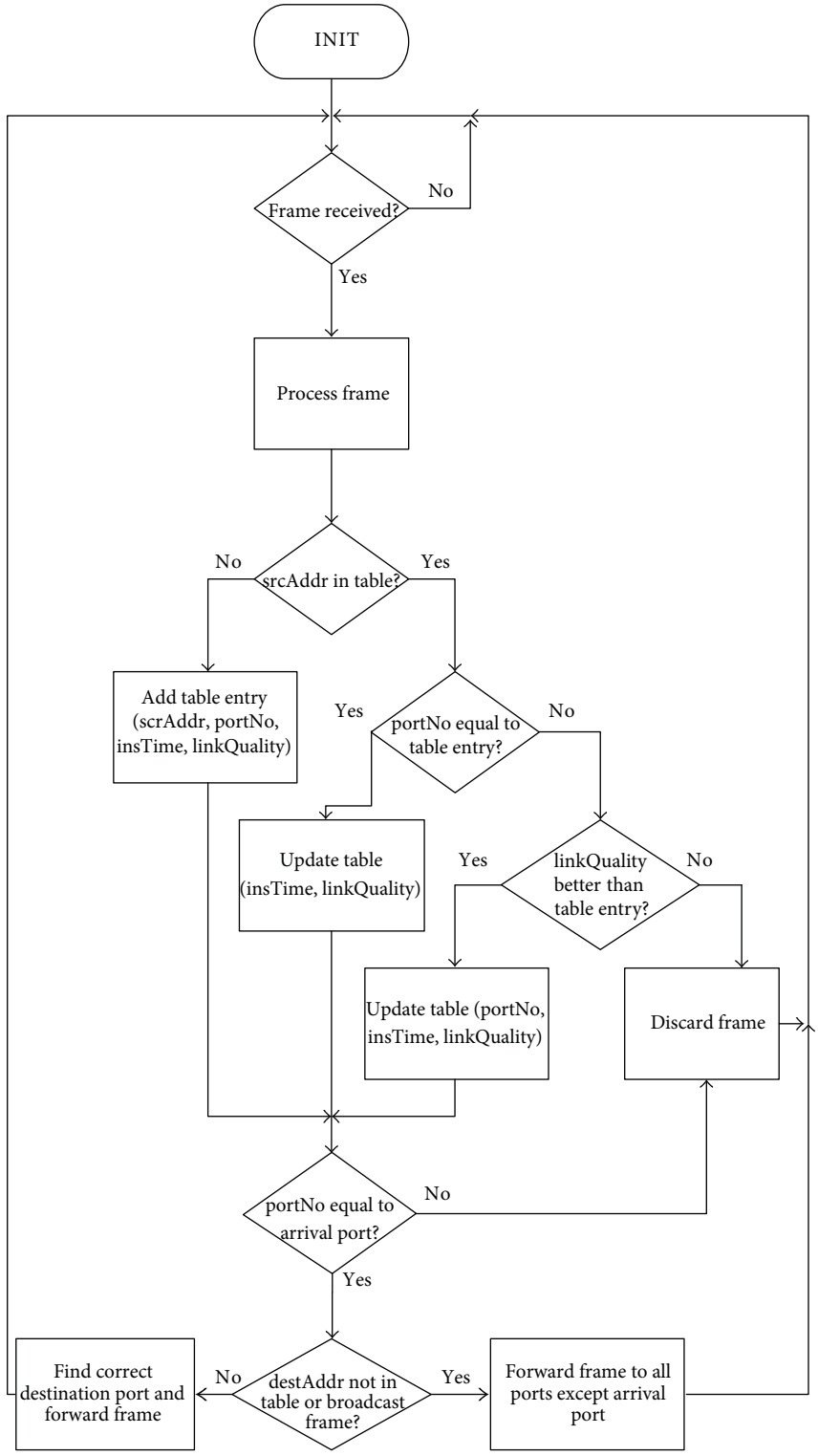

Figure 4: Switch flow chart.

platform [27] that consists of a pair of NB-PLC OFDM based modems whose parameters are very similar to the ones specified by G3-PLC (see Section 2). We have performed two trial campaigns connecting, at each time, this pair of modems to two power sockets within a house. The first campaign took place in a single floor house. Whereas, the second took place in a three-floor house, whose electrical power is distributed from the main panel (MP) to each floor through a floor circuit breaker (CB) located at the MP. In the latter case, we have considered either the transmission between outlets belonging to the same floor or between outlets belonging to different floors. Appliances, for example, television, washing machine,

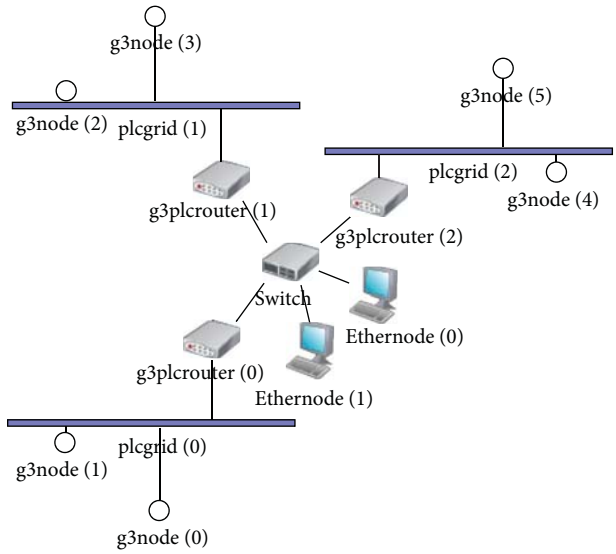

Figure 5: Screenshot of an example of convergent network simulation in OMNET++.

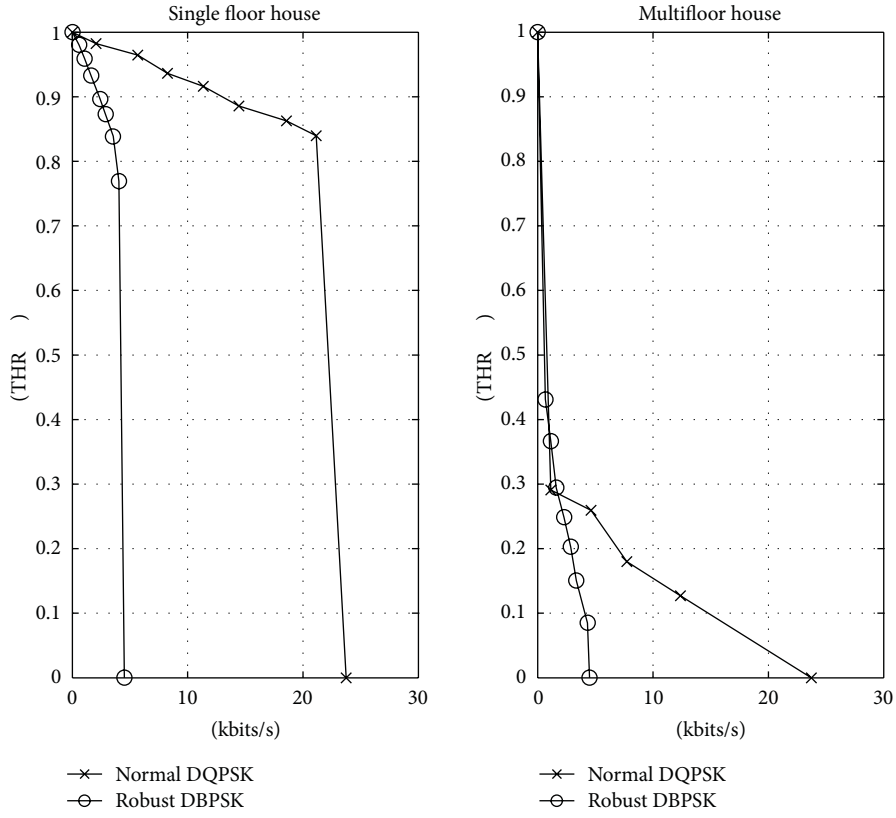

Figure 6: CCDF of the measured THR for G3-PLC technology.

battery charger, fluorescent lamps, fridge, and so on, have been plugged and unplugged.

Figures 6 and 7, respectively, show the complementary cumulative distribution function (CCDF) of the THR, and the cumulative distribution function (CDF) of the FER for normal and robust mode for both the considered scenarios. As we can see, both the THR and the FER are much more degraded for channels belonging to the multifloor house. This is simply explainable observing that channels associated to multifloor houses cover in average larger distances than those in single floor houses, and they experience higher attenuation. From the obtained results, we computed the distribution of the FER. In particular, for the single floor house, the FER can be assumed to be exponentially distributed with mean

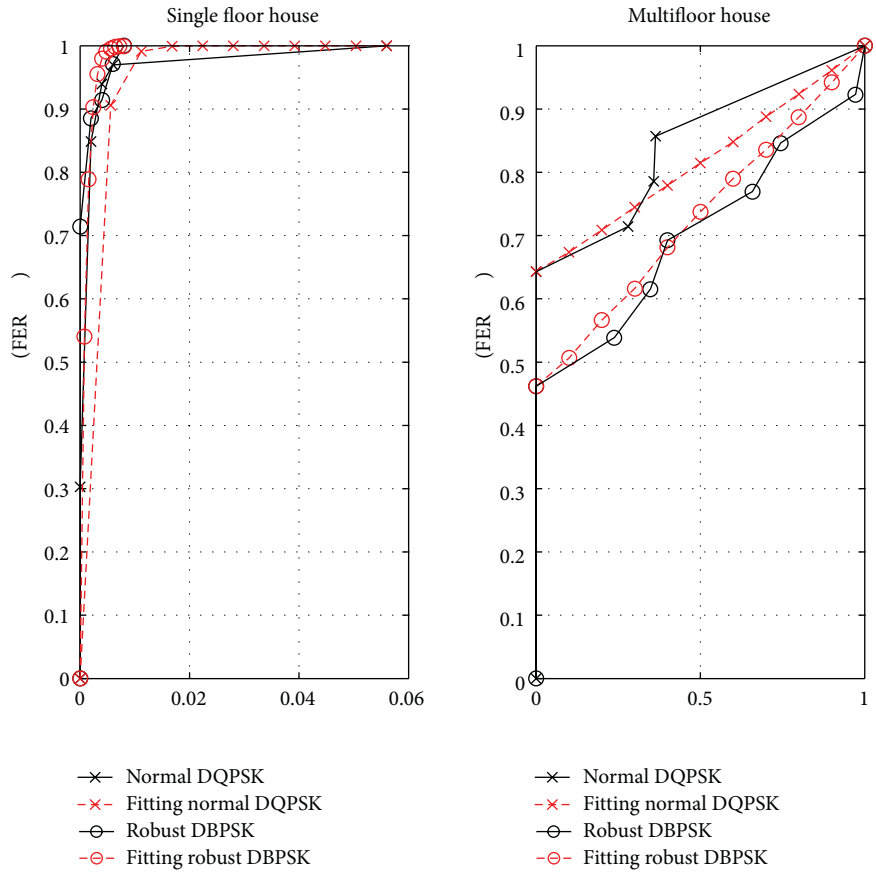

Figure 7: CDF of the measured FER for G3-PLC technology. The distribution fitting is also shown.

equal to 0.0024 and 0.001, respectively, for normal DQPSK and robust DBPSK mode. Regarding the multifloor house, we model the FER as uniformly distributed in the range $(0.6429, 1)$ or $(0.4615, 1)$, respectively, for normal DQPSK and robust DBPSK mode. The obtained statistics are depicted in Figure 7 (red dotted lines). More results regarding the test campaigns are reported in [23].

It is important to note that in the case of a multi-floor house, the G3-PLC network can be naturally split into several subnetworks, one for each floor. The subnetworks can then be connected through Ethernet. The same architecture can be used in large buildings that may already have a wired Ethernet deployment.

We now turn our attention to the convergent network behavior. To do that, we consider the saturation throughput (STH), which is defined as the limit reached by the THR when the offered load increases, and it represents the maximum load that the system can carry [28]. In STH conditions, each node has immediately a packet available for transmission, after the completion of each successful transmission.

Now we build the simulation scenario using from 6 up to 60 G3-PLC nodes and we evaluate the STH when no Routers are introduced, and when two and three Routers—for example, one per each floor—are considered. The traffic is generated among G3-PLC nodes belonging to the same subnetwork or to different subnetworks in DQPSK mode.

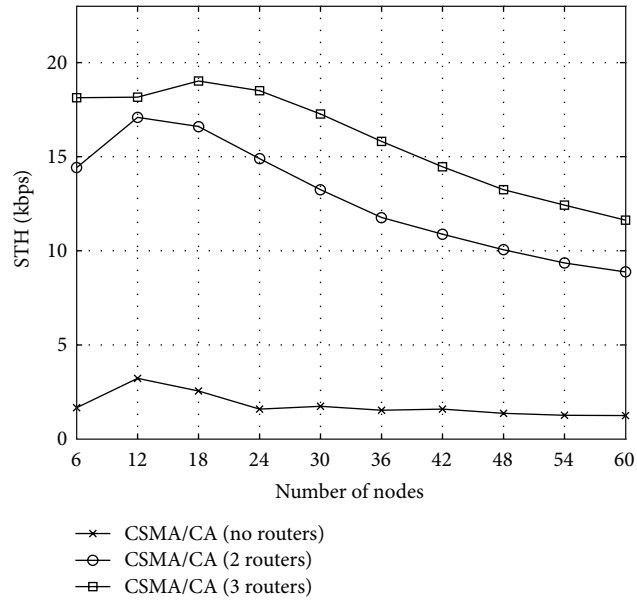

Figure 8: Simulated STH for different network configurations.

Figure 8 shows the STH. As we can see, the introduction of 2 and 3 routers substantially improves the performance. It is worth noting that the STH improvements directly translate in a coverage increase.

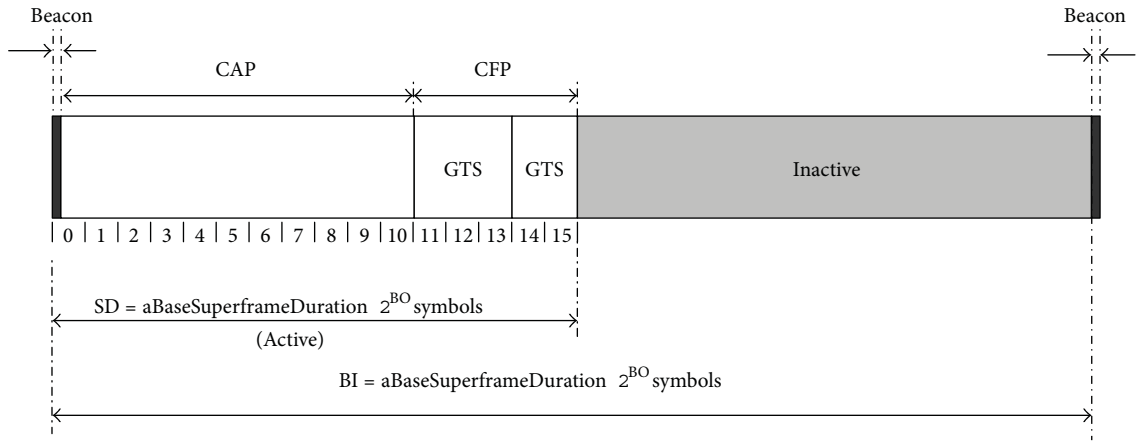

Figure 9: An example of superframe structure [24].

Table 2: Superframe parameters and values.

Parameters	Value
aBaseSuperframeDuration	*aBaseSlotDuration* ∗ *aNumSuperframeSlots*
aBaseSlotDuration	50
aNumSuperframeSlots	16
SO = BO	2

5. Further Improvements Using Time Division Multiple Access

Despite the STH improvements related to the introduction of routers, the bottleneck of the network is represented by the degradation of the performance with the increasing number of G3-PLC nodes within each subnetwork (see Figure 8). To prevent this occurrence, we envision the G3-PLC communication technology proposing a different channel access method that provides a higher QoS, namely, time division multiple access (TDMA). To do this, we implement the *beacon-enabled* mode of the IEEE 802.15.4-2006 specifications [24]. It defines a *superframe* structure as depicted in Figure 9. Each superframe is characterized by an active and an inactive portion. The active portion, which is defined by the superframe duration (SD), consists of a contention access period (CAP) and a contention-free period (CFP). In the CAP period, data packet transmission follows a CSMA/CA algorithm while during the CFP the channel access is based on TDMA. The network coordinator, represented by the router, assigns a guaranteed time slot (GTS) to each node. We notice that the coordinator may assign more than one GTS to each station, in order to satisfy given QoS constraints. Therefore, the CFP grows or shrinks dynamically fulfilling the minimum CAP length (440 symbols). We further denote with N_{TStot} the number of time slots present in the CFP.

It is worth noting that the beacon frame, which is periodically sent by the WPAN coordinator for synchronization purposes, can be replaced by synchronization via the exploitation of the mains cycle.

The values of the parameters used in beacon-enabled mode simulations are reported in Table 2.

The GTS assignment is done by each router solving the following optimization problem:

$$\begin{aligned} &\max_{\underline{N}_{TS}} \sum_{u=1}^{N} \frac{N_{TS}^{(u)}}{N_{TStot}} \mathrm{THR}^{(u)} \\ &\text{s.t.} \quad \sum_{u=1}^{N} \frac{N_{TS}^{(u)}}{N_{TStot}} = 1, \\ &\frac{N_{TS}^{(u)}}{N_{TStot}} \mathrm{THR}^{(u)} \geq p^{(u)} \mathrm{THR}^{(u)}, \quad \forall u = 1, \ldots, N, \end{aligned} \tag{4}$$

where N is the number of nodes, $N_{TS}^{(u)}$ is the number of time slots assigned to node u, and $\underline{N}_{TS} = [N_{TS}^{(1)}, N_{TS}^{(2)}, \ldots, N_{TS}^{(N)}]$. Furthermore, $\mathrm{THR}^{(u)}$ is the throughput of node u in bps. It can be obtained as $\mathrm{THR}^{(u)} = 8n(1 - \mathrm{FER}^{(u)})/T_s$, with T_s denoting the time slot duration in seconds. $p^{(u)} \in [0, 1]$ are QoS coefficients, each indicates the percentage of the throughput that the uth node has to achieve with respect to the one that it would achieve in the corresponding single user scenario. Finally, the condition in the second line of (4) forces all the time slots in a CFP to be used.

Problem (4) is an integer linear programming problem. Therefore, it is, in general, NP hard. To simplify the problem, we solve (4) using linear programming (LP) and we round the obtained coefficients to the lower closest integer value. Clearly, there could be cases where the number of slots assigned to one or more nodes is zero. In these cases, the correspondent nodes are deferred to transmit in the CAP. Furthermore, when some time slots are not occupied as result of the rounding of the coefficients, these will be assigned to the nodes that have the highest throughput, leaving the CAP free of transmissions. Finally, we assume $\sum_{u=1}^{N} p^{(u)} \leq 1$. The latter assures that the LP always give a feasible solution if $N \leq N_{TStot}$.

It is easy to prove that when $\sum_{u=1}^{N} p^{(u)} = 1$, for example, $p^{(u)} = 1/N$, the optimal solution to (4) can be found

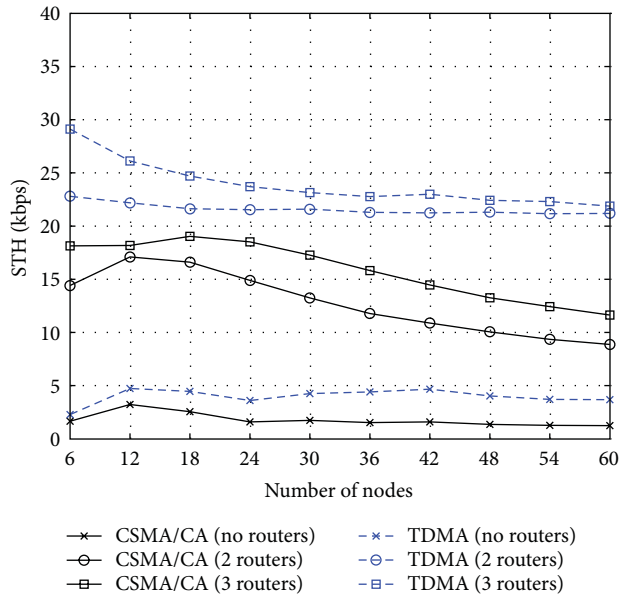

Figure 10: STH comparison between CSMA/CA and TDMA.

imposing the Karush Kuhn Tucker (KKT) conditions [29] and it is given by $N_{TS}^{(u)} = N_{TStot}/N$ for all $u = 1, \ldots, N$. In the following, we assume the last condition holds true.

Now, in Figure 10, we consider the comparison between the CSMA/CA and the optimized TDMA increasing the number of network nodes. From Figure 10, we notice that the TDMA scheme allows for a substantial increase of the aggregate network throughput with respect to CSMA. Furthermore, it solves the bottleneck problem of CSMA represented by a considerable degradation of the performance with the increasing number of nodes within each subnetwork. We finally notice that the minimum CAP length constraint, specified by the 802.15.4 standard, affects the behavior of the aggregate throughput. In fact, the throughput exhibits a faster decay when considering 2 and 3 routers with respect to the no router case. This is because the negative effect of the CAP is present in each subnetwork, namely twice or three times, respectively.

6. Conclusions

G3-PLC devices show poor performance when working over large in-home/building PLC networks whose links can be severely attenuated. A convergent network, consisting of Ethernet and G3-PLC devices, can be built using routers and switches nodes to cope with this problem. Through simulation results, obtained implementing the convergent network in the OMNET++ simulator, we have shown the feasibility of such a solution. After that, we have analysed the behavior of the CSMA/CA protocol implemented in the G3-PLC devices and we have found that its performance decreases as the number of network nodes increases. To cope with this problem, we have proposed to implement a TDMA scheme and we have seen that it sensibly improves the network performance.

Acknowledgments

The work of this paper has been partially supported by the Friuli Venezia Giulia region under the POR/FESR 2007–2013 programme, project LAK—Living for All Kitchen.

References

[1] European Commission, *Energy 2020—A Strategy for Competitive, Sustainable and Secure Energy*, 2010.

[2] L. Lampe, A. Tonello, and D. Shaver, "Power line communications for automation networks and smart grid," *IEEE Communications Magazine*, vol. 49, no. 12, pp. 26–27, 2011.

[3] A. Zaballos, A. Vallejo, and J. Selga, "Heterogeneous communication architecture for the smart grid," *IEEE Network*, vol. 25, no. 5, pp. 30–37, 2011.

[4] H. C. Ferreira, L. Lampe, J. Newbury, and T. G. Swart, *Power Line Communications: Theory and Applications for Narrowband and Broadband Communications Over Power Lines*, Wiley & Sons, New York, NY, USA, 2010.

[5] V. C. Gungor, D. Sahin, T. Kocak et al., "Smart grid technologies: communication technologies and standards," *IEEE Transactions on Industrial Informatics*, vol. 7, no. 4, pp. 529–539, 2011.

[6] M. M. Rahman, C. S. Hong, S. Lee, J. Lee, M. A. Razzaque, and J. H. Kim, "Medium access control for power line communications: an overview of the IEEE 1901 and ITU-T G.hn standards," *IEEE Communications Magazine*, vol. 49, no. 6, pp. 183–191, 2011.

[7] HomeGrid Forum, *G.hn—Compatibility with Existing Home Networking Technologies*, 2009.

[8] V. Suraci, A. Cimmino, R. Colella, G. Oddi, and M. Castrucci, "Convergence in home gigabit networks: implementation of the inter-MAC layer as a pluggable kernel module," in *Proceedings of the IEEE 21st International Symposium on Personal Indoor and Mobile Radio Communications (PIMRC '10)*, pp. 2569–2574, Istanbul, Turkey, September 2010.

[9] V. Miori, L. Tarrini, M. Manca, and G. Tolomei, "An open standard solution for domotic interoperability," *IEEE Transactions on Consumer Electronics*, vol. 52, no. 1, pp. 97–103, 2006.

[10] S. Wolff, P. G. Larsen, K. Lausdahl, A. Ribeiro, and T. S. Toftegaard, "Facilitating home automation through wireless protocol interoperability," in *Proceedings of the International Symposium on Wireless Personal. Multimedia Communications*, September 2009.

[11] D. Elshani and P. Francq, "The anatomy of a universal domotics integrator for globally interconnected devices," in *Proceedings of the International Conference on Pervasive Systems and Computing*, pp. 17–23, June 2006.

[12] S. Tompros, N. Mouratidis, M. Draaijer, A. Foglar, and H. Hrasnica, "Enabling applicability of energy saving applications on the appliances of the home environment," *IEEE Network*, vol. 23, no. 6, pp. 8–15, 2009.

[13] *IEEE P1905. 1/D06, IEEE Draft Standard for A Convergent Digital Home Network for Heterogeneous Technologies*, IEEE, 2012.

[14] IEEE Standards Associacion, IEEE Std. 802. 11-2012—Part 11: Wireless LAN Medium Access Control (MAC) and Physical Layer (PHY) Specifications, IEEE, 2012, .

[15] L. Chang, *White Paper—Making of IEEE 802. 3 Compliant Equipment, National Semiconductor*, 2003.

[16] Multimedia over Coax Allinace, *MoCA 1. 1 Specification for Device RF Characteristics*, 2012.

[17] ZigBee Alliance, *ZigBee and Wireless Radio Frequency Coexistence*, 2008.

[18] *HomePlug Powerline Alliance, HomePlug AV White Paper*, 2005.

[19] ZigBee Alliance and HomePlug Powerline Alliance liaison, *Smart Energy Profile Version 2. 0 Technical Requirements*, 2012.

[20] ERDF, *PLC G3 Physical Layer Specification*.

[21] ERDF, *PLC G3 MAC Layer Specification*.

[22] V. Oksman and J. Zhang, "G.HNEM: the new ITU-T standard on narrowband PLC technology," *IEEE Communications Magazine*, vol. 49, no. 12, pp. 36–44, 2011.

[23] L. D. Bert, S. D'Alessandro, and A. M. Tonello, "An Interconnection approach and performance tests for in-home PLC networks," in *Proceedings of the IEEE International Symposium on Power Line Communications and Its Applications*, Bejing, China, March 2012.

[24] *IEEE Std 802. 15. 4-2006, Part 15. 4: Wireless Medium Access Control (MAC) and Physical Layer (PHY) Specifications for Low-Rate Wireless Personal Area Networks (WPANs)*, IEEE, 2006.

[25] A. Varga, *OMNeT++ User Manual*, 2011.

[26] *INET Framework For OMNeT++ Manual*, 2012.

[27] *MAX2990 Integrated Power-Line Digital Transceiver Programming Manual*, Maxim Integrated Products, 2010.

[28] G. Bianchi, "IEEE 802. 11-saturation throughput analysis," *IEEE Communications Letters*, vol. 2, no. 12, pp. 318–320, 1998.

[29] S. Boyd and L. Vandenberghe, *Convex Optimization*, Cambridge University Press, 2004.

Hindawi Publishing Corporation
Journal of Electrical and Computer Engineering
Volume 2012, Article ID 452402, 9 pages
doi:10.1155/2012/452402

Research Article

Improved Maximum Likelihood S-FSK Receiver for PLC Modem in AMR

Mohamed Chaker Bali and Chiheb Rebai

GRESCOM Research Laboratory, SUPCOM, University of Carthage, City of Communications Technologies, 2083 El Ghazala Ariana Tunis, Tunisia

Correspondence should be addressed to Chiheb Rebai, chiheb.rebai@supcom.rnu.tn

Received 3 August 2012; Accepted 26 October 2012

Academic Editor: Justinian Anatory

This paper deals with an optimized software implementation of a narrowband power line modem. The modem is a node in automatic meter reading (AMR) system compliant to IEC 61334-5-1 profile and operates in the CENELEC-A band. Because of the hostile communication environments of power line channel, a new design approach is carried out for an S-FSK demodulator capable of providing lower bit error rate (BER) than standard specifications. The best compromise between efficiency and architecture complexity is investigated in this paper. Some implementation results are presented to show that a communication throughput of 9.6 kbps is reachable with the designed S-FSK modem.

1. Introduction

International concerns about natural environment preservation have been increasingly serious during the last decades. In fact, one of the most ecologically influencing factors is energy. Besides, energy consumption rise was unexpectedly important and quick, neglecting efficiency and ecological considerations. These facts have pushed several countries to try to change their energy consumption policies.

The widest idea behind operating energy efficiently is called SmartGrid. This concept, as its name suggests, involves integrating intelligence into the whole power grid; generation, transmission, distribution, and management are concerned. The goal is to increase power generation, transmission, distribution, and usage efficiency by reducing power waste, favoring renewable energies, and sensitizing consumers about their actual consumption [1].

This big concept was only expressed lately after arise of more specific and actually applicable ideas. The first is automatic meter reading (AMR), enabling automated remote meter reading. Later were introduced automatic meter infrastructure (AMI) and automatic meter Management (AMM), which are two expansions providing more consumer- and management-oriented services.

Despite its obvious advantages, AMR have not been yet rolled out significantly. Actually, a major broad deployment inconvenient of smart meters was the lack of reliability on hostile communication environments of power line channel. In fact, early implementations of PLC modems were basic on ordinary amplitude shift keying (ASK) or frequency shift keying (FSK) techniques.

In this paper, we investigate the importance of spread frequency shift keying (S-FSK) modulation scheme to make transmissions robust against narrowband noise and attenuation in such hostile channel. Hence, an intelligent power line communication (PLC) modem solution for automatic meter reading using International Electrotechnical Commission (IEC) S-FSK profile is simulated and implemented using digital signal processor (DSP) [2].

The paper is organized as follows. In Section 2 we will start by presenting PLC-based automatic meter reading solution. The chosen S-FSK profile is briefly introduced. A description of the proposed S-FSK receiver is presented in Section 3. In Section 4 we focus on implementation of S-FSK modulation scheme using DSP architecture. The efficiency of the proposed design was illustrated by some implementation results that show the performances of the

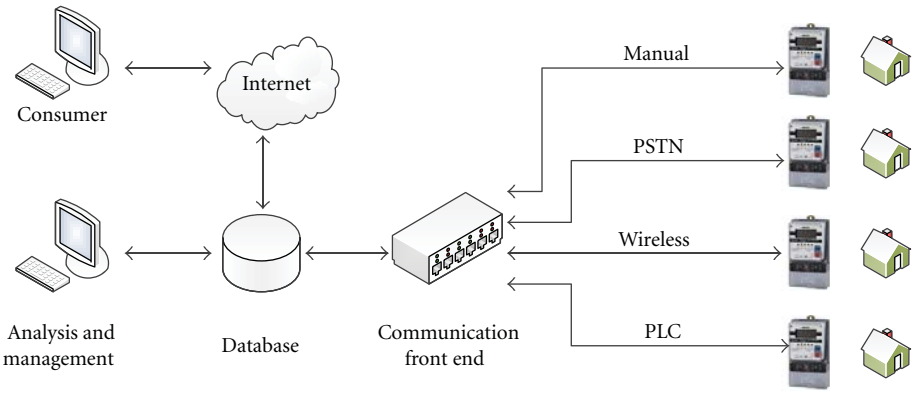

Figure 1: Different automatic meter reading techniques.

realized PLC Modem. Finally some conclusions are outlined in Section 5.

2. PLC Modems for AMR

The evolution of meter reading has been outstanding during the last decades. Several power suppliers, distributers jointly with their technological partners, have tried several novel approaches in order to automate meter reading.

The evolution from traditional manual meter reading to actual and future intelligent infrastructures passing through e-meters, semiautomatic meter reading, and fully automated meter reading gave these actors a great experience in this ever-evolving field.

Despite the abundance of the available technologies, power line communication has been agreed to be the best fit for last-mile meter reading and meter management communication. In fact, this technology has one of the lowest costs and is easily set up. Moreover, the technology is now considered as sufficiently ripe to be widely deployed.

PLC, as a technology, is very wide. A myriad of techniques are available using different modulation techniques and different protocols. From another side, the regulation is still under work. Nevertheless, some profiles have already been standardized and are being adopted by the market. The IEC S-FSK profile, for example, is actually one of the most used for AMR because it proved its simplicity and maturity.

In this section, we will briefly introduce automatic meter reading concepts, then present PLC from both technical and technological sides, and finally give a short survey on S-FSK PLC modems.

2.1. Automatic Meter Reading. Automatic meter reading is a technique used to collect data from electricity, gas, water, or other utility meters. Unlike manual meter reading, automatic meter reading relies on communication technologies to collect users' consumption. Meters send data automatically through a communication network to the management system. Collected data can be then transferred to a central database to be analyzed and used for billing. This means that billing can be based on actual consumption rather than on an estimate based on previous consumption statistics, giving customers better control of their usage of electric energy, gas, or water. From the other side, predicting energy usage remains a key advantage for energy distributors. With AMR, distributors can get accurate information of consumption profile of each consumer and monitor the network in order to prevent or capture defects.

The advantages of AMR are several and obvious:

(i) increasing meter reading and billing accuracy and security;

(ii) permitting a flexible tariff changing;

(iii) giving user the control over its consumption;

(iv) enabling a better grid monitoring and load management;

(v) remote power disconnection and reconnection.

Automatic meter reading system is summarized by Figure 1. Meters' data are collected using one of the available ways of communication into a database. This database is then accessible for analysis and management purposes in the information system center. A subset of these data can also be accessed by customers using dedicated services.

Several automatic meter reading technologies can be used depending on grid topology. Most important ones are as follows

(i) handheld, walk-by, and drive-by AMR;

(ii) public switched telephone network-based AMR;

(iii) wireless communication-based AMR;

(iv) power line communication-based AMR.

2.2. Power Line Communication-Based AMR. Power line communication consists of the use of the power lines as a physical communication medium. PLC has been used for data transfer for both indoor and outdoor networks. Anyhow, the profile of these applications is different.

Concerning PLC use for AMR and outdoor communication, PLC is the most approved technology by electricity distributors. In fact, electric network is already well expanded and offers a great coverage. Thus, no additional wireless

or wired communication medium needs to be used and deployment costs are then cut.

The main idea behind PLC is the use of the power line to carry radio frequency signals. Actually, a low power modulated signal containing information is added to the electric signal. Data then propagates over the electric network and is detected by remote stations.

Several modulation techniques can be used to transport data over power lines. But most of them are based on frequency modulation. Actually, data is converted to a higher frequency signal which is superimposed to the 50 Hz/60 Hz electrical signal. The signal is then repeatedly transmitted over the network until it reaches the destination node.

Several PLC communication profiles have been proposed and each profile is essentially based on the modulation scheme chosen.

Two different modulation scheme classes can be distinguished:

(i) single-carrier modulations;

(ii) multicarrier modulations.

The first technique is the simpler one. It uses a narrow frequency band for data transfer. Examples of these modulation schemes are FSK, S-FSK, and continuous phase frequency shift keying (CPFSK). These modulation schemes are often chosen for their maturity and implementation simplicity. Though, they do not offer great data transfer rates. Actually, data rates generally range from 300 bps to 2.4 kbps [3]. Narrowband PLC has been receiving widespread attention due to its applications in the SmartGrid.

The second uses multiple adjacent carriers in order to transfer data. Usually orthogonal frequency division multiplexing (OFDM) or a derived modulation scheme is used. These modulation schemes are applied in order to increase raw data throughput and/or to cope with harsh channel conditions. Broadband PLC is seen as an exciting and effective technology for multimedia distribution within homes.

In either case, AMR PLC technique must handle poor channel quality. In fact, outdoor power lines are exposed to several noise sources. Furthermore, power lines present highly varying impedance due to topology changes and high attenuation. Hence, power line channel quality is considered as time, space, and frequency dependent [4].

In order to overcome these impairments, high performance processing is unavoidable. This includes channel estimation and equalization, strong forward error correction algorithms, and signal repetition.

In addition to noise and channel quality difficulties, PLC-based AMR has two other main challenges. The first is that unlike usual communication techniques where transfer speed is the most significant criteria, cost and reliability are the most important factors in AMR. The second is the existence of a lot and very different protocols and standards, their specific underlying problems, and interoperability issues.

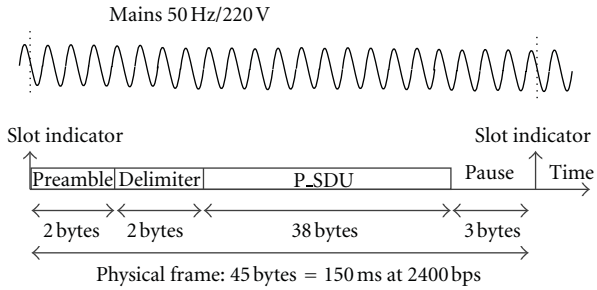

Figure 2: Physical frame structure.

2.3. PLC Modem Based on S-FSK Profile. The communication profile described by the IEC 61334-5-1 standard is based on the S-FSK modulation technique.

S-FSK is a modulation and demodulation technique which combines some of the advantages of a classical spread spectrum system (e.g., immunity against narrowband interferers) with the advantages of a classical FSK system (low-complexity, well-investigated implementations).

As the classical FSK, S-FSK uses two frequencies to transmit binary information at each bit time. By spreading the two used frequencies, S-FSK makes these two channels independent. This characteristic is then used by the demodulator and ensures a better reception quality than FSK. In fact, if signal qualities of the two channels are close, the demodulator makes the decision by comparing the signal on both channels. Otherwise, demodulation is based only on the channel having a better reception quality. Channel quality estimation is calculated using a predefined preamble preceding transmitted data.

Synchronization in this profile is based on zero crossing detection of electric signal. Therefore, the transmission and reception must start on the main zero cross. Due to the phase shift between 50 Hz and the carrier, the zero cross signal may provide incorrect timing of the bit-wise synchronization. To recover this delay the bit synchronization adjustment method is implemented in the modem software. This algorithm based on correlation method can move bit border during reception.

Time is divided into system wide synchronized time slots, and physical frames are only transmitted with the beginning of timeslots.

Timeslot synchronization is achieved using detection of any frame's preamble and delimiter as described in Figure 2. After physical synchronization, each station must keep track of slot indicator using an internal clock.

As described earlier, communication between meters and management system is done through a special node called access node usually placed at the medium/low voltage (MV/LV) transformer stations. Access nodes are specific nodes that manage the communication on a specific meter network.

This profile uses a master/slave communication paradigm based on polling mechanism. In fact, meters can only respond to queries made by master station. This method combined with slotted time simplifies considerably medium access control.

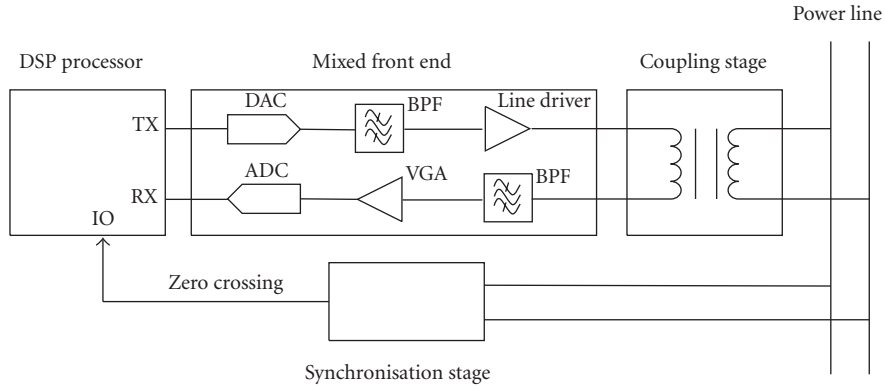

Figure 3: PLC modem functional block diagram.

The modem that we propose in this paper is an AMR PLC modem using IEC61334-5-1 compliant profile and operates in the CENELEC—A band [5]. It is based on three main stages as described in Figure 3; DSP processor, mixed front end, and a coupling interface:

(i) digital stage including DSP processor and external memories. DSP processor provides flexible software implementation and easily upgrade to new software version or merging standards;

(ii) mixed front end based on digital to analog converter (DAC) and line driver for transmitter section, analog to digital converter (ADC) and variable gain amplifier (VGA) for receiver section, and external band-pass filter (BPF);

(iii) coupling interface makes connection between the mixed front end and the power lines. It provides protection from high voltage and peak voltage/current, attenuation of 50/60 Hz signal, impedance matching to the mains for both transmitter and receiver paths, and nonisolated power supply.

The use of a DSP permits a greater control over the signal processing stage and a greater flexibility of the implemented S-FSK modem.

3. S-FSK Modulation Technique

This section details S-FSK modulation principle and gives theory and simulations of suboptimum receiver.

3.1. The S-FSK Principle. S-FSK modulation consists of a binary FSK modulation in which the frequency deviation Δf is large enough to generate a spectrum with two separate lobes. For this reason, the concept of dual channel is introduced: channel 0 refers to the signal placed around a frequency f_0 and channel 1 refers to the signal placed around a frequency f_1, with $\Delta f = |f_1 - f_0|/2$ [6, 7].

The symbols to be transmitted are generated with a rate $1/T$, where T is the symbol period, and belong to the alphabet $\{-1, +1\}$. Therefore, binary hypotheses H_0 and H_1 can be associated with 0 and 1 being transmitted, respectively.

A digital signal waveform with binary signaling consists of two kinds of signals $s_0(t)$ and $s_1(t)$ for $nT \le t \le (n+1)T$, n is a positive integer:

$$\begin{aligned} H_0 &: s_0(t) = A\sin(2\pi f_0 t), \\ H_1 &: s_1(t) = A\sin(2\pi f_1 t), \end{aligned} \tag{1}$$

where A is a real constant.

A frequency selective channel with an additive nonwhite Gaussian noise is considered; however, the channel gain G_i and the noise power spectral density N_i are assumed to be flat around the frequency f_i. Therefore, at the receiver input, the signal-to-noise ratio (SNR) for the channel i is

$$\mathrm{SNR}_i = \frac{A^2 G_i^2/2}{N_i/T}, \quad \text{with } i \in \{0, 1\}. \tag{2}$$

The SNR_i completely characterize the quality of the received signal. Moreover, another characterization of the quality of the received S-FSK signal may be made through the unbalancing factor x and the average signal-to-noise ratio $\mathrm{SNR}_{\mathrm{av}}$. This last term is defined as the ratio of the signal energy and the average noise power densities. These parameters are related to (2) as follows:

$$\mathrm{SNR}_{\mathrm{av}} = 2\frac{\mathrm{SNR}_0\ \mathrm{SNR}_1}{\mathrm{SNR}_0 + \mathrm{SNR}_1}, \qquad x = \frac{\mathrm{SNR}_1}{\mathrm{SNR}_0}. \tag{3}$$

3.2. The Maximum Likelihood S-FSK Receiver. In practical channels, the received signal phase is very difficult or even impossible to track. Thus, the detection process may have to disregard the phase information to avoid complex circuits, at some expense of performance degradation. This is called noncoherent detection [8, 9].

Using the channel model early presented the received signal under hypotheses H_0 and H_1 is

$$r(t) = \begin{cases} G_0 s_0(t, \theta) + n_0(t) & \text{under } H_0, \\ G_1 s_1(t, \theta) + n_1(t) & \text{under } H_1, \end{cases} \tag{4}$$

where $s_i(t, \theta)$ is the signal with an unknown phase θ and $n_i(t)$ is the white Gaussian noise with zero mean and a noise power spectral density $N_i/2$, with $i \in \{0, 1\}$.

The unknown phase is random with a power density function $p_\theta(\theta)$. We assume that θ is uniformly distributed on $[0, 2\pi]$, that is,

$$p_\theta(\theta) = \frac{1}{2\pi}, \quad 0 \le \theta \le 2\pi. \tag{5}$$

The correlation receiver correlates the input signal $r(t)$ with a stored replica of the signal $s_i(t)$. The outputs r_i are necessary to discriminate whether $+1$ or -1 has been transmitted.

The modulus of the envelop detectors' outputs may be modeled as follows for two orthogonal S-FSK signals:

$$r_0 = \begin{cases} |n_0| & \text{under } H_1 \\ |s_0 + n_0| & \text{under } H_0, \end{cases}$$
$$r_1 = \begin{cases} |n_1| & \text{under } H_0 \\ |s_1 + n_1| & \text{under } H_1, \end{cases} \tag{6}$$

where n_i is an additive circularly Gaussian noise with zero mean and variance σ_i^2, with $i \in \{0, 1\}$.

Under the assumption that the noise is Gaussian, the sampled outputs of the envelope detectors r_0 and r_1 are Rician or Rayleigh distributed depending on which of the two signals $s_0(t)$ and $s_1(t)$ is transmitted.

Under hypothesis H_0, the probability density function $p(r_i \mid H_0)$ of the amplitude of the signal r_i with $i \in \{0, 1\}$ is

$$p(r_0 \mid H_0) = \frac{2r_0}{\sigma_0^2}\, I_0\left(\frac{2r_0 a_0}{\sigma_0^2}\right) \exp\left(-\frac{r_0^2 + \mu_0^2}{\sigma_0^2}\right),$$
$$p(r_1 \mid H_0) = \frac{2r_1}{\sigma_1^2} \exp\left(-\frac{r_1^2}{\sigma_1^2}\right). \tag{7}$$

Under hypothesis H_1, the probability density function $p(r_i \mid H_1)$ of the amplitude of the signal r_i with $i \in \{0, 1\}$ is

$$p(r_0 \mid H_1) = \frac{2r_0}{\sigma_0^2} \exp\left(-\frac{r_0^2}{\sigma_0^2}\right),$$
$$p(r_0 \mid H_1) = \frac{2r_1}{\sigma_1^2}\, I_0\left(\frac{2r_1 a_1}{\sigma_1^2}\right) \exp\left(-\frac{r_1^2 + \mu_1^2}{\sigma_1^2}\right), \tag{8}$$

where $\mu_0 = \int_0^T s_0(t)^2 dt$ and $\mu_1 = \int_0^T s_1(t)^2 dt$. $I_0(\cdot)$ is the modified Bessel function of the first kind of order 0.

Assuming the symbols $\{+1, -1\}$ to be transmitted with the same probability and to deal with independent noises n_0 and n_1 (typical in the S-FSK modulation), the maximum likelihood (ML) decision turns out to be the optimum decision rule [10].

In particular, the decision rule uses the following decision values:

$$p(r \mid H_0) = p(r_0 \mid H_0) p(r_1 \mid H_0),$$
$$p(r \mid H_1) = p(r_0 \mid H_1) p(r_1 \mid H_1). \tag{9}$$

The decision rule is to compare likelihood functions and choose the largest:

$$\text{detect } 0 \; p(r \mid H_0) \gtrless p(r \mid H_1) \text{ detect } 1. \tag{10}$$

3.3. Improved ML S-FSK Receiver. Implementation of the ML receiver is difficult due to the complexity of formulae from (8) to (9). An improved method of estimating log-likelihood metric is proposed for a practical realization.

In order to describe the receiver, the log-likelihood ratio $l_i(r_i)$ of the signal r_i is introduced:

$$l_i(r_i) = \log\left(\frac{p(r_i \mid H_1)}{p(r_i \mid H_0)}\right). \tag{11}$$

Using the distributions (8)–(9), (11) can be simplified into the following equation:

$$l_i(r_i) = (2i - 1)\left(\log\left(I_0\left(\frac{2r_i\mu_i}{\sigma_i^2}\right)\right) - \frac{\mu_i^2}{\sigma_i^2}\right). \tag{12}$$

Logarithm and Bessel function are approached using approximating function. Let $g(\cdot)$ be a piecewise linear approximation of the composed function $\log(I_0(\cdot))$ defined as

$$g(X) = A_j X + B_j. \tag{13}$$

The approximation is defined over M intervals $I_1, I_2, \ldots, I_M$. A_j and B_j are calculated by imposing $g(\cdot)$ to be equal to $\log(I_0(\cdot))$ on the boundary of each interval that defines the piecewise approximation:

$$g(X) = \log(I_0(X)) \quad \text{with } X \in \{0, 2^1, 2^2, \ldots\}. \tag{14}$$

Using (14) in (12), an approximated estimation of the loglikelihood $l_i'(r_i)$ ratio is obtained with the equation:

$$l_i'(r_i) = (2i - 1)\left(g\left(\frac{2r_i\mu_i}{\sigma_i^2}\right) - \frac{\mu_i^2}{\sigma_i^2}\right). \tag{15}$$

The proposed receiver decides accordingly to (10) on the following decision values:

$$p(r \mid H_1) = l_1'(r_1), \qquad p(r \mid H_0) = l_0'(r_0). \tag{16}$$

Assuming to have knowledge of the first P symbols creating the Preamble (alternative 1 and 0 symbols), the channel and noise parameters may be estimated using the signals (6) as follows:

$$\tilde{\sigma}_0^2 = \frac{2}{P} \sum_{k \in H_1} r_0(k)^2, \qquad \tilde{\sigma}_1^2 = \frac{2}{P} \sum_{k \in H_0} r_1(k)^2,$$
$$\tilde{\mu}_0^2 = \left| -\tilde{\sigma}_0^2 + \frac{2}{P} \sum_{k \in H_0} r_0(k)^2 \right|,$$
$$\tilde{\mu}_1^2 = \left| -\tilde{\sigma}_1^2 + \frac{2}{P} \sum_{k \in H_1} r_1(k)^2 \right|. \tag{17}$$

3.4. Simulations' Results. The performance of different receiver is compared through communication schema implementation using Matlab. A packet-based transmission has been adopted, with preamble length P equal to 32 and

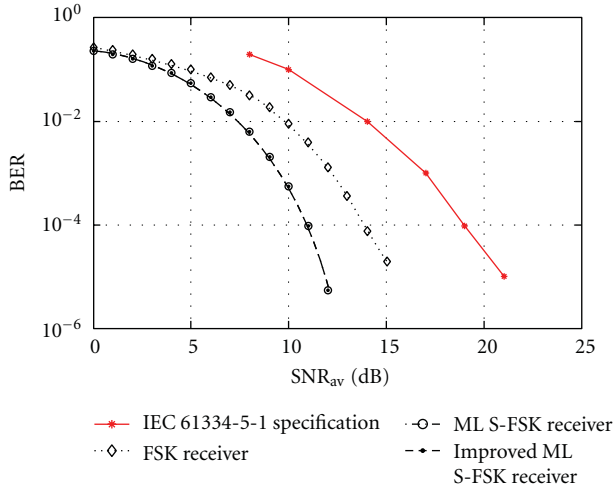

Figure 4: BER versus SNR$_{av}$ with $x = 5$ dB.

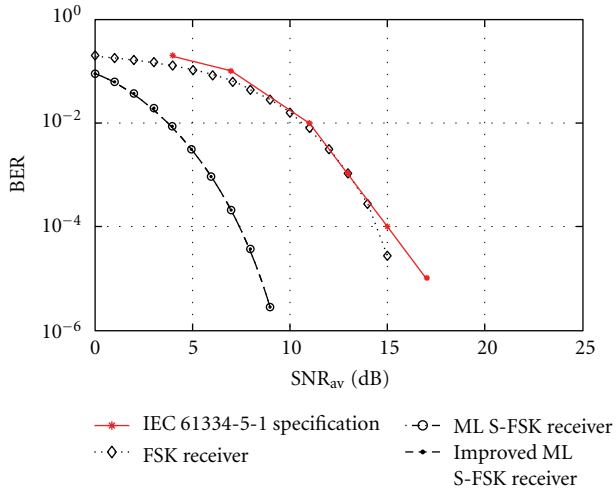

Figure 5: BER versus SNR$_{av}$ with $x = 10$ dB.

a payload of 304 random bits. The following curves are averaged over 1000 packets.

Figures 4, 5, and 6 show the bit error rate (BER) versus the average signal-to-noise ratio SNR$_{av}$ for three unbalancing factors $x \in \{+5, +10, +20\}$ dB.

From the previous figures, the FSK receiver loses in performance with the increasing of the unbalancing factor; however, the ML S-FSK receiver presents relevant improvement on balanced channels. For bit error rate equal to 10^{-4}, more than 6 dB gain at $x = 10$ dB.

For $X \in [0, 256]$ this approximation guarantees a mean square error lower than 10^{-3}, which is adequate to obtain negligible loss of performance between the ideal ML S-FSK receiver and the improved ML S-FSK receiver.

4. DSP Implementation Methodology

Priority in design was given to modularity, simplicity, low cost, and reliability. A 32-bit-fixed point general purpose DSP architecture is considered to optimize the software

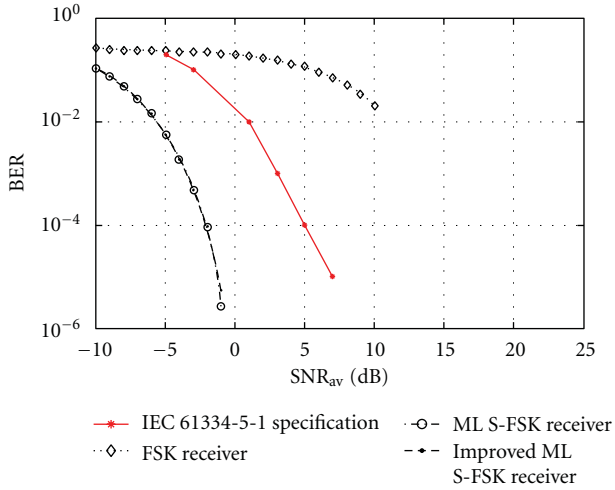

Figure 6: BER versus SNR$_{av}$ with $x = 20$ dB.

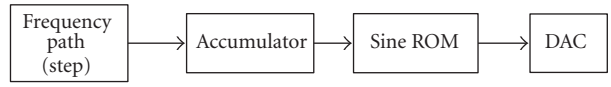

Figure 7: Modulator block diagram.

implementation of the S-FSK receiver. The DSP-based digital part communicates, through serial port in full duplex, with the host device. At the other end, DSP communicates, in half-duplex, through power line via a mixed front end coupling interface.

The DSP programming structure was defined to handle in real-time transmitting or receiving S-FSK signal.

The S-FSK base-band modem is obtained by the implementation of an S-FSK modulator at the transmitter side and an improved ML receiver at the receiver one.

4.1. Modulator Implementation. The transmitter is composed by three stages:

(i) a numeric stage involving a DSP that performs frequency synthesizing with a direct digital synthesizer (DDS);

(ii) a digital to analog convertor (DAC) capable to generate a linear signal up to its full scale output;

(iii) line driver delivering amplified signal.

As described in Figure 7, DDS is based on storing the samples of a sinusoidal signal in a look-up table (LUT) and to read it by a specified integer step index which determines the phase increment, in order to generate the desired frequency f_i which is related to the step index k, the sampling frequency f_s and the LUT length N by the following relation:

$$f_i = \frac{k f_s}{N}. \tag{18}$$

It is important to minimize the LUT size since the implementation will be done in an embedded processor where the resources especially the memory size are limited.

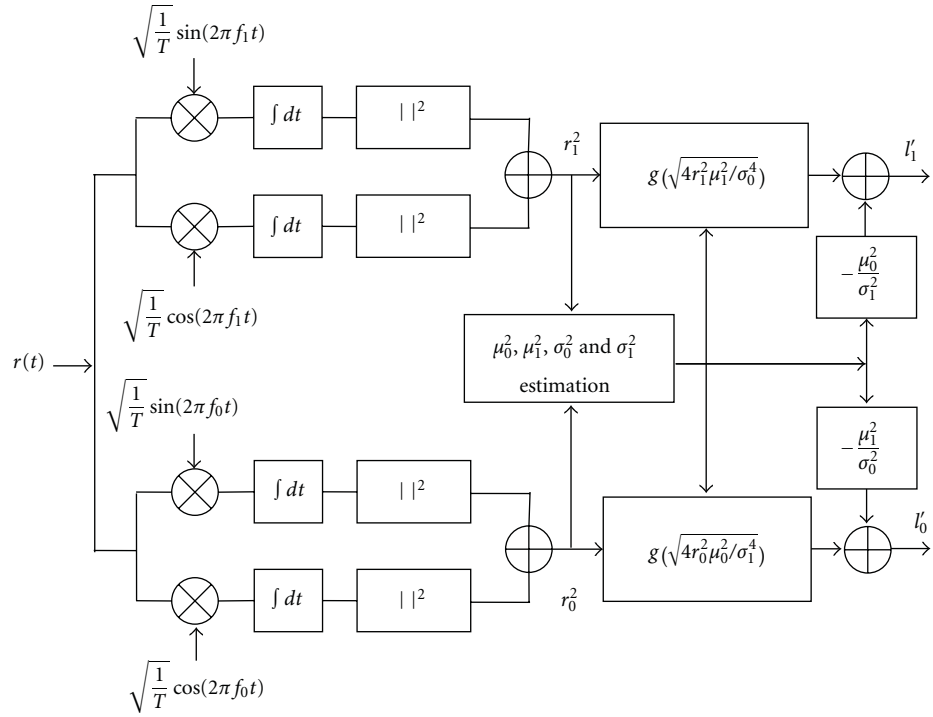

Figure 8: Implemented improved ML S-FSK receiver architecture.

The sampling frequency f_s is chosen as multiple of the data rate $1/T$, thus the number of samples in a bit period is an integer.

Once the appropriate sine samples are read they serve as input for the DAC. The generated signal by the DAC pin is amplified by the line driver.

The S-FSK modulator generates signal in the CENELEC band from 3 kHz to 95 kHz responding to the following specifications:

(i) frequency bandwidth $2\Delta f > 10$ kHz and multiple of bit rate D;

(ii) programmable bit rate D;

(iii) frequencies f_0 and f_1 are multiple of $D/2$.

The sampling frequency f_s is fixed at 3.125 MHz and the samples' number is set to 320 samples to optimize the error performance at the demodulator side. Therefore, the data rate is equal to 9.6 kbps.

The step index k is an integer; therefore, the resolution frequency is found by setting $k = 1$,

$$f_{\text{res}} = \frac{f_s}{N}. \tag{19}$$

Resolution frequency is set to 4.8 kHz to respect orthogonality constraint between two frequencies f_0 and f_1.

The minimum LUT lengths that satisfy the conditions already cited and the generation of the frequencies f_0 and f_1 with zero error are 656.

In Table 1, we present the possible choice of orthogonal frequency f_0 and f_1 in the case of S-FSK demodulator at baud rate 9.6 kbps.

Table 1: Orthogonality frequency choice for baud rate 9.6 kbps.

CENELEC band	Frequency (kHz)		Carrier frequency (kHz)
	f_0	f_1	
A band	91.2	72	81.6
	86.4	67.2	76.8
	81.6	62.4	72
	76.8	57.6	67.2
	72	52.8	62.4

4.2. Improved ML Receiver Implementation. Coherent FSK signals can be noncoherently demodulated to avoid the carrier recovery. The improved ML demodulator is a quadrature receiver capable of detecting signals with unknown phases.

It can be implemented with four correlators as shown in Figure 8, where the four reference signals are $\sin(2\pi f_0 t)$, $\cos(2\pi f_0 t)$, $\sin(2\pi f_1 t)$, and $\cos(2\pi f_1 t)$. We will use the same DDS module as the modulator one to generate those reference signals.

The signal consists of an in-phase component and a quadrature component. Thus, the signal is partially correlated with $\sin(2\pi f_i t)$ and partially correlated with $\cos(2\pi f_i t)$. Therefore, we use two correlators to collect the signal energy in these two parts.

The first P outputs are used to estimate channel parameters. Then, we apply probability function (15) to correlator output using estimated channel parameters and g function. The g function is a piecewise linear approximated and stored in data memory.

All samples of received bits are processed according to Figure 8. The main constraint in the receiver is to tune the sampling frequency of ADC f_{ADC} so as to have

$$\frac{f_s}{f_{ADC}} = M. \tag{20}$$

Different configurations are possible; we have to choose the one that maximizes f_{ADC}. In this case M is equal to 2 and the ADC sampling frequency f_{ADC} becomes equal to 1.565 MHz.

Thus, samples' count during bit time T is 160 samples. The number of samples per symbol period T must be multiple of 8 for direct memory access (DMA) use that offer transfer facility and rapidity.

4.3. Implementation Results. The DSP processor BF506F, sited to an evaluation board [11, 12], operates with frequency up to 400 MIPS with 32 Kbytes of L1 memory associated to instructions (L1_code), 32 Kbytes for data (L1_data) accessed at full processor speed, and 32 Mbytes of external flash memory.

To evaluate the complexity of the S-FSK modem software, it is important to determine the consumed cycles and the consumed data memory space [13].

We have used the data memory to store the LUT table that contains 656 samples encoded on 16 bits.

g function is stored also on data memory space. g function is defiened over 8 intervals and the affinity coefficients are encoded on 16 and 32 bits.

The cycles' consumption is limited by the available number of cycles per sample that is governed by the DSP speed which is 400 MIPS.

The DDS algorithm consumes only 2 cycles per sample, one cycle for memory access to read the sample from the LUT, and one cycle for incrementing the reading index. The transfer of DDS samples to DAC convertor requires 10 cycles per sample.

At the receiving site, the demodulator invokes 4 correlators. At each correlator, one sample is treated on 4 cycles to read, multiply, accumulate, and update index.

Finally, we apply g function on correlators' output at the end of symbol reception.

The cycle's consumptions per sample of these different modules are presented in Table 2. It is important to report that additional modules are implemented to ensure synchronization, build packets, and handling different events.

The cycle's consumption of the S-FSK modem software composed of the modulator, demodulator, and PHY layer functionalities according to IEC 61334-5-1 is lower than the available cycles per symbol period T.

By considering the DSP implementation, we measured an average cycles consumption of 9076 cycles during transmission (21.78% of available cycles) and 9232 cycles during reception (22.15% of available cycles).

Memory consumption is 10.25% for data memory and 45.17% for code memory.

Table 2: Memory and processing time analysis results for the PLC-modem DSP implementation.

Module	PM space (16-bit Word)	DM space (16-bit Word)	Number of cycles machine during T
Modulator module	1620	656	3840
ADC reception module	1066	160	1280
Correlation module	246	656	2560
S-FSK decision module	87	32	156
Initialization PHY module	513	10	2323
PHY layer FSM module	3869	822	5236

The physical layer is designed and implemented. The remaining available cycles and memory will be used to build upper layers: MAC layer and Application layer.

5. Conclusions

In this paper, we have described the design and optimized DSP implementation of an S-FSK profile for a PLC node in an AMR system. To overcome power line channel condition, an improved ML S-FSK receiver is used. Improved receiver presents close error performance to the ideal ML S-FSK receiver but has simplifier architecture.

Analysis of new receiver reveals excellent results in terms of memory occupations, required cycles, and BER performances.

Data rate of 9.6 kbps is easily provided with flexibility and programmability to change receiver parameters.

Acknowledgments

This work was supported by the Embedded Systems Technology (EBSYS) SmartGrid Division and GRESCOM Research Laboratory of Higher School of Communication of Tunis.

References

[1] H. C. Ferreira, L. Lampe, J. Newbury, and T. G. Swart, *Power Line Communications—Theory and Applications for Narrowband and Broadband Communications over Power Lines*, Wiley, 2010.

[2] IEC 61334-5-1, 2.0 b: Distribution automation using distribution line carrier systems—part 5-1: Lower layer profiles—the spread frequency shift keying (S-FSK) profile, 2001.

[3] A. Lotito, R. Fiorelli, D. Arrigo, and R. Cappelletti, "A complete narrow-band power line communication node for AMR," in *Proceedings of the IEEE International Symposium on Power Line Communications and Its Applications (ISPLC '07)*, pp. 161–166, March 2007.

[4] D. Cooper and T. Jeans, "Narrowband, low data rate communications on the low-voltage mains in the CENELEC frequencies—part I: noise and attenuation," *IEEE Transactions on Power Delivery*, vol. 17, no. 3, pp. 718–723, 2002.

[5] CENELEC EN 50065-1:2001.Signaling on low-voltage electrical installations in the frequency range from 3 kHz to 148.5 kHz—part I: General requirements, frequency bands and electromagnetic disturbances.
[6] T. Schaub, "Spread frequency shift keying," *IEEE Transactions on Communications*, vol. 42, no. 2, pp. 1056–1064, 1994.
[7] T. Schaub and B. Steinle, "Minimax noncoherent detection of BFSK signals in nonwhite gaussian noise," *IEEE Transactions on Communications*, vol. 34, no. 9, pp. 955–958, 1986.
[8] B. Sklar, *Digital Communications: Fundamentals and Applications*, Prentice Hall, 2001.
[9] F. Xiong, *Digital Modulation Techniques*, Artech House, London, UK, 2000.
[10] D. Veronesi, L. Guerrieri, and P. Bisaglia, "Improved spread frequency shift keying receiver," in *Proceedings of the 14th Annual International Symposium on Power Line Communications and its Applications (ISPLC '10)*, pp. 166–171, March 2010.
[11] ADSP-BF50x Blackfin Processor Hardware Reference. Rev 1.0, Analog Devices, 2010.
[12] [12] ADSP-BF506F EZ-KIT Lite Evaluation System Manual. Rev 1.0, Analog Devices, 2009.
[13] H. Hajji and A. Ghazel, "Design and implementation of a correlation-based DSP software for narrowband power line communication receiver," in *Proceedings of the 13th IEEE International Conference on Electronics, Circuits and Systems (ICECS '06)*, pp. 114–118, December 2006.